SAND2020-10787R

Advances in GDSA Framework Development and Process Model Integration

Spent Fuel and Waste Disposition

Prepared for
U.S. Department of Energy
Spent Fuel and Waste Science Technology

P.E. Mariner, M.A. Nole, E. Basurto, T.M. Berg, K.W. Chang, B.J. Debusschere, A.C. Eckert, M.S. Ebeida, M. Gross, G.E. Hammond, J. Harvey, S.H. Jordan, K.L. Kuhlman, T.C. LaForce, R.C. Leone, W.C. McLendon III, M.M. Mills, H.D. Park, F.V. Perry, A. Salazar III, D.T. Seidl, S.D. Sevougian, E.R. Stein, L.P. Swiler*

Sandia National Laboratories
**Los Alamos National Laboratory*

September 14, 2020
M2SF-20SN010304042
SAND2020-xxxxx R

DISCLAIMER

This information was prepared as an account of work sponsored by an agency of the U.S. Government. Neither the U.S. Government nor any agency thereof, nor any of their employees, makes any warranty, expressed or implied, or assumes any legal liability or responsibility for the accuracy, completeness, or usefulness, of any information, apparatus, product, or process disclosed, or represents that its use would not infringe privately owned rights. References herein to any specific commercial product, process, or service by trade name, trade mark, manufacturer, or otherwise, does not necessarily constitute or imply its endorsement, recommendation, or favoring by the U.S. Government or any agency thereof. The views and opinions of authors expressed herein do not necessarily state or reflect those of the U.S. Government or any agency thereof.

DISCLAIMER

This is a technical report that does not take into account contractual limitations or obligations under the Standard Contract for Disposal of Spent Nuclear Fuel and/or High-Level Radioactive Waste (Standard Contract) (10 CFR Part 961). For example, under the provisions of the Standard Contract, spent nuclear fuel in multi-assembly canisters is not an acceptable waste form, absent a mutually agreed to contract amendment.

To the extent discussions or recommendations in this report conflict with the provisions of the Standard Contract, the Standard Contract governs the obligations of the parties, and this report in no manner supersedes, overrides, or amends the Standard Contract.

This report reflects technical work which could support future decision making by DOE. No inferences should be drawn from this report regarding future actions by DOE, which are limited both by the terms of the Standard Contract and Congressional appropriations for the Department to fulfill its obligations under the Nuclear Waste Policy Act including licensing and construction of a spent nuclear fuel repository.

Sandia National Laboratories is a multi-mission laboratory managed and operated by National Technology & Engineering Solutions of Sandia, LLC., a wholly owned subsidiary of Honeywell International, Inc., for the U.S. Department of Energy's National Nuclear Security Administration under contract DE-NA0003525.

U.S. DEPARTMENT OF ENERGY

Sandia National Laboratories

APPENDIX E
NFCSC DOCUMENT COVER SHEET[1]

Name/Title of Deliverable/Milestone/Revision No.	Advances in GDSA Framework Development and Process Model Integration / M2SF-20SN010304042
Work Package Title and Number	GDSA – Framework Development – SNL / SF-20SN01030404
Work Package WBS Number	1.08.01.03.04
Responsible Work Package Manager	Paul Mariner (Name/Signature)
Date Submitted	

Quality Rigor Level for Deliverable/Milestone[2]	☐ QRL-1 ☐ Nuclear Data	☐ QRL-2	☒ QRL-3	☐ QRL-4 Lab QA Program[3]

This deliverable was prepared in accordance with Sandia National Laboratories
(Participant/National Laboratory Name)

QA program which meets the requirements of

☒ DOE Order 414.1 ☐ NQA-1 ☐ Other

This Deliverable was subjected to:

☒ Technical Review ☐ Peer Review

Technical Review (TR)
Review Documentation Provided

☐ Signed TR Report or,
☐ Signed TR Concurrence Sheet or,
☐ Signature of TR Reviewer(s) below

Peer Review (PR)
Review Documentation Provided

☐ Signed PR Report or,
☐ Signed PR Concurrence Sheet or,
☐ Signature of PR Reviewer(s) below

Name and Signature of Reviewers

David Sassani

NOTE 1: *Appendix E should be filled out and submitted with the deliverable. Or, if the PICS:NE system permits, completely enter all applicable information in the PICS:NE Deliverable Form. The requirement is to ensure that all applicable information is entered either in the PICS:NE system or by using the NFCSC Document Cover Sheet.*

- *In some cases there may be a milestone where an item is being fabricated, maintenance is being performed on a facility, or a document is being issued through a formal document control process where it specifically calls out a formal review of the document. In these cases, documentation (e.g., inspection report, maintenance request, work planning package documentation or the documented review of the issued document through the document control process) of the completion of the activity, along with the Document Cover Sheet, is sufficient to demonstrate achieving the milestone.*

NOTE 2: *If QRL 1, 2, or 3 is not assigned, then the QRL 4 box must be checked, and the work is understood to be performed using laboratory QA requirements. This includes any deliverable developed in conformance with the respective National Laboratory / Participant, DOE or NNSA-approved QA Program.*

NOTE 3: *If the lab has an NQA-1 program and the work to be conducted requires an NQA-1 program, then the QRL-1 box must be checked in the work Package and on the Appendix E cover sheet and the work must be performed in accordance with the Lab's NQA-1 program. The QRL-4 box should not be checked.*

ACKNOWLEDGEMENTS

This report incorporates principal contributions in Sections 3.1 and 3.2 from the following coauthors:

- K-Won Chang (3.1.8 Evolution of Buffer and DRZ Porosity and Permeability)
- Mohamed Ebeida and Will McLendon III (3.2.2 VoroCrust Meshing)
- Aubrey Eckert (Appendix C: GDSA Framework Graphical Workflow)
- Michael Gross (3.2.3.3 Geologic Framework Model for the Mimbres Basin Unsaturated Zone Alluvial Model)
- Glenn Hammond (Appendix A: Dynamic KD – A Reduced-Order Sorption Model)
- Jacob Harvey (Appendix B: Fuel Matrix Degradation Modeling in FORTRAN)
- Rosie Leone (3.1.2 Quality Assurance)
- Paul Mariner (3.1.3 Process Model Coupling, 3.1.7.1 FMD Surrogate Models, 3.1.10 AGGREGATE Function for Recording Maximum Concentrations in a Region, 3.2.5 Tracer Method for Quantifying Repository Hydraulic Characteristics, and 3.2.6 Tracer Method for Quantifying Mean Travel Time)
- Melissa Mills (3.1.6.4 Corrosion Model Database)
- Michael Nole (3.1.1 Code Management, 3.1.2 Quality Assurance, 3.1.3 Process Model Coupling, 3.1.8 Evolution of Buffer and DRZ Porosity and Permeability, and 3.1.10 AGGREGATE Function for Recording Maximum Concentrations in a Region)
- Heeho Park (3.1.4 Convergence Improvements)
- Frank Perry (3.2.3 Geologic Framework Model)
- Alex Salazar III and Kris Kuhlman (3.1.9 Temperature-Dependent Thermal Conductivity)
- Laura Swiler (3.2.4 Uncertainty Quantification and Sensitivity Analysis).

The authors thank David Sassani of Sandia National Laboratories (SNL) for his thoughtful technical review, Emily Stein (SNL) for her informal review of sections of the report, and the staff from U.S. Department of Energy Office of Nuclear Energy (DOE-NE), Prasad Nair (DOE NE-81) and Tim Gunter (DOE NE-81), for their discussions, oversight, and guidance on topics addressed in this report.

EXECUTIVE SUMMARY

The Spent Fuel and Waste Science and Technology (SFWST) Campaign of the U.S. Department of Energy (DOE) Office of Nuclear Energy (NE), Office of Spent Fuel & Waste Disposition (SFWD) is conducting research and development (R&D) on geologic disposal of spent nuclear fuel (SNF) and high-level nuclear waste (HLW). A high priority for SFWST disposal R&D is to develop a disposal system modeling and analysis capability for evaluating disposal system performance for nuclear waste in geologic media.

This report describes fiscal year (FY) 2020 advances of the Geologic Disposal Safety Assessment (GDSA) Framework and PFLOTRAN development groups of the SFWST Campaign. The common mission of these groups is to develop a geologic disposal system modeling capability for nuclear waste that can be used to probabilistically assess the performance of disposal options and generic sites. The capability is a framework called GDSA Framework that employs high-performance computing (HPC) capable codes PFLOTRAN and Dakota. In FY 2020 advances included:

- New model capabilities in PFLOTRAN (e.g., buffer and disturbed rock zone evolution, temperature-dependent thermal conductivity, fuel matrix degradation (FMD) surrogate models)
- Improved model representations (e.g., new and improved Geologic Framework Models for shale and unsaturated alluvium)
- New approaches for enhanced model fidelity (e.g., dynamic adsorption model, waste package degradation, VoroCrust meshing)
- Improved speed and convergence (e.g., new Newton Trust Region Dogleg-Cauchy solver method for PFLOTRAN, fuel matrix degradation surrogate model coupling, coding fuel matrix degradation processes using advanced Fortran solvers)
- Enhanced workflow and infrastructure (e.g., release of PFLOTRAN v3.0, new prototype graphical user interface for GDSA Framework, new process model coupling workflow, automated quality assurance testing suite, adoption of Agile and Jira code management system, new HPC resources)
- New analytical methods for performance assessment (e.g., calculation of bulk characteristics of stochastically-affected regions using tracers, graphical analysis of DFN realizations, a new PFLOTRAN function to find and record maximum concentrations in a region)
- Continued integration with other SFWST Disposal Research R&D work packages
- Enhanced international engagement (e.g., Task F of DECOVALEX-2023 on performance assessment, international collaborations in uncertainty and sensitivity analysis)
- New 5-year plan for SFWST Disposal Research R&D priorities and schedules

The scope and impact of the GDSA FY 2020 accomplishments are substantial. The advances in PA modeling capabilities listed above allow for emulation of fuel matrix degradation (FMD) processes (e.g., radiolytic oxidation) at each waste package in a repository simulation, simulation of changes to buffer and disturbed rock zone (DRZ) properties over time, improved simulation of heat flow, improved PFLOTRAN convergence for multiphase systems, and improved assessment of performance using a new function that finds the highest concentrations of radionuclides in a region. New quantitative methods allow for characterization of regions affected by stochastically-generated discrete fracture networks, e.g., in terms of mean or shortest travel time from the repository to an aquifer and mean residence time of an initial tracer in the repository region. In addition, new modeling approaches under development in FY 2020 include advanced meshing capabilities, a new approach for dynamically simulating adsorption as affected by changing local conditions, new concepts for simulating waste package degradation, and

advanced biosphere modeling. Progress in simulation workflow, quality assurance (QA) workflow, process model coupling workflow, and other forms of supporting infrastructure in FY 2020 was also extensive and is expected to greatly facilitate continued model development, user-friendliness, and user adoption going forward.

An important responsibility of the GDSA team is to integrate with disposal R&D activities across the SFWST Campaign to ensure that R&D activities support the portions of generic safety cases being developed. In FY 2020, the GDSA team participated with other scientists and engineers at ORNL, LANL, DOE, and SNL in the development of a new high-temperature shale reference case. That effort resulted in new reference case designs, new options for waste package materials and other EBS components, and new conceptual process models. Other activities involved integration with LANL, ANL, LBNL, and PNNL, including development of dfnWorks for the crystalline reference case, Geologic Framework Modeling for the unsaturated alluvium reference case, FMD model integration, DECOVALEX-2023 Task F performance assessment, and planning for the development of an advanced biosphere model.

Another important accomplishment in FY 2020, at the request of DOE, was the preparation of a 5-year plan for high priority activities of the Disposal Research R&D of the SFWST Campaign. In the prepared plan, evaluation and prioritization of current and planned activities for each technical area in Disposal Research R&D are discussed, and schedules are outlined (Sassani et al. 2020). This plan will be revised each year to align with changes in objectives and funding.

Each year, GDSA Framework improves as additional modelers and programmers from around the world use, apply, and contribute to its development. GDSA Framework is accessible to everyone because the primary codes, PFLOTRAN and Dakota, are open source, available for free download, and have supporting documentation online. The GDSA team has worked to increase the number of users and participants by (1) maintaining a collaborative web site (pa.sandia.gov), (2) expanding online documentation of verification testing, generic reference cases, and code features, (3) developing quality assurance documentation and a user manual, (4) conducting PFLOTRAN short courses, (5) presenting papers and posters on GDSA Framework capabilities at international forums, and (6) engaging in international collaborations such as DECOVALEX. Outreach and collaborations support a primary objective of the GDSA work package by facilitating testing of, and feedback on, PFLOTRAN and GDSA Framework and by increasing the likelihood outside users will contribute directly to code development in the future.

The ability to simulate increasingly complex repository reference cases continues to affirm that HPC-capable codes can be used to simulate important multi-physics couplings directly in a total system safety assessment demonstration. The generic repository systems modeled to date indicate that PFLOTRAN and its coupled codes can simulate complex coupled processes in a multi-kilometer domain while simultaneously simulating sub-meter-scale coupled behavior in the repository. Continued development is needed to ensure GDSA Framework is ready for application to potential sites that may be selected in the future. The challenge is to address the remaining needs using available resources. Meeting this challenge will require close integration with technical teams across the SFWST Campaign.

This report fulfills the GDSA Framework Development Work Package Level 2 Milestone – *Advances in GDSA Framework Development and Process Model Integration*, M2SF-20SN010304042.

CONTENTS

Page

FIGURES

Page

TABLES

NOMENCLATURE

1D, 2D, 3D, 4D	one-, two-, three-, and four-dimensional
ANDRA	French national radioactive waste management agency
ANL	Argonne National Laboratory
ANN	artificial neural network
CPU	central processing unit
DECOVALEX	Development of COupled models and their VALidation against Experiments
DFN	discrete fracture network
DGR	deep geologic repository
DOE	U.S. Department of Energy
DR	disposal research
DRZ	disturbed rock zone
EBS	engineered barrier system
ECPM	equivalent continuous porous medium
EDZ	excavation disturbed zone
Eq.	equation
ERB	example reference biosphere
FEP	feature, event, and process
FMD	Fuel Matrix Degradation
FY	fiscal year
GB	gigabytes
GDSA	Geologic Disposal Safety Assessment
GFM	geologic framework model
GUI	graphical user interface
GWd	gigawatt day
HDF5	hierarchical data format, version 5
HIC	hydrogen induced cracking
HLW	high-level radioactive waste
HPC	high-performance computing
IAEA	International Atomic Energy Agency
IGA	intergranular grain boundary attack
IWM	Integrated Waste Management
K	Kelvin
K_D	distribution coefficient
km	kilometer
kNNr	k Nearest-Neighbors regressor
LANL	Los Alamos National Laboratory
LBNL	Lawrence Berkeley National Laboratory
LGPL	lesser general public license
LHS	Latin hypercube sampling
m	meter
MB	megabytes
MIC	microbially-influenced corrosion
mm	millimeter
mol	mole

MPa	megapascal
MRT	mean residence time
MTHM	metric tons of heavy metal
MTT	mean travel time
MWd	megawatt day
NA	not applicable
NBS	natural barrier system
NE	Office of Nuclear Energy
NEA	Nuclear Energy Agency
NGW	Next-Generation Workflow
NM	New Mexico
NMF	net mass flux
NT	Newton's method
NTR	Newton trust region
NTRDC	Newton Trust Region Dogleg-Cauchy
OECD	Organization for Economic Co-operation and Development
OFCT	Office of Fuel Cycle Technology
OoR	out of reactor
ORNL	Oak Ridge National Laboratory
PA	performance assessment
PDE	partial differential equation
PETSc	Portable Extensible Toolkit for Scientific Computation
PFLOTRAN	massively parallel reactive flow and transport model for describing subsurface processes (pflotran.org)
pH	negative logarithm of hydrogen ion activity
PNNL	Pacific Northwest National Laboratory
PWR	pressurized water reactor
QA	quality assurance
RAM	random access memory
R&D	research and development
s	seconds
S&D	step and direction
S&T	Storage and Transportation
SA	sensitivity analysis
SCC	stress corrosion cracking
SDA	SFWD Document Archive
SFWD	Spent Fuel and Waste Disposition
SFWST	Spent Fuel and Waste Science and Technology
SKB	Swedish Nuclear Fuel and Waste Management Company
SNF	spent nuclear fuel
SNL	Sandia National Laboratories
TBD	to be determined
TCC	thermal characteristic curve
THC	thermal-hydrologic-chemical
THM	thermal-hydrologic-mechanical
THMC	thermal-hydrologic-mechanical-chemical
TRL	technical readiness level

UFD	Used Fuel Disposition
ULR	unclassified limited release
UNF	used nuclear fuel
UO_2	uranium dioxide
UQ	uncertainty quantification
URL	underground research laboratory
U.S.	United States of America
USA	United States of America
UUR	unclassified unlimited release
V&V	verification and validation
W	watt
WF	waste form
WP	waste package
yr	year

(This page left intentionally blank.)

1. INTRODUCTION

The Spent Fuel and Waste Science and Technology (SFWST) Campaign of the U.S. Department of Energy (DOE) Office of Nuclear Energy (NE), Office of Spent Fuel & Waste Disposition (SFWD) is conducting research and development (R&D) on geologic disposal of spent nuclear fuel (SNF) and high-level nuclear waste (HLW). A high priority for SFWST disposal R&D is disposal system modeling (DOE 2012, Table 6; Sevougian et al. 2019a). The SFWST Geologic Disposal Safety Assessment (GDSA) work package is charged with developing a disposal system modeling and analysis capability for evaluating disposal system performance for nuclear waste in geologic media.

The capability being developed is a software package referred to as GDSA Framework. The primary codes used by GDSA Framework are PFLOTRAN and Dakota (Section 2.2). Each code is designed for massively-parallel processing in a high-performance computing (HPC) environment.

- The purpose of the GDSA Framework Development work package is to develop a GDSA capability that:
- Integrates updated conceptual models of subsystem processes and couplings developed under this and other disposal research work packages,
- Is used to evaluate disposal research R&D priorities,
- Leverages existing computational capabilities (e.g., meshing, visualization, HPC) where appropriate, and
- Is developed and distributed in an open-source environment.

The long-term goal for the GDSA team is to develop a safety assessment capability that can simulate all potentially important FEPs for a given repository environment. Such a capability is years away, but a DOE timeline suggests that a performance assessment (PA) model for a potential candidate site will likely not be needed before at least 2037 (DOE 2013). Although the specific timing is more uncertain, with additional time, continued advances in computing speed, and continued code development, it is expected that much progress will be made for these capabilities applied to generic geologic system analyses in the SFWST Campaign and toward the long-term goal by the time the capability is applied for its ultimate purpose in a different future program.

For the near term, GDSA objectives are focused on adding FEPs to the PA model and on developing a suite of probabilistic repository reference case applications. These near-term objectives are in line with the long-term goal. In addition, the products of the near-term objectives are useful for evaluating the effects of FEPs and input parameters on repository performance, which is useful for R&D planning.

For FY 2020, eight tasks were addressed:

- Identify additional capabilities needed to advance GDSA Framework (e.g., multiphase processes, temperature dependencies, colloids, engineered barrier system (EBS) degradation processes, computational efficiency, gridding capability). The GDSA Framework work package will work closely with other work packages as applicable in identifying these needs, determining what is required to sufficiently address them, and working to fulfill them.
- Integrate subsystem models developed under this and other SFWST work packages into GDSA software and safety assessments (e.g., waste form degradation, waste package degradation, colloid stability and transport, EBS chemistry, EBS flow and transport, fracture representation, thermal-hydrological-mechanical/chemical processes, natural system flow and transport).
- Develop and implement methods for computationally efficient multi-scale, multi-physics modeling (e.g., surrogate models, reduced order models, physics-based machine learning, nested

models, block grid refinement, etc.). This task aims to improve integration of complicated FEPs in probabilistic safety assessments and to reduce uncertainty in performance metrics.

- Develop, perform, and document verification and validation analyses of relevant GDSA model processes, expand regression testing to demonstrate and assure continued quality, and work toward a prototype GDSA Framework release package.
- Demonstrate the open-source and freely-available PFLOTRAN GDSA Framework and modeling capability at national and international forums, support an international DECOVALEX proposal for a multi-year PA modeling comparison of reference repository systems, and potentially conduct one or more workshops to promote accelerated use of the capability worldwide. Expanding the user base provides additional testing of the code and opportunities for additional development by outside contributors.
- Attend, as appropriate, technical training (e.g., classes/workshops in Python, simulation and analysis software, or computational and analysis methods), technical conferences, and international clubs and initiatives with direct benefit to GDSA.
- Develop a plan with descriptions of R&D priorities and schedules for Disposal Research over the next five fiscal years.
- Purchase 16 nodes on new Sandia National Laboratories (SNL) HPC cluster Boca to greatly improve availability of computational resources for probabilistic reference case repository simulations.

As documented in this report, good progress was made on each of these tasks. Section 2 describes the conceptual model framework and the PFLOTRAN-based computational framework for GDSA Framework. Section 3 describes FY 2020 advances in general code development, meshing, uncertainty quantification, workflow, and infrastructure. Section 4 inspects how the FY 2020 GDSA efforts address objectives highlighted for GDSA PA in the 2109 Roadmap Update (Sevougian et al. 2019a). Section 5 summarizes the development of a new Disposal Research R&D 5-Year Plan and identifies the thrusts for GDSA and how they align with current GDSA efforts. Conclusions are summarized in Section 6.

This report fulfills the requirements of the GDSA Framework Development work package (SF-20SN01030404) Level 2 Milestone – *Advances in GDSA Framework Development and Process Model Integration*, M2SF-20SN010304042. It includes, in Section 3.1, Appendix A, and Appendix B, FY 2020 accomplishments of the GDSA PFLOTRAN Development work package (SF-20SN01030406). The work presented in this report builds on previous work described in the following supporting milestones: Freeze et al. (2013a), Sevougian et al. (2013), Sevougian et al. (2014), Mariner et al. (2015), Mariner et al. (2016), Mariner et al. (2017), Mariner et al. (2018), Mariner et al. (2019), Sevougian et al. (2019a), Sevougian et al. (2019b).

2. GDSA FRAMEWORK

A performance assessment (PA) for underground disposal of nuclear waste utilizes a comprehensive analysis of features, events, and processes (FEPs) potentially affecting the release and transport of radionuclides to the biosphere. In a comprehensive PA, plausible scenarios and processes that may affect repository performance are addressed. FEPs and scenarios are evaluated and screened. Potentially pertinent FEPs are identified for simulation in a quantitative PA model. Probabilistic simulations are performed, and results are evaluated against performance metrics. Uncertainty and sensitivity analyses may also be performed to inform prioritization of additional research and model development.

The PA framework consists of a conceptual model framework (Section 2.1) and a computational framework (Section 2.2). An overview of PA methodology and terminology is presented in Sevougian et al. (2014, Section 2.2), Meacham et al. (2011, Section 1) and elsewhere (Rechard 2002).

2.1 Conceptual Framework

A safety case for a deep geologic disposal facility is a comprehensive analysis designed, in part, to assess regulatory compliance with safety standards. More specifically, it is a widely accepted approach for documenting the basis for the understanding of the disposal system, describing the key justifications for its safety, and acknowledging the unresolved uncertainties and their safety significance (OECD 2004, IAEA 2006, Freeze et al. 2013b). A full safety case may only be constructed for a specific site with an integrated design, but aspects of a safety case may also be developed for generic systems evaluated in the SFWST Campaign. In general, building such a safety case requires three primary components related most directly to post-closure safety assessments: a safety strategy, technical bases, and a safety assessment.

- The safety strategy provides direction and boundaries for the safety case. It guides the safety case by identifying requirements for site location, repository design, and safety objectives.
- Technical bases are the laws of nature and the physical and chemical barriers that govern the system. They address each feature, event, and process (FEP) that could potentially facilitate or inhibit the transport of radionuclides from the repository to the biosphere. Development of the technical bases involves site characterization, FEPs identification including waste inventory, barriers to radionuclide release and migration, radionuclide behavior, and using natural analogs, model validation, code verification, and uncertainty quantification.
- Safety assessment involves the analysis of technical bases to evaluate whether the objectives of the safety strategy are met. In safety assessment, each FEP included in the technical bases is either incorporated into the probabilistic PA model or is addressed in separate analyses or process model simulations. In the PA model, probabilistic predictions of regulatory metrics (e.g., annual dose rate) are calculated to compare to regulatory limits.

The goals and objectives of the GDSA team focus on safety assessment and, more specifically, on the development of the PA model. Conceptually, the long-term vision for the GDSA effort is to ensure that the GDSA modeling capability can adapt to, and take advantage of, future advances in computational software and hardware and future advances in process modeling. In line with this vision, the near-term mission is to develop a robust suite of fully functional generic repository reference case applications (1) for evaluation of the effects of FEPs and input parameters on repository performance to inform R&D planning and (2) for application to candidate sites by the time they are selected.

Consistent with the long-term vision, two open-source, HPC codes serve as the core of the GDSA Framework: PFLOTRAN and Dakota. PFLOTRAN is a thermal-hydrologic-chemical (THC) flow and transport code, and Dakota is a versatile probabilistic code (Section 2.2). The PFLOTRAN code is being developed by the GDSA team to accommodate new geologic disposal process models and capabilities

through additional code development and coupling with external process models. The HPC capabilities of PFLOTRAN and Dakota allow for ever higher fidelity in total system performance assessment modeling as more powerful HPC resources become available.

As the GDSA modeling capability evolves, the GDSA team will continue to generate and refine three-dimensional models of disposal repository concepts complete with surrounding geospheres and connected biospheres. Sensitivity analyses will be performed on these models to distinguish the importance of features, processes, and parameters on model results. These analyses are expected to assist prioritization of future disposal R&D.

A conceptual model framework requires a coherent representation of pertinent FEPs. Figure 2-1 schematically illustrates the conceptual model framework for a repository system. To calculate a dose to a receptor in the biosphere, radionuclides released from the waste form must pass through the repository engineered barrier system (EBS) and the surrounding natural barrier system (NBS).

A FEPs database like the one developed and described in Freeze et al. (2011) can be used to help identify a full set of potentially important FEPs for a specific conceptual repository model. Many of the FEPs in a FEPs database may be directly simulated in the PA model. In a comprehensive PA, excluded FEPs (i.e., FEPs not simulated in the PA model) must be addressed in separate analyses and arguments.

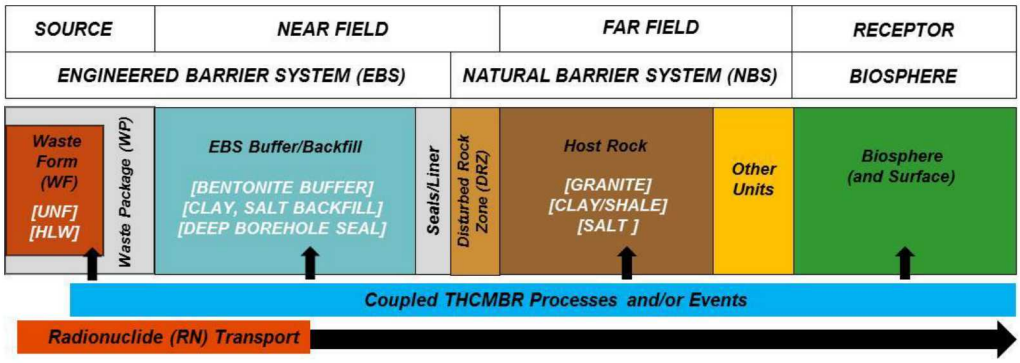

Figure 2-1 Schematic diagram of the conceptual model framework of a generic geologic disposal system

2.2 Computational Framework

Performance assessment of a geologic repository is aided by directly modeling the important coupled processes in the system and by executing multiple probabilistic realizations. The approach of using detailed models directly in a PA is a continuation of the successful modeling approach adopted for the Waste Isolation Pilot Plant (WIPP) PAs (Rechard 1995, Rechard 2002, Rechard and Tierney 2005) and differs from the modeling approach adopted for past PAs for disposal of spent nuclear fuel (SNF) and high-level radioactive waste (HLW) in volcanic tuff (Rechard and Stockman 2014). For this reason, GDSA Framework is designed for massively-parallel processing in a HPC environment.

GDSA Framework consists of the following components:

- Input parameter database
- Software for sampling, sensitivity analysis, and uncertainty quantification (Dakota)
- Petascale multiphase flow and reactive transport code (PFLOTRAN), working in concert with coupled process model codes (e.g., Fuel Matrix Degradation (FMD) Model)
- Computational support software and scripts for meshing, processing, and visualizing results (e.g., CUBIT, dfnWorks, Python, ParaView, VisIt).

The two primary components of this computational framework are PFLOTRAN and Dakota. PFLOTRAN is a thermal-hydrologic-chemical multi-physics code (Hammond et al. 2011a; Lichtner and Hammond 2012) that is used to simulate coupled multi-physics processes affecting waste isolation in a repository system and transport of released radionuclides to the biosphere over time. Simulated processes include heat flow, fluid flow, waste dissolution, radionuclide release, radionuclide decay and ingrowth, precipitation and dissolution of secondary phases, and radionuclide transport. Dakota is an uncertainty sampling and propagation code (Adams et al. 2012; Adams et al. 2013). Dakota is used to propagate uncertainty in PFLOTRAN simulations and to analyze PFLOTRAN results to assess sensitivities of model processes and inputs. These two codes are described in more detail in Sections 2.2.1 and 2.2.2.

The flow of data and calculations through the components of GDSA Framework is illustrated in Figure 2-2. In a probabilistic simulation, Dakota generates stochastic input for each PA realization based on parameter uncertainty distributions and input parameter correlations. The sampled inputs are used by PFLOTRAN and its coupled process models to simulate source term release, EBS evolution, flow and transport through the EBS and NBS, and uptake in the biosphere. After the simulation, various software may be used to reduce and illustrate the output results of parameters and performance metrics. Dakota may also be used to evaluate the effects of parameter uncertainty on specific outputs.

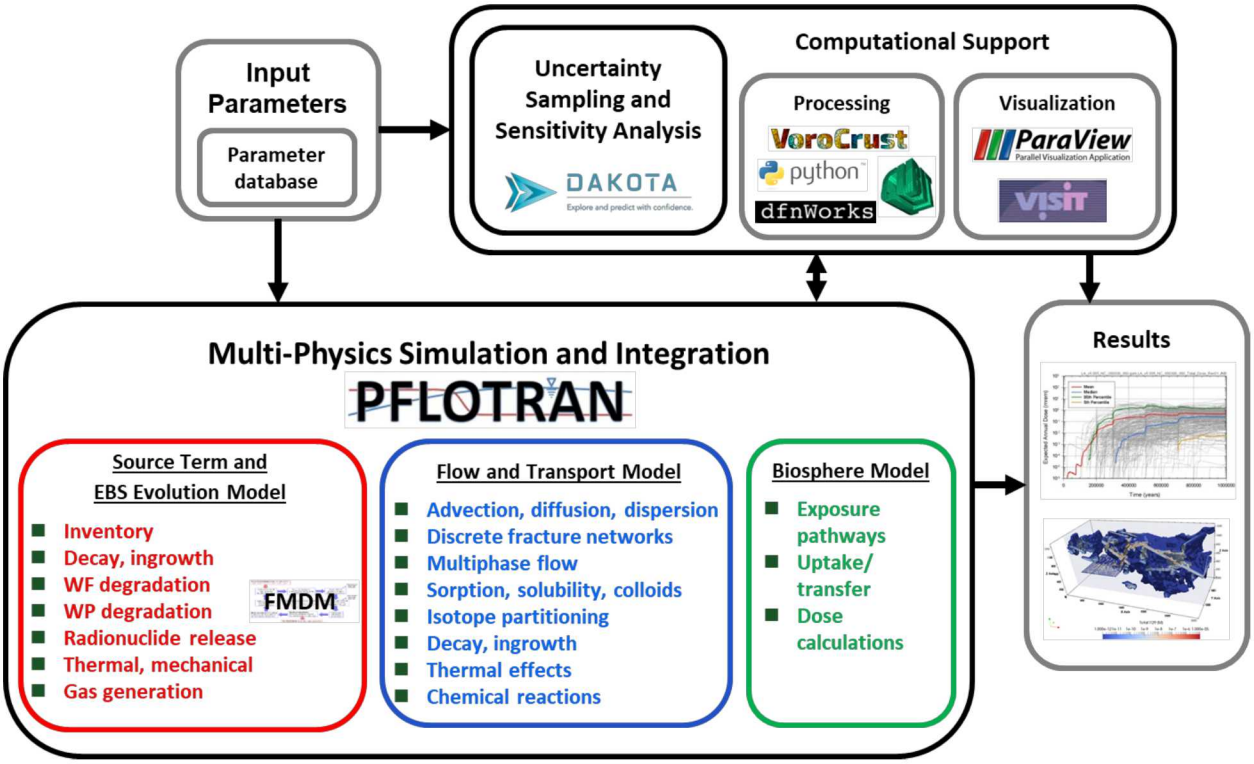

Figure 2-2 GDSA Framework structure

2.2.1 PFLOTRAN

PFLOTRAN (Hammond et al. 2011a; Lichtner and Hammond 2012) is an open source, reactive multi-phase flow and transport simulator designed to leverage massively-parallel high-performance computing to simulate subsurface earth system processes. PFLOTRAN has been employed on petascale leadership-class DOE computing resources (e.g., Jaguar [at Oak Ridge National Laboratory (ORNL)] and Franklin/Hopper [at Lawrence Berkeley National Laboratory (LBNL)]) to simulate THC processes at the Nevada Test Site (Mills et al. 2007), multi-phase CO_2-H_2O for carbon sequestration (Lu and Lichtner

2007), CO_2 leakage within shallow aquifers (Navarre-Sitchler et al. 2013), and uranium fate and transport at the Hanford 300 Area (Hammond et al. 2007, Hammond et al. 2008, Hammond and Lichtner 2010, Hammond et al. 2011b, Chen et al. 2012, Chen et al. 2013). PFLOTRAN is also under development for use in PA at the Waste Isolation Pilot Plant (WIPP).

PFLOTRAN solves the non-linear partial differential equations describing non-isothermal multi-phase flow, reactive transport, and geomechanics in porous media. Parallelization is achieved through domain decomposition using the Portable Extensible Toolkit for Scientific Computation (PETSc) (Balay et al. 2013). PETSc provides a flexible interface to data structures and solvers that facilitate the use of parallel computing. PFLOTRAN is written in Fortran 2003/2008 and leverages state of the art Fortran programming (i.e. Fortran classes, pointers to procedures, etc.) to support its object-oriented design. The code provides "factories" within which the developer can integrate a custom set of process models and time integrators for simulating surface and subsurface multi-physics processes. PFLOTRAN employs a single, unified framework for simulating multi-physics processes on both structured and unstructured grid discretizations (i.e. there is no duplication of the code that calculates multi-physics process model functions in support of structured and unstructured discretizations). The code requires a small, select set of third-party libraries (e.g., MPI, PETSc, BLAS/LAPACK, HDF5, Metis/Parmetis). Both the unified structured/unstructured framework and the limited number of third-party libraries greatly facilitate usability for the end user.

2.2.2 Dakota

The Dakota software toolkit is open source software developed and supported at Sandia National Laboratories (Adams et al. 2012, Adams et al. 2013). Dakota provides deterministic codes an extensible interface for propagating uncertainty into a set of realizations and for performing sensitivity analysis and optimization. GDSA Framework uses Dakota's sampling schemes, principally Latin Hypercube Sampling (LHS), to propagate input value uncertainty into probabilistic PFLOTRAN simulations. Dakota is also used in sensitivity analyses to analyze the effects of input value uncertainty on probabilistic GDSA Framework results.

3. GDSA FRAMEWORK DEVELOPMENT

GDSA Framework has become a powerful PA modeling tool. Over the years, important features and processes for repository PA have been added, several generic repository reference cases have been developed, and probabilistic tools have been established and exercised. These advances were aided by collaboration with other work packages of the Used Fuel Disposition (UFD) and SFWST Campaigns and by interactions with the international community. A summary of the major GDSA Framework developments over previous years is provided in Mariner et al. (2019).

In FY 2019 the status of the GDSA Framework modeling capability was evaluated against the 2012 Disposal Research Roadmap. Based on the results of that evaluation, much progress had been made, but more work was identified for certain areas (Sevougian et al. 2019a).

Guided by the results of the Roadmap exercise in FY 2019, the GDSA team continued to make advances in FY 2020. This chapter describes advances pertaining to general code development, meshing, uncertainty quantification, and workflow. In some cases these advances were used in the development of enhanced repository reference case simulations (LaForce et al. 2020; Swiler et al. 2020). Additional advances in uncertainty quantification and sensitivity analysis capabilities in FY 2020 are documented in Swiler et al. (2020).

3.1 PFLOTRAN Development

This year saw the fulfillment of a broad set of significant PFLOTRAN development objectives. These code development objectives included:

- Theory development and implementation of advanced linear and nonlinear solvers to overcome challenges inherent to simulating multiphase miscible flow and heat transport in porous media (Section 3.1.4). This significantly impacts reference cases where phase changes are likely, including the unsaturated alluvium reference case and reference cases subjected to large waste package thermal loading;
- Development of a general framework within GDSA Framework for dynamic K_D modeling for use in rapidly estimating adsorption in place of a slow surface complexation model (Section 3.1.5 and Appendix A);
- Preparatory work for advancing waste package degradation modeling (Section 3.1.6);
- Development of a Fortran code to speed up the numerical solution of the Fuel Matrix Degradation (FMD) process model and improve coupling with PFLOTRAN (Section 3.1.7 and Appendix B);
- Addition of geomechanical reduced-order models to simulate evolution of bentonite buffer and disturbed rock zone porosity and permeability during re-saturation in the shale repository reference case (Section 3.1.8);
- Functionality to adjust composite medium thermal conductivity as a function of both temperature and water saturation, as opposed to solely water saturation as was previously available. This functionality is important for reference cases involving high thermal loading from waste packages (Section 3.1.9);
- Capability to record metrics associated with specified regions of a simulation domain, referred to as “Aggregate Metrics” (Section 3.1.10). This capability is particularly useful for post-processing, statistical analysis, and uncertainty quantification.

In addition to these physical process model developments, a number of structural and organizational improvements to the GDSA Framework were achieved, which include:

- Implementation of an Agile framework for software development and interfacing between developers and users working on the GDSA project (Section 3.1.1);
- Copyright of PFLOTRAN and release of PFLOTRAN version 3.0 (Section 3.1.1);
- Development of a centralized Quality Assurance (QA) framework to be flexible for meeting the design specification needs of future work at higher levels in a graded QA system (Section 3.1.2);
- Design of a framework for coupling in new process models from GDSA collaborators across laboratories (Section 3.1.3).

These accomplishments advance the GDSA framework by offering higher fidelity modeling techniques, increasing code stability, asserting GDSA ownership over significant portions of PFLOTRAN, and offering a streamlined system for bug reporting and prioritization of future development tasks. Care has been taken to strengthen collaborations across laboratories and provide the infrastructure for future collaborations between labs and internationally.

3.1.1 Code Management

The PFLOTRAN code development infrastructure has been overhauled to allow for clearer linkage between project goals and development tasks, to promote transparency and allow for input to the code development process from GDSA users, and to offer structure for submitting and prioritizing bug reports or new capability requests. This has been achieved by adopting an Agile development framework through use of Atlassian's Jira© issue and project tracking software (Figure 3-1). Through this software, the GDSA PFLOTRAN development team is able to outline code development priorities that are categorized as either stories, bugs, or tasks. Stories generally encompass new process model implementation or extension of existing process models. Tasks are used for routine code maintenance work. Bugs describe instances where the code is not performing as expected or is crashing when running with a specific set of user inputs.

GDSA now uses a sprint structure for software project management internally, which entails working in "sprints" of two weeks intervals. Prior to the start of the sprint the developers identify a list of issues they plan to undertake, and those issues are placed on the sprint board (Figure 3-1). Through the duration of the sprint, issues are categorized as "To Do", "In Progress", "Under Review", or "Done". GDSA users have access to the site as well and can submit bug reports or requests for new capabilities at any time, with the expectation that the issues will be prioritized accordingly in advance of the following sprint. This results in a traceable structure for issue identification and a clear timeline for how/when issues will be re-prioritized. It also puts in place a clearer review process for approving new code development.

The public PFLOTRAN repository has also been modified to streamline the code change review and approval process. When a new pull request (a request to have new code developments added to the main code distribution) is submitted to the master branch of the code, a series of checks must be passed before the request can be approved. First, the development branch is automatically built on a continuous integration server, Travis CI. If the development branch passes all regression and unit tests, it passes the first check. If the development branch merged with the master branch passes all regression and unit tests, it passes the second check. Finally, one of the software administrators must approve of the pull request for it to pass the final check. Software administrators review each other's pull requests. This structure removes the need for administrators to manually pull and merge the new branch of the code and then run regression tests locally, which eliminates sources of error due to e.g. compiler differences between a local build and the CI server build or a failure to manually pull and test the new branch.

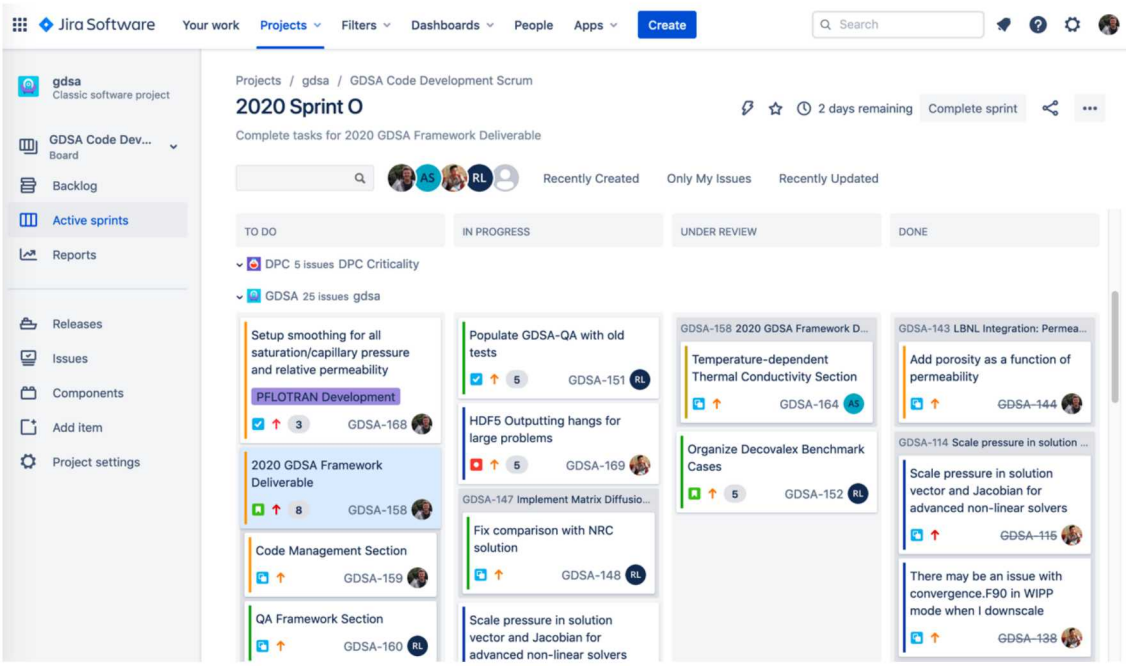

Figure 3-1 An example of a GDSA sprint using Jira issue and project tracking software

PFLOTRAN has undergone a major release, to version 3.0. As part of the latest release, Sandia has asserted copyright over GDSA-related process models that have been added to the code since the release of version 2.0. This establishes Sandia as the owner of these additions to the code, but it does not conflict with PFLOTRAN's LGPL (lesser general public license) open source licensing, which allows the source code to be freely downloaded from anywhere in the world. The release of PFLOTRAN v3.0 has also introduced a new versioning structure that the software will adhere to moving forward (Figure 3-2). Upon release, a maint/vX.X branch will be created. All bug fixes that affect the current release will be corrected in branches originating from the current maint/vX.X branch and merged or cherry-picked to the master branch. vX.X.X patches will be released at points in time when the number of bug fixes merit a patch release. All patches within a major release are expected to be backward compatible within that release. Any update that breaks backward compatibility will require a major version release (e.g., to version 4.0).

As part of the PFLOTRAN version 3.0 release, a significant refactor to the input deck structure has introduced the NUMERICAL_METHODS input block which encompasses NEWTON_SOLVER, LINEAR_SOLVER, and TIMESTEPPER blocks that contain keywords that were previously scattered in other blocks of the code, such as the OPTIONS sub-block of the PROCESS_MODEL block. This has resulted in better organizing of keywords and less cluttered input decks. PFLOTRAN v3.0 is incompatible with input decks designed for previous versions of the code, but a Python script named "refactor_numerical_methods.py" has been added to the repository to aid input deck migration to v3.0.

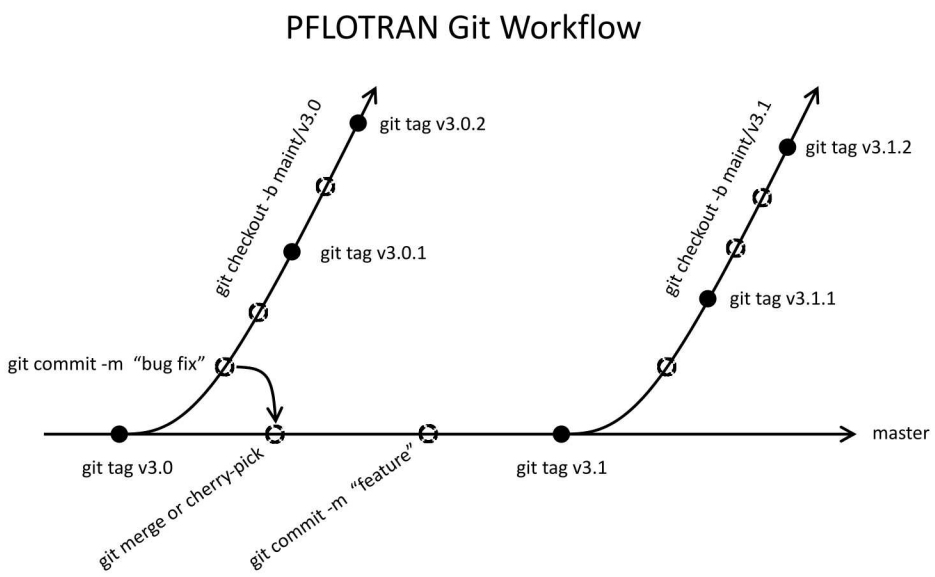

Figure 3-2 PFLOTRAN Git workflow after v3.0

3.1.2 Quality Assurance

Quality Assurance (QA) is vital to establish confidence in PFLOTRAN calculations and technical requirements. In code development, QA includes performing verification and validation (V&V) studies to compare simulation outputs with other simulators, analytical solutions, or experimental data. In complex scenarios analytical solutions may be too simple for comparison and other simulators must be used to validate results. Therefore, it is important for a V&V framework to be flexible to allow comparison with multiple simulators to ensure validation across the entire code. PFLOTRAN has been compared with several other simulators including TOUGH3 (Jung, 2017), CrunchTope (Steefel, 2009), and TDycore (https://github.com/TDycores-Project/TDycore).

A QA-toolbox was developed to perform code V&V for PFLOTRAN. The toolbox is a modular, Python-based V&V testing framework for vetting GDSA tests. The toolbox is therefore flexible to accommodate addition of new tests, and it is written in a common programming language with established data visualization and analysis libraries. The testing framework installs multiple simulators and suites of test problems to compare PFLOTRAN solutions against existing simulators, analytical solutions, and/or datasets. The toolbox is designed to be completely automated and user friendly when adding new tests or simulators to compare against. Simulator templates use Python wrappers to read simulator output and plot solutions and error metrics. The most current version of the toolbox can be found at https://github.com/TDycores-Project/qa-toolbox.

The test suite is designed to run automatically in the cloud. Simulators and tests are installed on a virtual machine and the QA-toolbox is called to run and plot installed tests and simulators. Once complete, the V&V testing framework documents results in reStructuredText, generates HTML using Sphinx (http://www.sphinx-doc.org), and pushes the HTML to a website.

QA documentation is automatically created using the input parameters specified by the user and the accompanying results calculated from the QA-toolbox. This includes a results summary, problem description, detailed results, and links to download the input decks that were used to run the simulations. The results summary includes output values, simulation times, and locations of the maximum and average errors within the model domain with links to more detailed results at these locations. Detailed results include a table of the average and maximum errors, their associated locations or times, and plots of the

solution and error for each point in time or space the user specifies. The documentation will also automatically group together tests in a hierarchical structure as requested by the user.

The advantage of the new QA-toolbox compared to the old test suite (Frederick, 2018) is that more complex models are now allowable and multiple simulators can be added using new Python wrappers. Documentation of results generated through the new test suite is also more flexible because documentation is automatically created by the Python code. The use of templates allows the user to enter in specific variables and labels in place of hard-coding simulation parameters and documentation. For example, the user can decide to perform mesh convergence testing by having the toolbox shrink the grid size until a certain error threshold has been met. Tests can also be created in a separate repository from the toolbox to allow for better organization. Thorough documentation has been created to allow other code developers to easily use the new toolbox.

The QA-toolbox has built-in regression testing that is implemented before tests are run. Regression testing verifies the build of the toolbox and the output of the documentation. Results of the regression test suite are printed to the online documentation after running the tests.

To provide a proof of concept for the QA-toolbox, PFLOTRAN was compared to the TDycore model, a code being developed under DOE's Scientific Discovery through Advanced Computing (SciDAC) program (https://github.com/TDycores-Project/TDycore). A 2D, steady state, saturated groundwater flow benchmark case was chosen to compare PFLOTRAN and TDycore. The problem domain consists of a unit square divided into quadrants with linear pressure gradients at the boundaries. Figure 3-3 shows the problem domain used for the benchmark case and Figure 3-4 shows an example of the output HTML documentation for the detailed results. Overall error metrics are shown in the table in Figure 3-4, and the solutions are plotted as contoured lines and fill. Absolute and relative error are also plotted over the entire domain.

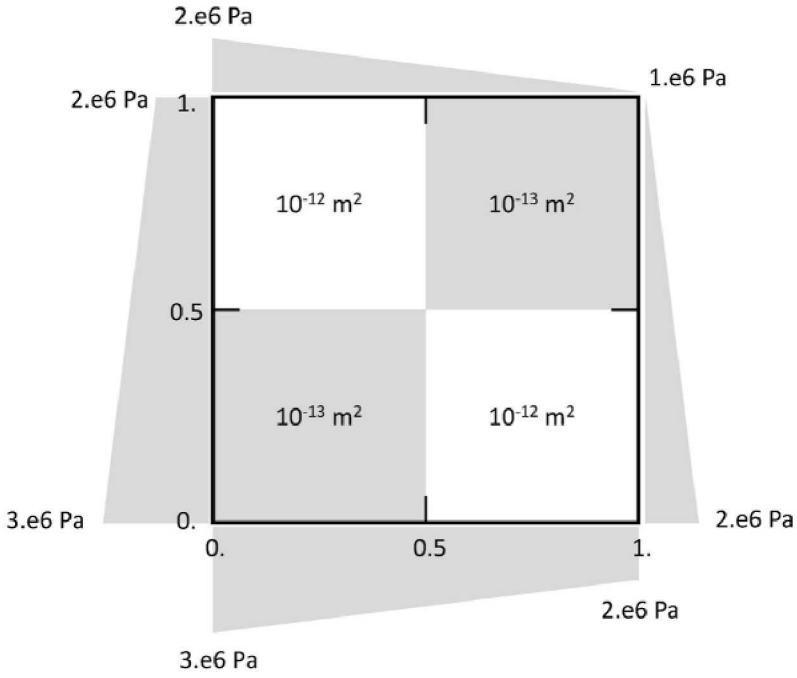

Figure 3-3 Problem domain for the PFLOTRAN and TDycore benchmark case

Detailed Results

Scenario 1 - Time Slice

Comparison of Liquid Pressure at steady state for Scenario 1 - Time Slice: tdycore vs pflotran

```
Average Absolute Error = 1582.2024844264765
Average Relative Error = 0.08020896112895463 %
Maximum Absolute Error = 6346.666977404617
Maximum Relative Error = 0.36442093831914657 %
X Location of Maximum Absolute Error = 0.495 m
Y Location of Maximum Absolute Error = 0.185 m
X Location of Maximum Relative Error = 0.975 m
Y Location of Maximum Relative Error = 0.505 m
```

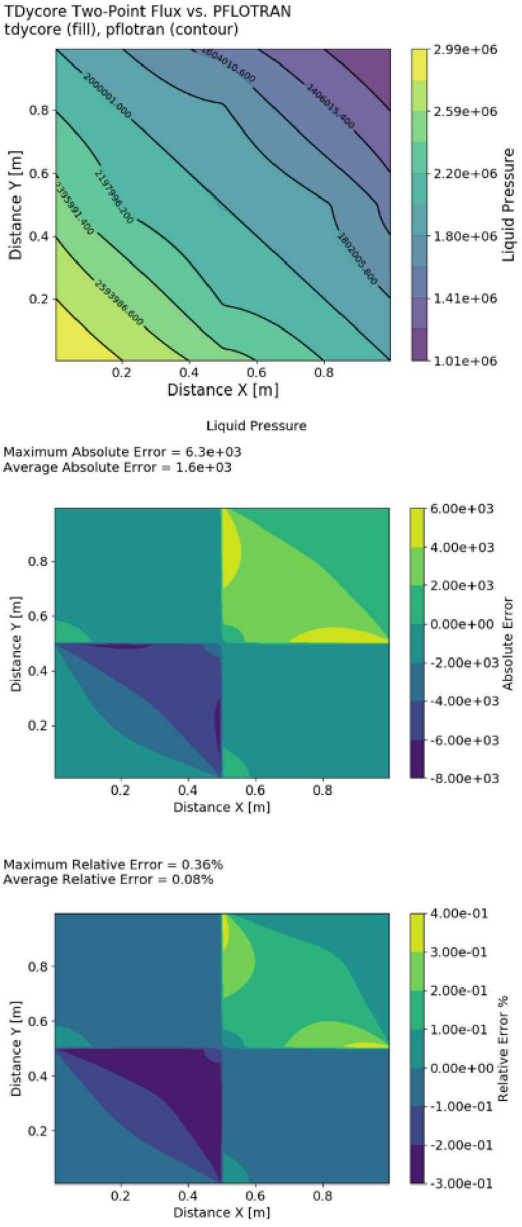

Figure 3-4 Example output of documentation from the QA-toolbox for the TDycore and PFLOTRAN benchmark case

3.1.3 Process Model Coupling

To facilitate a more streamlined process of integrating process models into the PFLOTRAN code while preserving the look and feel of PFLOTRAN as a unified simulator, a general workflow was developed for approaching process model coupling. This workflow is specifically designed to be worked through by users and developers when deciding how to design and implement new process models in the code. It is expected that in the future, users and developers will interface through GDSA's Jira issue and project tracking software when applying this workflow to clearly plan out code development targets that meet the goals of process modelers.

3.1.3.1 Type of Model Implementation

The first, preliminary stage of process model coupling requires identifying the style of model implementation that will be pursued. Type of model implementation can fall into one of three categories: direct process implementation, coupled process model, and coupled surrogate model.

Direct process implementation. Pursuing direct process implementation is the most rigorous option from the standpoint of PFLOTRAN development. It involves description of all relevant equations and constitutive relationships by the process modelers for the code developers to implement. This can take the form of physics-derived equations or reduced-order models. This option will build the model in as a standard PFLOTRAN feature or option, and as such it will be supported with successive versioning (but not guaranteed to be maintained/compatible with future code capabilities). Direct process implementation may be computationally demanding, so it might not be the best option if the process can be emulated by a separate surrogate model.

Coupled process model. The coupled process model approach is to design a standalone process model that can be called by PFLOTRAN. This approach works best for process models that are loosely coupled or otherwise have no feedback on processes simulated by PFLOTRAN (e.g., a biosphere model). Typically, the coupling is one-way from PFLOTRAN to the process model, so that PFLOTRAN runtime is not significantly affected. Two-way coupling can be achieved, but this can be a more computationally demanding approach; a separate surrogate model might be a better approach in this instance.

Coupled surrogate model. The coupled surrogate model approach involves creating a standalone process model emulator that can be called by PFLOTRAN. This approach is most useful when the process model is too computationally intensive to execute as often as may be desired. The surrogate model can instead be trained by a standalone process model or dataset and feed results to PFLOTRAN. This approach is built for speed, but attention must be paid to ensure its accuracy. Accuracy must be quantified and, if possible, traceable in a simulation. Surrogate models tend to not have trouble converging if they are not simulating systems of coupled nonlinear partial differential equation (PDEs), so they can sample a broad range of parameter space and their results can be readily available to PA simulations. Surrogates may be parametric (e.g., polynomial regression, neural network) or non-parametric (e.g., k-Nearest Neighbors regression).

3.1.3.2 Steps for Implementation

To implement a new model, the process modeler will first pre-qualify the model for implementation by outlining specific model requirements and working with a PFLOTRAN developer to identify the best model implementation approach. The process modeler will then submit a request for implementation. This will formally be achieved through PFLOTRAN's issue and project tracker, which is currently Atlassian's Jira software. In this request, the process modeler will provide a brief summary of the model and general ideas for how it will be implemented, provide an example simulation of the process model and plots of outputs, and address all model input requirements (Section 3.1.1).

Once a request is received, the PFLOTRAN developers will evaluate the request. This will involve iterating with the process modelers to discuss how development would meet the modelers' needs while preserving computational efficiency and optimizing time spent implementing the model. Once the developers understand the process modelers' needs and communicate to the modelers what resources would likely be required to achieve process model coupling (e.g., time, expertise), resources will be allocated and prioritized.

After acceptance and resource allocation, it is expected that until the process model is fully implemented/coupled to PFLOTRAN, recurring meetings will take place between developers and modelers to communicate project status. When unforeseen issues arise, or if expanded capabilities are desired, future work can be planned accordingly.

3.1.3.3 Model Requirements for Implementation in PFLOTRAN

Before implementation in PFLOTRAN, the model must first be approved by applicable work package managers. To be approved, the process model must be demonstrated to align with work package objectives and have sufficient priority relative to other items in the work package scope given available resources. Additionally, the model must be sufficiently documented, supported, and defensible. A few key questions to consider include:

- Do we expect the model to have significant effects on important repository performance metrics or provide important answers to key questions?
- Are all model assumptions affecting the validity of the model and the valid ranges of input values acceptable for the intended use?
- Is there a better approach with more defensible assumptions that covers the same or larger range of applicability?

Before implementation, standalone execution of the process model must be shown to produce expected results for the expected ranges of application. This qualification can take the form of comparison to laboratory data, concurrence with analytical solutions, or consistency with other benchmarks of an identical process. It should be expected that this qualification will be independently reviewed and approved. Furthermore, qualification should be performed over all applicable input ranges, and all regions of poor model convergence and/or instability must be identified. Qualification will involve identifying all model assumptions for conceptual model consistency, documenting applicable spatiotemporal convergence studies, providing plots showing input/output relationships, and developing a plan for filtering out specific model iterations that provide erroneous or highly suspect results with appropriate justification for doing so. It is expected that through this process the modeler will provide a table of all input parameters, their ranges of validity for the model, and their expected ranges of application to the PFLOTRAN developers.

In addition, it is expected that the following couplings will be identified prior to implementation:

Inputs

- Inputs to define in the PFLOTRAN input deck for the new process model
    - Fixed or sampled process model input parameters (e.g., solver options, boundary conditions, material properties)
    - Initial values (e.g., initial concentrations)
- Inputs directly provided by PFLOTRAN when the coupled model is called (e.g., temperature, time, local species concentrations)

- Time: If called during a large PFLOTRAN time step, can the model directly produce results for that moment in time or does it perform its own time-stepping?
- State variables: What existing capability is the process model intending to leverage? For example, is temperature dependence required? This would limit scope to non-isothermal flow modes.

Database Files

- Text or binary files that the model uses to perform its calculations (e.g., response surfaces, thermodynamic data)

Outputs

- Outputs to return to PFLOTRAN
  - Certain outputs may be used in internal PFLOTRAN calculations
  - Others may simply be stored by PFLOTRAN and used as input to the implemented model at the next call
- Outputs of the model to include in a model-specific output file

3.1.3.4 Software Requirements

The PFLOTRAN repository consists of Fortran 90 simulator source code files and Python libraries for post-processing. It is expected that direct process implementation will be pursued in Fortran and be consistent with PFLOTRAN's style guide. Coupling with external process models will require identifying options for coding languages and any required external libraries so that any potential interface issues can be addressed up front. PFLOTRAN developers will provide recommendations for available options to support database reading/writing. It is expected that process models directly implemented in PFLOTRAN will output in PFLOTRAN-consistent formats.

3.1.4 Convergence Improvements

As a part of convergence improvement goals, more innovative solver options have been explored this year. The innovative solvers can largely reduce computation time by applying more mathematically and algorithmically optimized methods for solving coupled mass and energy transport in porous media equations, whether they describe single-phase, multi-phase, immiscible, miscible, isothermal or non-isothermal flow.

This year an innovative nonlinear solver, Newton Trust Region Dogleg-Cauchy (NTRDC), has been developed and implemented in PETSc and PFLOTRAN. A type of trust region method was most recently introduced by Li and Tchelepi in 2015 (Li and Tchelepi 2015). They applied what is called the "Numerical Trust Region" method to the discrete transport (mass conservation) equation for immiscible, incompressible, two-phase flow in porous media in the presence of viscous and buoyancy forces. The method was very robust even with large timesteps, and it was shown to improve computation time by up to 50%. This application was very specific to the model, but NTRDC implementation is more generally applicable to many different flow modes in PFLOTRAN and possibly for transport. The solver now is under the testing and debugging process before beta release. This report presents some preliminary results.

3.1.4.1 Newton Trust Region Dogleg-Cauchy (NTRDC)

On Figure 3-5, the goal of the nonlinear algorithm is to find one minimum (potentially of a set of local minima) in the contour plot from the "Start" position. When solving a coupled system of PDEs, the contour plot would describe the residual of a given PDE, which must be minimized to declare

mass/energy conservation and can be a function of multiple primary independent variables. The algorithm goes through multiple iterations to get to one of the minima, and the algorithm should be heading towards one of the minima at every iteration. As a default, the basic PFLOTRAN Newton-Raphson method (Newton for short, NT) uses the Jacobian to determine both the search direction and step size for the solution update at each iteration, referred to here as a combined "step and direction" (S&D). This method is the starting point from which more advanced techniques are being developed.

From Figure 3-5, the original Newton (NT) nonlinear solver takes its first iteration at the end of the thinner white line that overshoots, and it will calculate a new S&D on the next iteration from the end of the thinner white line. Newton Trust Region Dogleg-Cauchy (NTRDC), on the other hand, gets to one of the minima in one iteration (from "Start" to "End" as seen on Figure 3-5). The algorithm recognizes that the original NT S&D produces a step beyond a computed maximum step-size, which was determined from knowing that there was a point somewhere in a circular "trust region" associated with a lower contour value than where the original NT algorithm ended up. Therefore, it reduces the trust region size to where it reaches a lower contour value than NT S&D.

Another series of statements realizes that an application of Cauchy's (C) steepest descent S&D may improve the nonlinear solution update, but in this example, Cauchy (a white line labeled "Cauchy S & D") did not minimize the solution more than truncated NT by trust region (a thicker white line towards "Newton Step & Direction" label). Lastly, the combination of the two S&D's in a quadratically calculated ratio, τ, is examined (a combination of red-line (NT) and yellow-line (C)). The algorithm recognizes that the combination of the two methods with the ratio, τ, reaches the smallest residual; thus, it chooses the combo solution which happens to reach the "End" minimum solution in just *one iteration*. If we had used the original NT in this case, the algorithm would have ended up in *a saddle point* between the two minima without a minimum solution. When this occurs, PFLOTRAN cuts the time step which in effect initializes the "Start" point closer to "End" point, which is easier to solve. If we had used Cauchy only for this case, it would have gotten to the minimum point, but it would have taken *17 iterations*. This method is pending for a journal publication and the details are therefore withheld from this report.

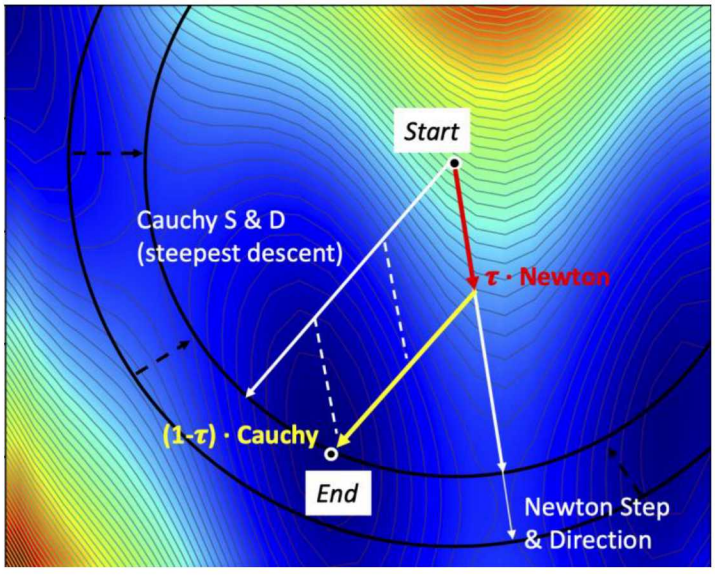

Figure 3-5 A demonstration of Newton Trust Region method. The algorithm corrects the appropriate Newton step-and-direction by reducing the trust region and adds Cauchy step-and-direction if the solution update can be improved further in the same iteration.

The NTRDC algorithm is being developed for the GDSA project to resolve many strong nonlinearities that occur when using PFLOTRAN's GENERAL mode (non-isothermal miscible multi-phase flow) during state changes. However, the algorithm can also be applied when using Richards mode (single-phase flow) and PFLOTRAN's isothermal immiscible multi-phase flow (WIPP-FLOW) mode. The sequence of development was to apply the NTRDC algorithm from the easiest to hardest governing equations; this report presents below the final results for both single-phase flow and isothermal immiscible multi-phase flow, and a preliminary result for non-isothermal miscible flow which is still in the testing and debugging phase of development.

3.1.4.2 NTRDC single phase performance: Drilling intrusion in a generic salt repository

The Richards flow equation solves conservation of water mass using either pressure or saturation as primary independent variables (Equations below) and then calculates the other via a capillary pressure function. Therefore, there is one unknown quantity, e.g. pressure, to solve per each grid cell in this model:

$$\frac{\partial}{\partial t}(\phi s \eta) + \nabla \cdot (\eta \vec{q}) = 0 \tag{1}$$

$$\vec{q} = -\frac{k k_r(s)}{\mu}(\nabla p - \rho \vec{g}). \tag{2}$$

The human borehole intrusion model simulates a hypothetical event where a waste room in bedded salt rock is penetrated by a human drilling activity 100 years after the disposal of wastes. This model uses the Richards flow equation to simulate the pressure propagation and flow before and after the event. The model has 68,894 structured grid cells hence 68,894 unknowns; the intrusion event occurs at 100 years by changing material properties in the domain, and then additional self-healing/closing transition at 200 and 1200 years after the intrusion. These events are clearly visible on the pressure line plot of Figure 3-6. The center of the domain is the waste room pressurized at year 100 by the borehole connecting the deep lithostatic or hydrostatic formation (the very bottom of the domain) to the waste room, driving excess pressurized brine up the borehole to the room. As the borehole sealant degrades, the pressure in the waste room decreases, which is simulated with instant changes in permeability in year 300 and 1300. There are four test cases: borehole intrusion at year 100 for (1) lithostatic pressure (15 MPa) in the deep formation and for (2) hydrostatic pressure (12 MPa); borehole intrusion at year 350 for (3) lithostatic pressure (15 MPa) in the deep formation and for (4) hydrostatic pressure (12 MPa).

Nonlinearity response is significant in these simulations because of sudden material changes that occur during the human borehole intrusion event. As shown in Table 3-1, NTRDC outperformed NT by up to a factor of 38 in terms of computation time, reduced the number of nonlinear iterations by a factor of 17, and reduced the number of linear iterations by a factor of 101. The final solutions are verified to each other to make sure that NTRDC is producing the consistent results.

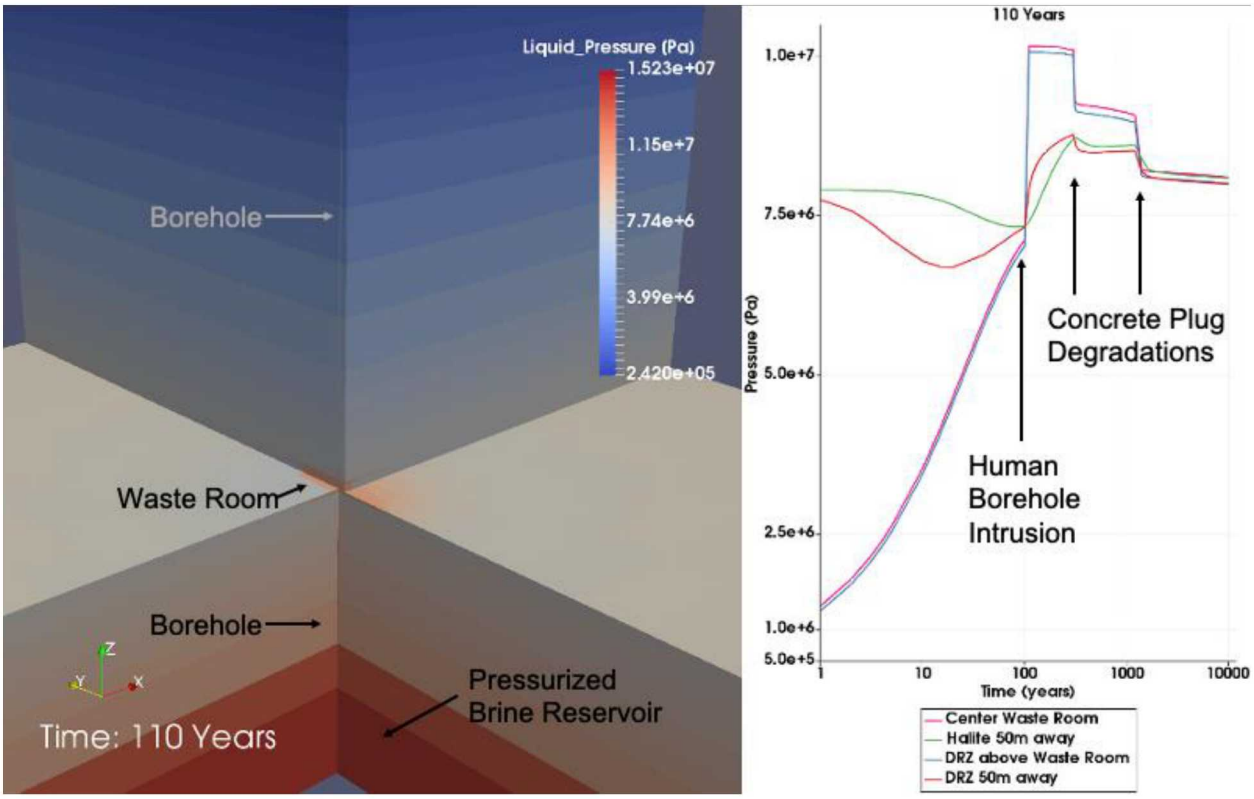

Figure 3-6 **Illustrates the hypothetical scenario where an excavated room is penetrated at 100 years after repository closure. The right figure shows the spike in pressure due to the lithostatic pressure from beneath the excavated room.**

Table 3-1 **Performance of NTRDC compared to NT**

3D Model Test Cases (Richards Flow)	Compute Time [Minutes]	Nonlinear Iterations	Linear Iterations
100-year intrusion lithostatic			
Newton's method (NT)	68.6	8019	3026014
Trust Region Dogleg (NTRDC)	1.77	482	29975
100-year intrusion hydrostatic			
NT	32.2	1931	1363055
NTRDC	1.77	412	31386
350-year intrusion lithostatic			
NT	75.7	3457	3919579
NTRDC	3.42	621	60134
350-year intrusion hydrostatic			
NT	25.6	1812	1191325
NTRDC	2.85	510	51534

3.1.4.3 NTRDC isothermal immiscible performance

The multiphase isothermal immiscible flow mode in PFLOTRAN has no energy balance (isothermal) in the system of governing equations; moreover, liquid and gas have interfaces across which pressure discontinuities exist (immiscible). The difference between the liquid and gas pressure is termed capillary pressure. Therefore, the immiscible model assumes that all phases exist in all simulation grid cells. PFLOTRAN uses the generalized flux form of Darcy's law. Each phase is denoted by subscripts g for gas and w for water (liquid). The governing equations are

$$\frac{\partial}{\partial t}(\phi \rho_w s_w) = \nabla \cdot \left[\frac{\rho_w k k_{rw}}{\mu_w} (\nabla p_w - \rho_w g \hat{z}) \right] + Q_w, \tag{3}$$

$$\frac{\partial}{\partial t}(\phi \rho_g s_g) = \nabla \cdot \left[\frac{\rho_g k k_{rg}}{\mu_g} (\nabla p_g - \rho_g g \hat{z}) \right] + Q_g. \tag{4}$$

In order to couple these two mass balance equations, there are saturation and capillary pressure constraints to complete the set of constitutive relations:

$$s_g + s_w = 1, \tag{5}$$

$$p_c = p_g - p_w. \tag{6}$$

The test simulation domain spans 30 km from south to north and 28 km from west to east as shown in the regularized depiction in Figure 3-7. Neighboring grid cells can have extreme contrasts in porosity, permeability, and volume. The domain discretization is created by using Cubit (cubit.sandia.gov), a mesh generation toolkit developed by Sandia National Labs. Cubit provides a pave algorithm to expand the unstructured grid cell sizes outward in x- and y-directions; the model is a structured grid in the z-direction. There are two levels of expansion from the repository features to the domain edges as shown in Figure 3-8. The domain has a total of 460,020 grid cells or 920,040 unknowns in the solution update vector.

The Newton trust region (NTR) method is also a new algorithm implemented during NTRDC development as a subset of NTRDC where it only considers the Newton step and direction and is truncated with the trust region. Cauchy step and direction are not considered in the NTR method. Both advanced methods, NTR and NTRDC, generally performed 6% to 37% faster than the Newton method in the numerical experiments (a few shown on Figure 3-9).

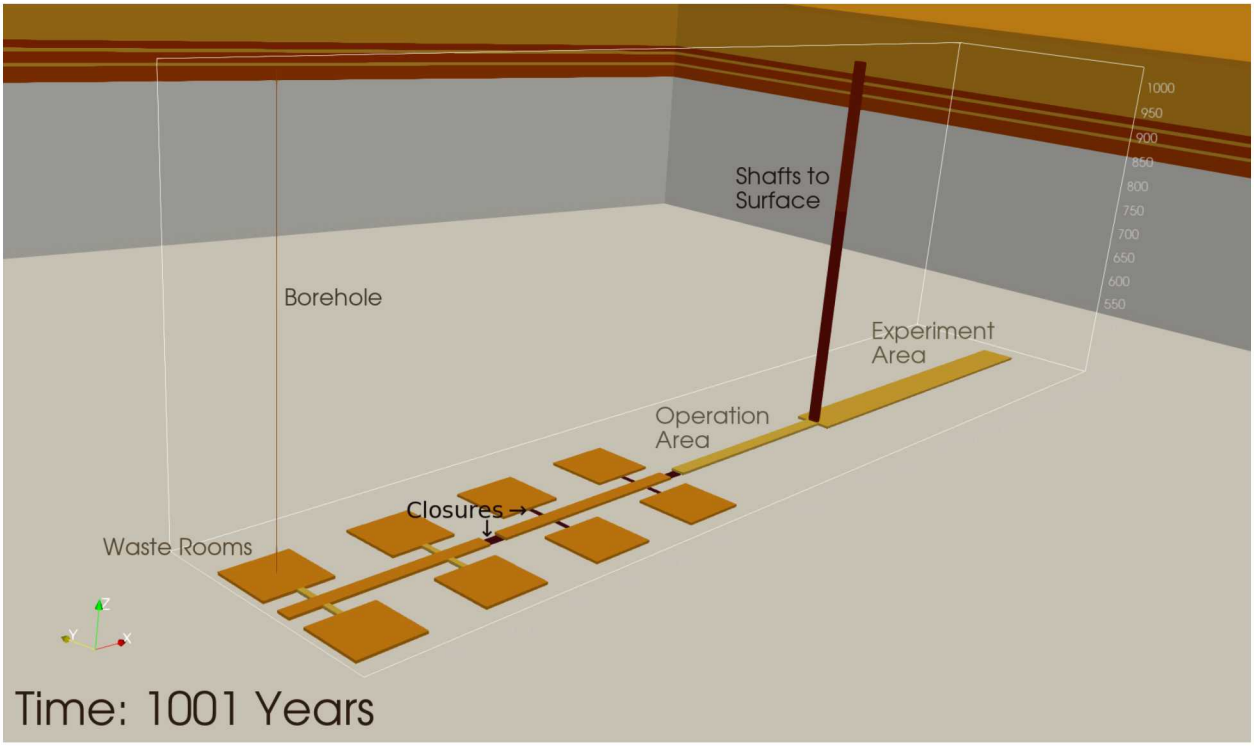

Figure 3-7 A structure view of the simulation domain

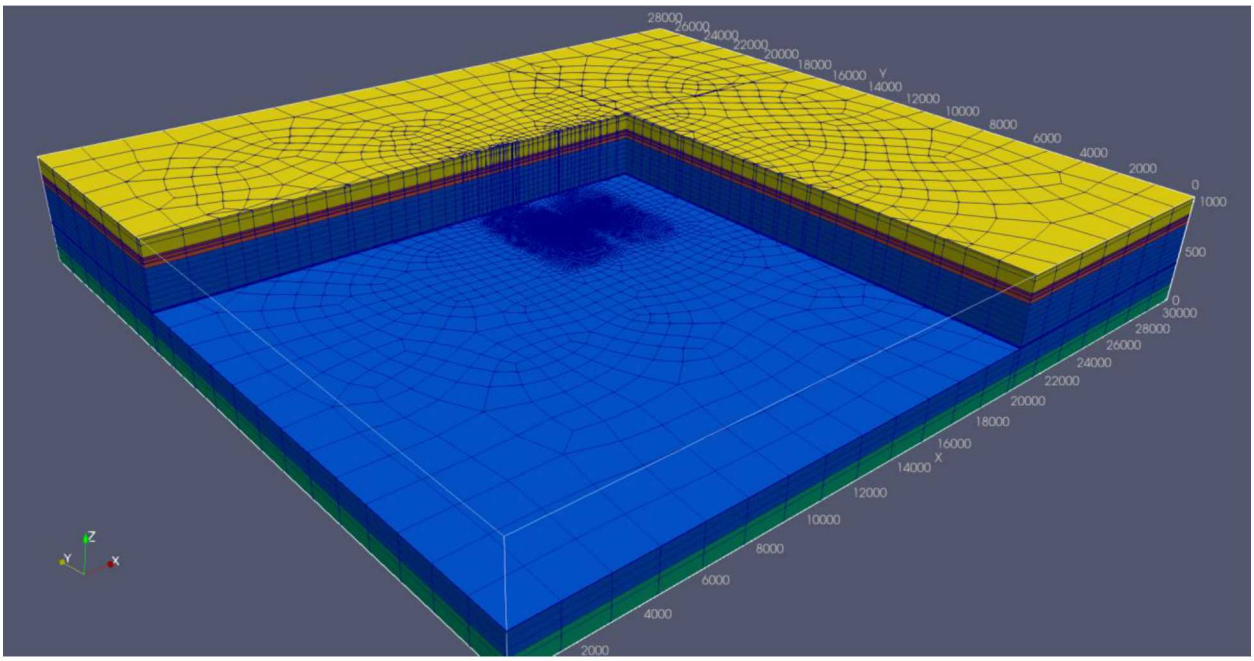

Figure 3-8 A discretization of the simulation domain. The domain has 460,020 grid cells. The cutaway in the image is used to illustrate vertical simulation resolution in the vicinity of the repository.

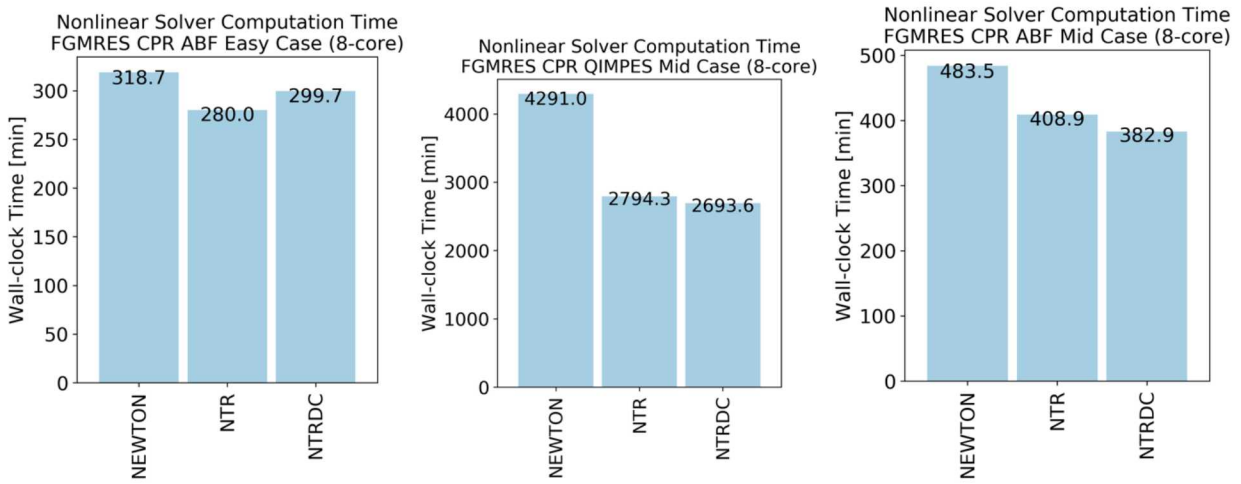

Figure 3-9 6 to 37% shorter computation time with NTR and NTRDC methods as compared to NEWTON

Before going over the scalability analysis of NTR and NTRDC, the physical architecture of Skybridge cluster must be understood properly. Sandia's Skybridge cluster nodes have Intel Xeon E5-2670 2.60 GHz processors, 20MB Cache. Each processor has 2 sockets, 4 cores per socket, and 2 threads per core that totals to 16 central processing units (CPUs). However, when all 16 CPUs are used, there can be a bottleneck in accessing cache and memory for each. Figure 3-10 illustrates the efficiency of each processor when it is relieved from the bottleneck. All of the cases use 16 CPUs in total, but each case uses a different number of nodes and different number of cores per node. When one uses 1 node and all 16 cores, this simulation takes close to 250 minutes, but when one uses 2 cores per node and 8 nodes, the simulation takes about 170 minutes. The one-node simulation took 47% longer to finish even though the same number of CPUs were involved. Of course, there is communication time loss when using MPI as seen between (8 n, 2 cpn) case and (16 n, 1 cpn) case, but that seems to be minimal compared to the bottleneck to cache and memory within the node.

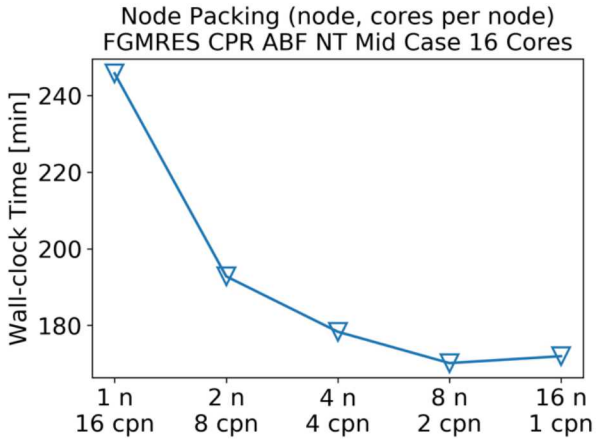

Figure 3-10 When a simulation uses all the resources available in a compute node, there is a clear decrease in efficiency

The strong scaling follows the trend of ideal scaling for NT and NTR in Figure 3-11. One thing to note is that the NTR algorithm requires two additional matrix-vector multiplications compared to Newton and NTRDC also requires two matrix-vector multiplications and a third one if Cauchy direction calculation is

needed. This may be why the 8-core example is performing better than 16 cores (more cache and memory access needed due to node packing); they lose scalability a bit compared to Newton for 16 and 32 cores, but they re-gain the scalability on 64 cores, because each core is loaded more lightly compared to 16 and 32 cores. When one unpacks the nodes and uses 4 cores per node, the scalability improves dramatically. The default linear (BCGS-ILU) and nonlinear solver (NT) for PFLOTRAN showed parallel inconsistency: 32 cores performed better than 64 cores in this particular test case.

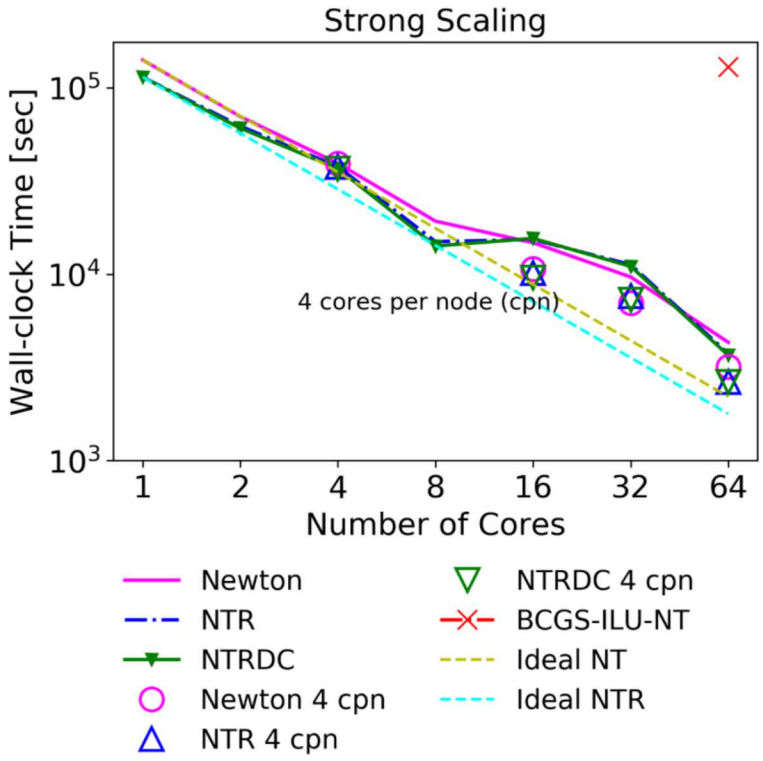

Figure 3-11 Strong scaling of Newton, NTR, and NTRDC with FGMRES-CPR-ABF solver-preconditioner combination. It follows the trend of ideal strong scaling for all methods, and it follows even closer when node packing defect is considered.

3.1.4.4 NTRDC non-isothermal miscible performance

The GENERAL mode model involves a finite volume grid representing heat generating nuclear waste package along with miscible liquid and gas phases which diffuse into each other. There are three unknowns per grid cell in the system of three equations; however, unknown primary variables change spatially and temporally depending on which phases are present for the given pressure and temperature conditions for each grid cell (the primary variable switch method). The two mass balance equations are

$$\frac{\partial}{\partial t}\phi(s_l\rho_l x_w^l + s_g\rho_g x_w^g) + \nabla\cdot(\vec{q}_l\rho_l x_w^l + \vec{q}_g\rho_g x_w^g - \phi s_l D_l\rho_l\nabla x_w^l - \phi s_g D_g\rho_g\nabla x_w^g) = Q_w \quad (7)$$

$$\frac{\partial}{\partial t}\phi(s_l\rho_l x_a^l + s_g\rho_g x_a^g) + \nabla\cdot(\vec{q}_l\rho_l x_a^l + \vec{q}_g\rho_g x_a^g - \phi s_l D_l\rho_l\nabla x_a^l - \phi s_g D_g\rho_g\nabla x_a^g) = Q_a. \quad (8)$$

The energy conservation equation couples saturation and pressure of each phase to internal energy and enthalpy of each phase, and temperature. The equation is written in form

$$\sum_{\alpha=l,g}\left[\frac{\partial}{\partial t}(\phi s_\alpha \rho_\alpha U_\alpha)+\nabla\cdot(\vec{q_\alpha}\rho_\alpha H_\alpha)\right]+\frac{\partial}{\partial t}\left(((1-\phi)\rho_{rock}C_pT)-\nabla\cdot(\kappa\nabla T)\right)=Q, \quad (9)$$

The internal energy of each phase can be determined by the relationship

$$U_\alpha = H_\alpha - \frac{p_\alpha}{\rho_\alpha}. \quad (10)$$

The preliminary results model is a 3x3 cube model with a heating grid cell in the middle (Figure 3-12). All boundary conditions are no-flow except east-west boundaries, which are set by Dirichlet boundary conditions that are equal to the initial condition. This model experiences all three states: liquid state, two-phase state, and gas state. Initially, all cells are in the liquid state, but the center cell starts to heat up, causing the cells to change state to two-phase (water boils). Further heating causes the center cell to become gas-phase. Later on, the heater turns off and the whole domain re-saturates back to the initial condition caused by east-west boundary condition. The test case may look simple, but it is numerically challenging because of all the nonlinearity associated with state changes.

The model is solved with NT and NTRDC using a Direct linear solver for a comparison. There is about a 13% reduction in the number of nonlinear iterations. The development of this capability in non-isothermal miscible is yet completely tested and debugged yet. The final results will be out in the next report.

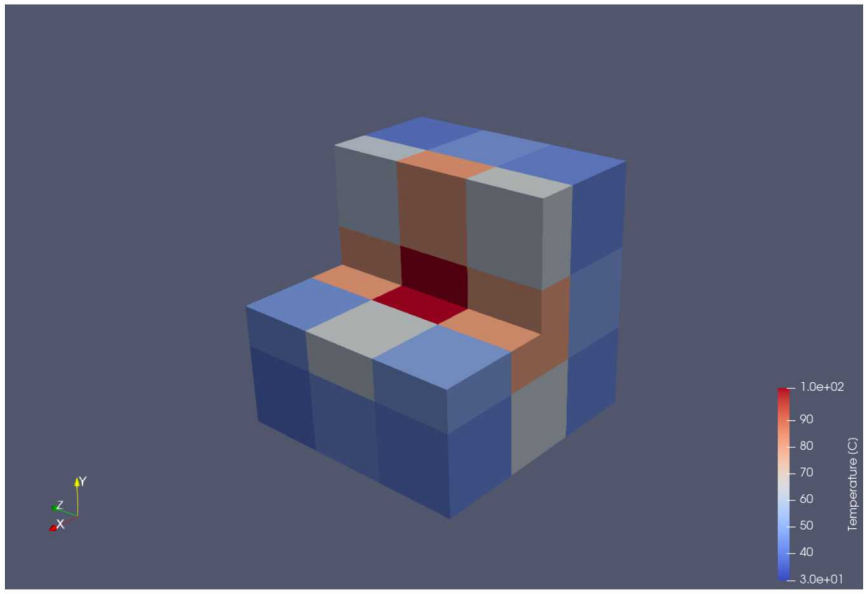

Figure 3-12 Cube model with a heating grid cell in the middle

Table 3-2 NTRDC performed faster with less nonlinear iteration counts.

Cube Model	Compute Time [s]	Nonlinear Iterations	Linear Iterations
Newton (NT)	1.2239	539	539
Trusted Region Dogleg (NTRDC)	1.0848	401	403

3.1.5 Dynamic K_D Adsorption Modeling

Adsorption of radionuclides to mineral surfaces can greatly affect radionuclide migration. The extent of adsorption depends on many factors including temperature, ionic strength, types and concentrations of mineral surface sorption sites, pH, and concentrations of aqueous solutes. Surface complexation models can be used to account for important parameters affecting adsorption to geologic media, but these models can be computationally demanding in a transport simulation, especially for a large number of grid cells. Consequently, instead of surface complexation modeling, a simple K_D approach is typically used. For constant K_D models, constant ratios of adsorbed to aqueous concentrations are selected from probability distributions for geologic materials for each realization.

The use of a surface complexation model can be emulated using a reduced-order, dynamic K_D approach that runs many times faster. To study this approach, a dynamic K_D model was developed for PFLOTRAN and tested on U(VI) (hexavalent uranium) plume simulations at the Hanford Site in southeastern Washington state. The dynamic K_D model was calibrated to maximum and minimum ratios of adsorbed to aqueous U(VI) based on batch geochemistry generated from the surface complexation model and concentrations from representative groundwater and river water at the site. The study compared both solution accuracy and speedup enabled by the dynamic K_D model in combination with HPC and operator splitting.

The results, documented in detail in Appendix A, indicate that the reduced-order dynamic K_D model is much faster than surface complexation models and is highly accurate. Figure 3-13 shows an example of the relative accuracy of the dynamic K_D model compared to the constant K_D model. A computational speedup factor of approximately 10 to 20 can be achieved over surface complexation models depending on whether a flow process model is included in the simulation. In addition, parallel processing and the decoupling of transport and reaction through operator splitting can further enhance simulator performance by 100-fold with speedup factors ranging from approximately 800 to 2300, again, depending on whether a flow process model is included in the simulation. The full study is documented in Appendix A.

This work shows that higher fidelity adsorption process modeling using a surface complexation model has a major effect on predicted U(VI) migration at the Hanford site compared to the constant K_D model. It also shows that the higher fidelity of the surface complexation model can be largely captured by a dynamic K_D model that runs many times faster than the surface complexation model. For these reasons, building a general framework within GDSA Framework for dynamic K_D modeling will likely be pursued further.

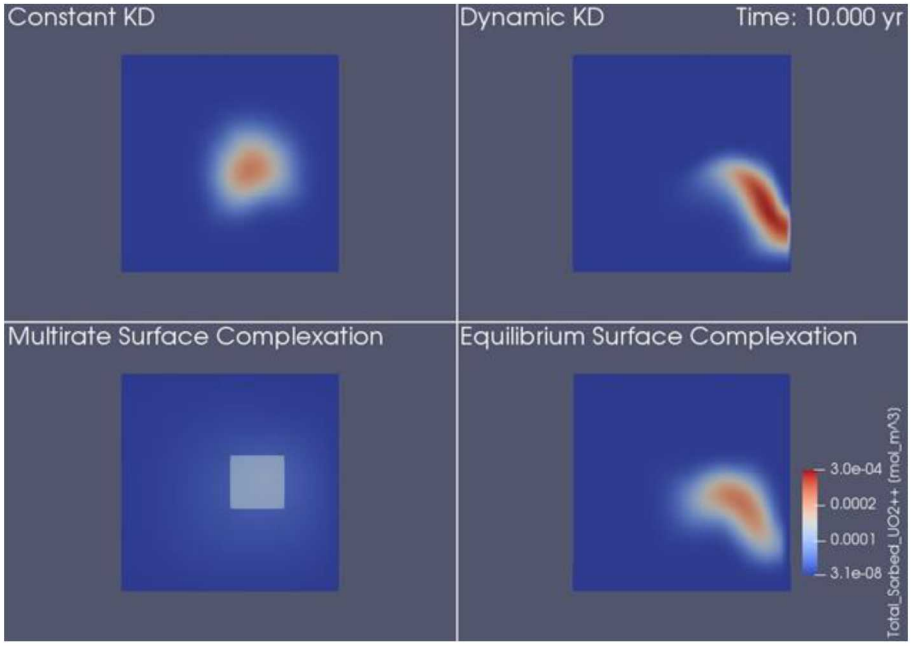

Figure 3-13 Total sorbed U(VI) at 10 years simulation time for each of the four sorption models using global implicit reactive transport with heterogeneous flow

3.1.6 Waste Package Degradation

Currently, PFLOTRAN options for waste package degradation modeling for high-level waste are simple and conservative. The options are 1) pre-specification of waste package breach time and 2) calculation of the general corrosion rate at each time step using an Arrhenius relationship. The latter tracks the decreasing thickness of the waste package barrier over time using a temperature-dependent corrosion rate. For each option, distributions can be specified so that all waste packages do not breach at once. Also, for each option, once a waste package breaches, the waste form is exposed in its entirety and there is no trace of the prior existence of the waste package.

Uncertainty in the metals or alloys that will likely be used for generic repository concepts has delayed development of more sophisticated waste package degradation models for GDSA Framework. This year, however, progress in this area has accelerated. A new high-temperature shale reference case has been developed that identifies several possibilities for outer waste package barrier materials, buffer materials, and degradation processes (Section 3.1.6.1). New waste package degradation studies are being conducted, and new steel degradation models are being developed (Section 3.1.6.2). Task F of DECOVALEX-2023 (Development of COupled models and their VALidation against Experiments) will likely spur enhanced PA modeling of waste package degradation in crystalline and salt repository environments (Section 3.1.6.3). In addition, we updated our database of international corrosion models (Section 3.1.6.4).

3.1.6.1 High-Temperature Shale Reference Case

In the fall of 2019, a team of experts across the SFWST Campaign formed to develop a conceptual model of a high-temperature shale reference case. The objective of this collaboration was to develop a shared concept for a high temperature shale repository to inform SFWST modeling and experiments. Much of the work focused on the properties of shales, repository design, EBS components, and how these components and designs may be appropriate for a high-temperature repository in shale. The progress to date of this initiative is summarized in Stein et al. (2020).

With regard to waste package degradation modeling in a high-temperature shale repository, several options for waste package and buffer materials were presented. Waste package material options include carbon steel, low-alloy steel, copper, titanium alloys, and amorphous metal and ceramic coatings. Buffer materials include the traditional bentonite option, saponite for certain harsh environments, and mixtures of buffer with silica or graphite filler to enhance heat transfer. A potential alternative for enhancing heat transfer is the installation of a copper mesh in the buffer region between the waste package and drift wall.

The high-temperature shale reference case report discusses several of the corrosion processes that may be relevant for iron-based alloys and copper, including general corrosion and different types of localized corrosion. Based on the broad range of options for waste package and buffer materials (Stein et al. 2020), options for waste package degradation models for the shale repository reference case remain numerous.

3.1.6.2 Corrosion Studies and Modeling

To understand the stability and interaction of steel, corrosion phases, and clay minerals, Los Alamos National Laboratory (LANL) has been conducting hydrothermal interaction experiments. Preliminary analysis of these interactions and potential mechanistic processes is presented in Jove-Colon et al. (2020).

Metallic copper remains an option for the outer barrier of waste packages, particularly for crystalline rock. The predominant corrosion mechanism for copper in reducing repository environments is attack by hydrogen sulfide. Lead or lead-alloy materials, however, appear not to be subject to sulfide attack under the same conditions (Wang et al. 2020). Long-term corrosion experiments in carbonate-bearing groundwater show that lead is passivated by low-solubility lead corrosion products (lead carbonates) that render sulfide attack thermodynamically unfavorable. To ensure sufficient carbonate for passivation, carbonate materials such as calcite or hydromagnesite could be included in the repository.

Steel corrosion is being simulated in the latest FMD/in-package chemistry model (Jerden et al. 2019). In this model, the corrosion mechanism is simulated based on chemical reactions using Geochemist's Workbench. Transport of reactants and products is simulated across a one-dimensional domain using the reactive transport code X1t. The 1D domain includes a single waste package, bentonite backfill, and near-field host rock. The model calculates the concentration of dissolved H_2 resulting from steel corrosion and tracks the masses, surface areas, and corrosion rates of each alloy over time. It was designed to couple with the FMD model because calculation of spent fuel degradation rate requires knowledge of the H_2 concentration at the fuel surface.

3.1.6.3 DECOVALEX-2023 Task F

DECOVALEX-2023 Task F is an international collaborative exercise to compare performance assessment models and results on common repository reference cases. Identical features, processes, initial conditions, and boundary conditions will be simulated by participating teams for crystalline rock and salt. The U.S. GDSA team is the lead for Task F and will develop reference cases for each host rock. Progress to date on this task is summarized in LaForce et al. (2020).

Waste package materials will be specified for each host rock, as will degradation processes. For the crystalline repository reference case, it is likely that the waste package outer barrier will be copper and that a mechanistic copper degradation model will be needed. The salt reference case may also require a mechanistic waste package degradation model. Whichever common materials and processes are chosen by the participants, this activity is expected to spur new waste package degradation modeling in GDSA Framework.

3.1.6.4 Corrosion Model Database

In preparation for development of new waste package degradation models, a literature review was performed to update the GDSA database of published corrosion models. This database includes

information from nuclear programs of over twenty countries with SNF, HLW, or both. Most of these countries are considering repositories in crystalline rock. Several are considering sedimentary and clay host rocks, and a few are considering salt. The stages of these programs range from having fully-developed safety cases to publishing little or no documentation of performance assessment models. Reports and papers found on waste package corrosion models were identified and, when possible, collected and saved in a common GDSA file directory with the corrosion database.

Several high-level observations can be made using this database. For example, among the 20-plus repository programs in the database, copper is the most commonly-selected outer barrier material. The thickness of copper in the various designs range from 0.3 to 5 cm. Other liner materials from international programs include stainless steel and carbon steel. Buffer materials are generally bentonite, but alternatives do exist, such as cement in the Belgium and Hungary concepts for clay repositories.

Waste package corrosion can occur via many processes. Key processes include (Bennett and Gens 2008):

- Atmospheric corrosion
- General (uniform) corrosion
- Crevice corrosion
- Pitting corrosion
- Stress corrosion cracking (SCC)
- Intergranular corrosion – grain boundary attack
- Galvanic corrosion
- Microbially influenced corrosion (MIC)
- Hydrogen embrittlement
- Radiation influenced corrosion
- Stray current corrosion
- Corrosion due to magnetic fields

Which processes occur to a significant extent in the repository depend on the waste package materials, buffer materials, and local environmental conditions. As indicated in Table 3-3, the most important corrosion processes in various national nuclear waste programs are general corrosion, pitting corrosion, localized corrosion, oxidation, and crevice corrosion. Other corrosion processes considered in these programs include stress corrosion cracking, intergranular grain boundary attack, hydrogen induced cracking, and microbially influenced corrosion.

As the GDSA waste package corrosion database develops, it will continue to provide a resource of the various approaches taken for modeling waste package corrosion. In addition, it will maintain a list of the various types of corrosion processes that could be important to repository safety assessment.

Table 3-3 Waste package corrosion processes in selected national nuclear waste programs (King and Kolar 2019)

Country	Reference container	General corrosion	Localized corrosion	Oxidation	SCC	IGA	HIC	MIC
Germany	Carbon steel	X	X (pitting)		x	x		
Spain	Carbon steel	X	X		x	x		
Belgium	Carbon steel	X			x			
France	Carbon steel	X		X				x
Switzerland	Carbon steel	X	X		x		x	
Sweden	Copper	X	x		x			x
Finland	Copper	X	x		x			x
Japan	Carbon steel	X	X		x		x	
Canada	Copper	X	x		x			x
	Carbon steel	X	X		x		x	x
USA	Alloy 22	X	X (crevice)					x
	Ti-7 (drip shield)	X			X		X	

X = most important corrosion processes; x = less important corrosion processes; SCC = stress corrosion cracking; IGA = intergranular grain boundary attack; HIC = hydrogen induced cracking; MIC = microbially influenced corrosion

3.1.7 Fuel Matrix Degradation

The Fuel Matrix Degradation (FMD) model is the uranium dioxide (UO_2) matrix degradation process model of GDSA Framework. It was developed collaboratively at Argonne National Laboratory and Pacific Northwest National Laboratory (Jerden et al. 2015b). This model, coded in MATLAB, calculates spent fuel degradation rates as a function of radiolysis, electro-kinetic reactions, alteration layer growth, and diffusion of reactants through the alteration layer. In more recent versions of the model, steel corrosion is included to provide a source of hydrogen (Jerden et al. 2018).

In FY 2015 a version of the FMD process model that excludes steel corrosion was coded in Fortran (Jerden et al. 2015a). This Fortran code was coupled to PFLOTRAN and successfully demonstrated (Mariner et al. 2015). Apart from the computational results, the demonstration indicated that the coupled model was computationally demanding. Mechanistic simulation of the FMD model processes requires a large number of calculations at each time step. For a probabilistic repository PA calculation there are thousands of waste packages and hundreds of realizations. Though the coupled Fortran FMD process model may be used for small scale problems, it is too expensive for higher-fidelity repository PA simulations that can propagate spatial variability in the values of inputs (e.g., local temperature and local environmental concentrations of chemical reactants) across the repository.

In FY 2019 and FY 2020, two approaches were undertaken to include the FMD process model in GDSA Framework. One approach, summarized in Section 3.1.7.1, was to develop surrogate models of the FMD process model for accurate and rapid emulation in PFLOTRAN. The other approach, described in Section 3.1.7.2, was to develop a new Fortran code that utilizes rapid solvers and flexible time steps for a more powerful standalone FMD process model that will smoothly couple to PFLOTRAN.

3.1.7.1 FMD Surrogate Models

In FY 2020, an artificial neural network (ANN) surrogate model and a k-Nearest-Neighbors regression (kNNr) surrogate model were implemented in PFLOTRAN for the FMD process model. The ANN surrogate is a parametric model that utilizes a network of artificial neurons with nonlinear activation functions. The kNNr surrogate is a nonparametric model that uses an advanced technique to interpolate between points in a multidimensional database. Both approaches were pursued to increase the chances of developing a useful surrogate and to allow comparison of the advantages and disadvantages of the approaches for incorporating surrogate models in GDSA Framework. A full report on the FMD surrogate model work is provided in Mariner et al. (2020).

As documented in Mariner et al. (2020), the two surrogates were trained on results generated by the MATLAB FMD V2 process model. Surrogate results were found to be highly accurate where training data were densely spaced. This finding underscores the importance of focusing surrogate model training data on the expected sample space of the application. Further, surrogate simulation was found to be rapid compared to the coupled process model, allowing full repository simulation of the shale repository reference case in a practical amount of time. These results indicate that each surrogate model will enable GDSA Framework to rapidly and accurately simulate spent fuel dissolution for each individual breached spent fuel waste package in a probabilistic repository simulation.

Figure 3-14 demonstrates the ANN FMD surrogate in a shale reference case simulation with emplacement of both 24 pressurized water reactor (PWR) and 37 PWR waste packages. For comparison, the figure includes the results of the traditional fractional dissolution rate (FDR) model that uses a dissolution rate of 10^{-7} yr^{-1}. Waste packages start to breach in these simulations around 300 years. Note that the surface-area-specific degradation rate (bottom plots) decreases over time in the ANN FMD simulation, as would be expected due to decreases in dose rate and temperature with time. For the FDR model, a surface-area-specific rate of ~3.7×10^{-7} mol m^{-2} yr^{-1} is maintained after breach for the rest of the simulation (both simulations assume a constant fuel specific surface area of 0.001 m^2 g^{-1}).

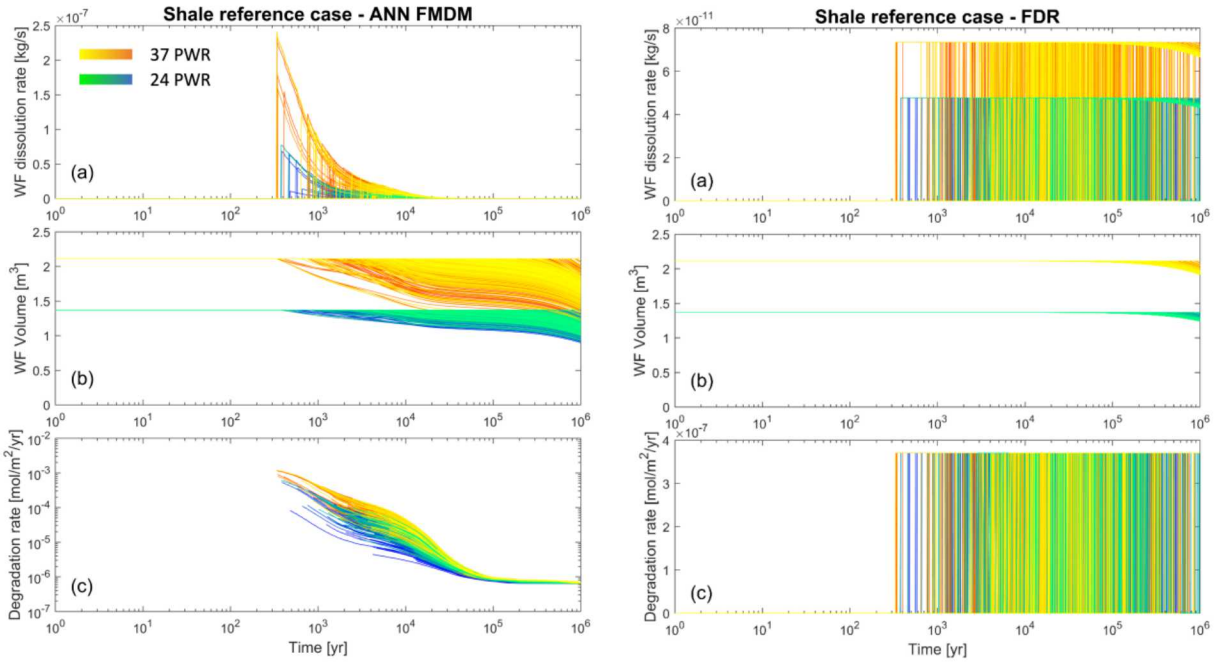

Figure 3-14 Fuel matrix degradation rates and remaining fuel volumes for breached 24 PWR (green and blue) and 37 PWR (yellow and orange) waste packages in a shale repository reference case using the ANN FMD surrogate (left) and traditional fractional dissolution rate (10^{-7} yr^{-1}) model (right).

3.1.7.2 Fortran Process Model

The original Fortran FMD code developed in FY 2015 and coupled with PFLOTRAN uses much of the same structure as the MATLAB code. Those codes recursively solve for corrosion potentials and new concentrations instead of coupling the solvers which leads to an increase in iterations and decrease in speed. Also, the Fortran code was not improved to allow for dynamic time stepping and was not set up for parallel computing.

Under the continued guidance of Glenn Hammond, development of a new Fortran code is underway for faster run times, smoother PFLOTRAN coupling, and parallel computing. The goals of this initiative are to develop a faster FMD process model with flexible coupling features, keep it open source, and help the process modelers transition to the new code so that they can continue to develop a code that is compatible with PFLOTRAN.

Appendix B documents progress in FY 2020 toward developing an improved solution scheme. Initial tests indicate that the number of iterations required to converge to a solution will be significantly reduced. In addition, the new code is expected to avoid the non-convergence issues often encountered with the MATLAB code.

3.1.8 Evolution of Buffer and DRZ Porosity and Permeability

An ongoing integration effort with Lawrence Berkeley National Laboratory to incorporate TOUGH-FLAC coupled thermal-hydrologic-mechanical (THM) nearfield modeling results into repository-scale thermo-hydrologic-chemical (THC) PA simulations in PFLOTRAN has led to the development of a suite of reduced-order models to approximate near-field geomechanical effects in PA simulations. This work is motivated by the fact that geomechanical effects are often localized to the near-tunnel environment and relatively early in the post-closure period (on the order of hundreds of years), when thermal loading from

waste packages is most significant. If localized, permanent geomechanical deformation occurs in the first hundreds of years of a simulation run for hundreds of thousands of years, it could be computationally inefficient to simulate geomechanics throughout the duration of a simulation at the PA scale. Therefore, by running a series of high-fidelity, high-resolution nearfield simulations in a THM simulator, TOUGH-FLAC, results can be compared to reduced-order models employed in PFLOTRAN to understand whether the relevant geomechanical phenomena can be adequately captured by reduced-order models.

Using a series of coupled THM models simulating the immediate vicinity of a shale-hosted repository tunnel backfilled with bentonite, Rutqvist et al. (2014a; 2014b) found that buffer swelling stress during repository re-saturation provides a significant increase in confining stress on the tunnel wall. This change in stress state can potentially work to close fractures in the disturbed rock zone (DRZ) and therefore reduce DRZ permeability and porosity. As a result, permeability evolution in a fractured DRZ could be an important geomechanical mechanism to consider for PA simulations as it can affect repository re-saturation behavior and consequently geochemical exchange between the repository and host rock.

It is likely that the swelling stress in the buffer can be adequately modeled analytically as a function of temperature and buffer saturation. By applying wellbore geomechanical stability analysis (Zoback 2010) for a cylindrical drift in a deep geological nuclear waste repository (Figure 3-15), the repository drift can be considered a horizontal wellbore parallel to the maximum horizontal stress ($S_{H,max}$). When buffer swelling occurs, the swelling stress is assumed to act homogeneously in the radial direction:

$$S_{rr} = \sigma_{swelling} \tag{11}$$

where, S_{rr} is the radial component of stress and $\sigma_{swelling}$ is the swelling stress exerted by the buffer on the side walls of the drift.

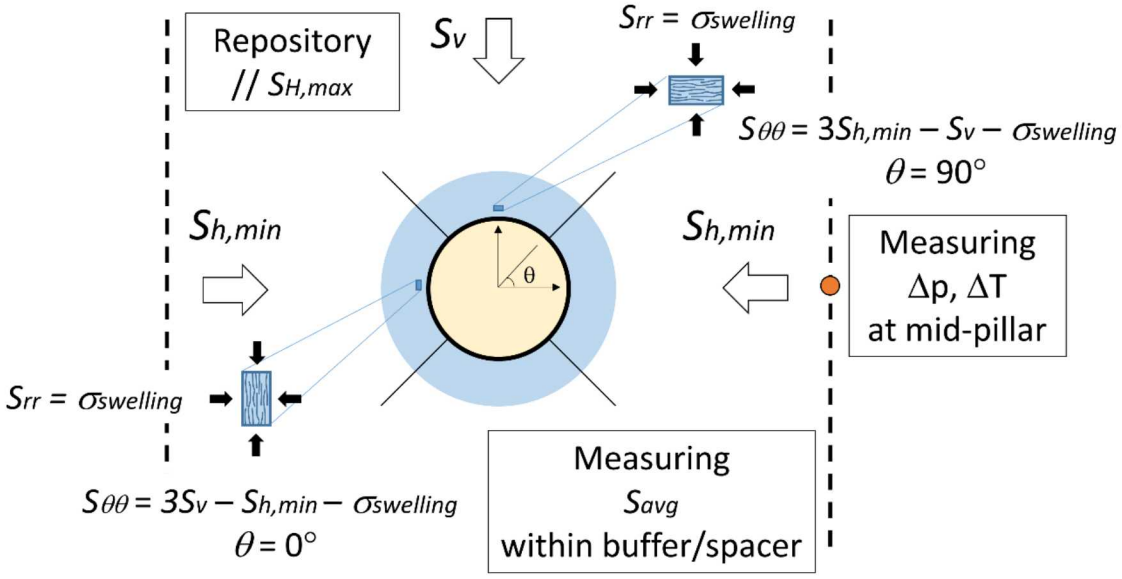

Figure 3-15 Schematic description of the geomechanical analysis of a cylindrical drift in 2D. The repository is assumed to be parallel to the direction of maximum horizontal stress ($S_{H,max}$).

In the simplest case, detailed here, the buffer swelling stress is set equal to the normal stress across fractures in the DRZ (Figure 3-15) and is used directly in one of a series of analytical functions relating fractured shale rock permeability to normal stress across the fractures. A more sophisticated advance will

be to link DRZ permeability to 3D stresses by considering both the local buffer swelling stress and tangential stresses related to the far-field stress state (Rutqvist et al. 2020).

The change in the swelling stress can be adequately captured as a linear function of the change in average liquid saturation within the buffer and spacer (Rutqvist et al. 2011):

$$\Delta\sigma_{swelling} = 3K\Delta S_l \beta_{sw} \quad (12)$$

where K is the bulk modulus and β_{sw} is a moisture swelling coefficient.

Waste packages in a repository generate heat and subsequently perturb the saturation and pressure fields in the near-field host rock. An initially unsaturated bentonite buffer/spacer will re-saturate over time by liquid water imbibition and vapor condensation from the host rock, which will increase the buffer swelling stress based on the linear relationship shown above.

The buffer material is required to have high swelling capacity and low hydraulic conductivity to minimize the penetration of ground water from the host rock; bentonite is therefore a widely favored buffer material. Swelling of bentonite enhances the sealing capacity of the buffer/spacer, such that high swelling stress will be favorable to prevent the seepage of fluids and accompanying transport of radionuclides. The β_{sw} value for a bentonite buffer material is approximately 0.238 (Rutqvist et al. 2011).

3.1.8.1 DRZ Permeability Evolution

Temporal perturbations in swelling stress caused by saturation changes can contribute to the changes in formation properties. During re-saturation, a swelling buffer exerts stress on the surrounding DRZ, which can in turn work to compress fractures in the DRZ. As fractures represent high-permeability pathways through the medium, closing them can result in reduction of the DRZ permeability. Therefore, as imbibition and condensation drive an increase in liquid saturation over time in the buffer, permeability of the surrounding DRZ will correspondingly decrease over time. In the current work, the closure or opening of the pre-existing fractures is assumed to be controlled mainly by the normal component of swelling stress acting across the fractures. The effective stress change can thus be defined as follows:

$$\Delta\sigma_{eff} = \Delta\sigma_{swelling} \quad (13)$$

The relationship between normal stress across fractures and bulk medium (fracture + matrix) permeability is highly dependent on fracture and matrix compressibility. There are multiple models in the literature to express this relationship for different shale rocks; in this work, three different models have been implemented in PFLOTRAN relating DRZ permeability to normal effective stress: an exponential function, a cubic law function, and a two-part Hooke's Law model.

Exponential Function

Previous studies of shale permeabilities have shown that experimental data fit well to an exponential functional form (e.g., Dewhurst et al. 1999, Dong et al. 2010). Bustin et al. (2008) showed the variation in permeability with effective stress for several shales (Figure 3-16).

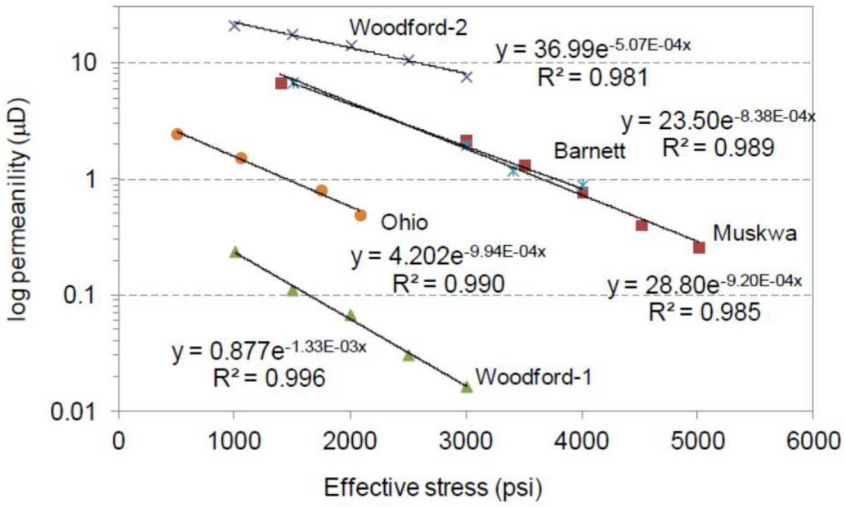

Figure 3-16 Experimental permeability data of five shales (modified from Bustin et al. 2008)

The experimental data are fitted to the following exponential function of the effective stress:

$$k = k_0 e^{-3C_{exp}\Delta\sigma_{eff}} \tag{14}$$

where c_{exp} (MPa^{-1}) is the compressibility coefficient and typically ranges from 7.35×10^{-2} to 1.93×10^{-1} MPa^{-1}.

Considering the presence of fractures within the shale host rock, the shale permeability declines exponentially with increasing effective stress (McKee et al. 1988) as a function of the fracture-volume compressibility.

Furthermore, the exponential relationship between permeability and effective stress can be refined to consider non-constant fracture compressibility as follows (Chen et al. 2015, Shi & Durucan 2016):

$$k = k_0 e^{-3C_f\Delta\sigma_{eff}} \tag{15}$$

where fracture compressibility is formulated itself as a function of effective stress as follows:

$$c_f = \frac{c_{f,0}}{\tau\Delta\sigma_{eff}}\left(1 - e^{-\tau\Delta\sigma_{eff}}\right) \tag{16}$$

where k_0 (m^2) is the reference permeability at zero effective stress, c_f (MPa^{-1}) is the mean compressibility over the effective stress range, $c_{f,0}$ (MPa^{-1}) is initial fracture compressibility ranging from 6×10^{-2} to 4×10^{-2} MPa^{-1} for shale, and τ (MPa^{-1}) is the declining rate of fracture compressibility with increasing effective stress ranging from 4×10^{-2} to 2×10^{-1} MPa^{-1} for shale. The experiments showed that larger initial fracture compressibility is associated with a larger declining rate coefficient. Note that over changes in swelling stress of about 5 MPa, the fracture compressibility (c_f) can be assumed as roughly constant.

Modified Cubic-Law Function

The measured permeability of illite-rich shale with different effective stresses ranging from 3 to 12 MPa gives the following equation (Kwon et al. 2001):

$$k = k_0 \left[1 - \left(\frac{\Delta\sigma_{eff}}{P_1}\right)^m\right]^3 \quad (17)$$

where P_1 (MPa) is the effective modulus of the equivalent asperities (P_1 = 19.3±1.6 MPa for shale), m is a constant between 0 and 1 (m = 0.159±0.007), and the reference permeability is ~10^{-17} m^2. This expression relates permeability with the equivalent fracture aperture, which can explain the decrease of permeability with the fracture compaction.

Two-Part Hooke's Law Model (TPHM)

The concept of TPHM represents non-uniform deformation of heterogeneous rock by dividing the rock body into 'soft' and 'hard' parts to describe different stress-strain behaviors (Liu et al., 2009). Dividing total porosity into soft and hard parts allows for the superposition of distinct relationships as functions of effective stress which combine to affect the total permeability.

In relatively high effective stress ranges, the hard part of the rock controls permeability, such that the soft part can be neglected (due to micro-crack closure at to high stress conditions). The hard-part permeability can be expressed as follows:

$$k_e = k_{e,0} e^{-\beta C_e \phi_{e,0} \Delta\sigma_{eff}} \quad (18)$$

where ϕ_e and k_e are the stress-dependent hard-part porosity and permeability, C_e is the compressibility of the hard part, and β is a constant stress sensitive coefficient. $\phi_{e,0}$ is the porosity under zero effective stress.

In low effective stress ranges, the permeability decreases mainly due to the deformation of the soft-part porosity, which experiences relatively large deformation, even though the soft-part porosity takes a small portion of the total pore volume. Soft part permeability can be expressed as follows:

$$k_t = \alpha \left[\gamma_t \exp\left(-\frac{\Delta\sigma_{eff}}{K_t}\right)\right]^m \quad (19)$$

where k_t is the soft-part permeability, γ_t is the volume fraction of the soft part under zero effective stress, α and m are material constants. Superimposing, the total permeability can be expressed as follows (Zheng et al. 2016):

$$k = k_e + k_t = k_{e,0} e^{-\beta C_e \phi_{e,0} \Delta\sigma_{eff}} + \alpha \left[\gamma_t \exp\left(-\frac{\Delta\sigma_{eff}}{K_t}\right)\right]^m \quad (20)$$

Due to the limitation of experimental methods, the porosity and the volume fraction of the soft part are obtained at the lowest effective stress ($k_{e,1}$ and $k_{t,1}$, respectively). The total permeability can thus be expressed as follows:

$$k = k_{e,1} + k_{t,1} = k_{e,1} e^{-\beta C_e \phi_{e,1} \Delta\sigma_{eff}} + \alpha \left[\gamma_{t,1} \exp\left(-\frac{\Delta\sigma_{eff}}{K_t}\right)\right]^m \quad (21)$$

Zheng et al. (2016) performed experiments for the four silty-shale samples to give a range of values for the TPHM model parameters (Table 3-4).

Table 3-4 Range of Parameter Values for TPHM Model

Parameter	Values
$\gamma_{t,1}$ (%)	0.07 to 0.09
K_t (MPa)	2.83 to 14.81
m	2.28 (loading), 2.08 (unloading)
α (m^2)	4.91×10^{-19} to 5.42×10^{-15}
C_e (1/MPa)	1.48×10^{-4} to 8.75×10^{-4}
$k_{e,1}$ (m^2)	1×10^{-19} to 3.66×10^{-17}
β	0.61 to 3.29

3.1.8.2 DRZ Porosity Evolution

In addition to affecting the bulk permeability of the DRZ, fracture closure can also reduce the overall porosity of the medium. Since fractures typically constitute a small volume but constitute an outsized contribution to the connectivity of the medium, relative porosity reduction due to fracture closure should generally be small compared to permeability reduction. Nonetheless, porosity reduction can alter geochemical transport behavior, specifically diffusive transport.

Log Formulation

Currently, a log formulation is implemented in PFLOTRAN to link permeability in the DRZ to porosity. This formulation is based on laboratory test data that show that permeability and porosity of shale rocks follow a log-linear trend (Neuzil, 2019):

$$\log k = \gamma\phi + \log k_0 \tag{22}$$

Then, the porosity can be expressed as:

$$\phi = \frac{1}{\gamma}\log\left(\frac{k}{k_0}\right) \tag{23}$$

where k_0 is the extrapolated intercept at zero porosity. Most data (Neuzil 2019) fall in a region defined by γ = 8.0, with $\log k_0$ values falling between -22.5 and -21.0.

Implementation of a Two-Part Hooke's Law model for porosity evolution as a function of permeability is currently under development. Once this is complete, the focus of the coming year will be on comparing results of these reduced order models to mechanistic models with the goal of producing a peer-reviewed journal publication.

3.1.9 Temperature-Dependent Thermal Conductivity

Recent developments in PFLOTRAN have focused on implementing temperature-dependent thermal conductivity by way of thermal characteristic curves (TCCs). TCCs express thermal conductivity as a function of temperature for a given material (e.g., Figure 3-17). Internally, this description resembles the way "characteristic curves," or combinations of capillary pressure and relative permeability functions, are implemented. A prototype of this capability was created to allow more physically realistic heat conduction modeling in salt, affiliated with the Brine Availability Test in Salt (BATS) heater test at the

Waste Isolation Pilot Plant (Kuhlman et al. 2020). Salt is well known to have thermal conductivity that decreases with increasing temperature (e.g., see lab test data in Kuhlman et al. 2020). The prototype capability developed for Salt R&D was expanded in scope and rigorously tested for GDSA. The goal of adding this functionality for broader GDSA purposes was to impart higher fidelity when modeling scenarios where significant thermal loading can lead to localized temperature anomalies; heat dissipation is linked to composite thermal conductivity, which can vary locally if there is significant local contrast in the temperature field and a strong dependence of host rock thermal conductivity on temperature. Thermal conductivity of a salt host rock, for instance, is understood to be heavily influenced by temperature in the relevant thermal regime for repository applications (Gilliam and Morgan 1987; Vosteen and Schellschmidt 2003). Furthermore, disposal of large waste packages, such as 37-PWR canisters, which contain a higher density of PWR assemblies (and thus a more significant decay heat load) than smaller waste packages, is an active area of study for multiple host rock scenarios. The decay heat itself will induce significant perturbation to the local temperature field, and potential consequence assessment of an in-package criticality event occurring is also an active area of research: during a criticality event, a huge local power spike in the waste form will result in significant local thermal perturbation.

Accurately capturing the capacity for the repository-host rock system to dissipate heat also affects material and geochemical properties that are temperature dependent and potentially irreversible. With the heat emission from a critical event in the canister, the mineral composition of the surrounding buffer is liable to be affected, which will directly impact sealing performance in the repository. Given the temperature-dependence of the smectite-to-illite transition, along with the potential non-linearity of the process, it is important to have expanded thermal modeling capability to accurately represent the phenomena involved for a consequence analysis.

3.1.9.1 Implementation of Thermal Characteristic Curves in PFLOTRAN

A new PFLOTRAN source code file was written that contains all variables and subroutines used to process thermal characteristic curve input and evaluate composite thermal conductivity. Modifications were made to the source code to read in curve parameters and produce error messages. Since functionality existed for function identification numbers for characteristic curves, these structures were largely mirrored for TCCs since both are employed in similar manner. To preserve backwards-compatibility with the legacy input format of specifying κ_T^{dry} and κ_T^{wet} by material, the default thermal characteristic curve (Eq. 24) is activated and tied to these parameters when this format is detected.

Previously, thermal conductivity (κ_T) in PFLOTRAN's non-isothermal flow modes was formulated as a function of wet (κ_T^{wet}) and dry (κ_T^{dry}) thermal conductivity values as well as liquid saturation (S_l) from Somerton *et al.* (1974) as shown in Eq. 24. In the context of current development, this equation is still used as the default (*D*) for effective thermal conductivity, and the implementation in PFLOTRAN is backward-compatible with input decks from PFLOTRAN v2.

$$\kappa_T^D(S_l)=\kappa_T^{dry}+\sqrt{S_l}\left(\kappa_T^{wet}-\kappa_T^{dry}\right) \tag{24}$$

In a given problem, these parameters are specified by material property along with heat capacity and density, but there are no additional parameters to determine temperature dependence. The effective thermal conductivity between two cells is applied at cell interfaces by computing a harmonic average thermal conductivity between the two cells. This average value is then used with the temperature difference across the cell to evaluate the heat flux and, depending on the phases involved, the derivative of internal energy and enthalpy with respect to temperature and saturation.

3.1.9.2 Supported Thermal Conductivity Function Types

Four new function types were employed to evaluate κ_T and are shown in Table 3-5 along with the previous functionality. The default TCC (Eq. 24) is actually used to determine saturation dependence for TCCs (Eq. 26, Eq. 27, and Eq. 28), while temperature dependence is handled elsewhere. The constant thermal characteristic curve (Eq. 25) removes all saturation and temperature dependence from the calculation. This can be advantageous for certain perturbation studies that need to isolate non-thermal phenomena. For example, in a criticality consequence study, the effect of water influx into the breached waste package can be better decoupled from the temperature-driven effects in the buffer using this setting, allowing for the moderator reactivity defect to be studied with a better degree of isolation.

The linear resistivity TCC (Eq. 26) assumes that the reciprocal of thermal conductivity can be modeled by a linear function with temperature, as suggested by Birch and Clark (1940) and fitted empirically by Blesch et al. (1983) for granite, basalt, shale, and salt. The latter study was a far-field thermal analysis of a repository to evaluate environmental impact based on temperature changes in various regions. In the linear resistivity function, a_0 is the resistivity shift parameter and a_1 is the scaling factor with the change in temperature. The temperature change is defined with respect to a reference temperature (T_{ref}), such that when $T_{ref} = 0$ °C, κ_T^{dry} and κ_T^{wet} for $\kappa_T^D(S_l)$ are assumed to have been evaluated at 0 °C as well.

The cubic polynomial TCC (Eq. 27) adds three orders of dependence on the change in temperature, which is once again based on a separate reference temperature T_{ref}. A polynomial form of equation was used by Flynn and Watson (1969) to evaluate effective thermal conductivity in soils reaching temperatures up to 1700 °C. This study was conducted in the context of reentry and earth-impact scenarios for space vehicles containing radioisotopes, and the soils that were sampled included limestone, granitic detritus, sand, and others within a particle diameter of 1.7 mm. The order of polynomial was chosen to reduce the residuals in a least-squares fit of test data. This model can be applied to rock and buffer regions near the waste package susceptible to being affected by high temperature transients.

Lastly, a power law TCC (Eq. 28) is provided that employs an exponent (γ) and reference temperature T_{ref}. The default reference temperature is defined as absolute zero, or -273.15 °C, which implies κ_T^{dry} and κ_T^{wet} values as pertaining to 26.85 °C. The temperature change is normalized by 300 K and then raised to the exponent γ. This type of model is relevant to studies of crystals, ceramics, and engineering materials, and can be useful in characterizing heat transfer through the canister and spent nuclear fuel.

Table 3-5 Options for thermal characteristic curves along with values used in the unit test problem

Name	Function	Unit Test Inputs
Default	$\kappa_T^D(S_l)=\kappa_T^{dry}+\sqrt{S_l}\left(\kappa_T^{wet}-\kappa_T^{dry}\right)$ (24)	κ_T^{wet} = 7.0 W/m-K κ_T^{dry} = 5.5 W/m-K
Constant	$\kappa_T=\kappa_T^C$ (25)	κ_T^C = 5.5 W/m-K
Linear Resistivity	$\kappa_T(S_l,T)=\frac{\kappa_T^D(S_l)}{a_1+a_2(T-T_{ref})}$ (26)	κ_T^{wet} = 7.0 W/m-K [0 °C] κ_T^{dry} = 5.5 W/m-K [0 °C] a_1 = 1 a_2 = 5.038×10^{-3} °C^{-1} T_{ref} = 0 °C
Cubic Polynomial	$\kappa_T(S_l,T)=\kappa_T^D(S_l)\left[1+\beta_1(T-T_{ref})+\beta_2(T-T_{ref})^2+\beta_3(T-T_{ref})^3\right]$ (27)	κ_T^{wet} = 7.0 W/m-K [0 °C] κ_T^{dry} = 5.5 W/m-K [0 °C] β_1 = -4.53398×10^{-3} °C^{-1} β_2 = $+1.41580\times10^{-5}$ °C^{-2} β_3 = -1.94840×10^{-8} °C^{-3} T_{ref} = 0 °C
Power Law	$\kappa_T(S_l,T)=\kappa_T^D(S_l)\left(\frac{T-T_{ref}}{300}\right)^{\gamma}$ (28)	κ_T^{wet} = 7.0 W/m-K [26.85 °C] κ_T^{dry} = 5.5 W/m-K [26.85 °C] γ = -1.18 T_{ref} = -273.15 °C

3.1.9.3 Unit Tests

Temperature-dependent thermal conductivity unit tests were added to the repository to ensure the functional forms described above were implemented correctly. To illustrate the differences in the thermal conductivity functions that are currently implemented, TCCs are plotted in Figure 3-17 for minimal and maximal values of $\kappa_T^D(S_l)$ for unsaturated and saturated cases, respectively. Relative to the default TCC, the power law TCC exhibits higher thermal conductivity at temperatures below 26.85 °C. Otherwise, at higher temperatures, the power law κ_T falls below the default thermal conductivity. Since κ_T^{dry} and κ_T^{wet} are universal in this problem setup and $\kappa_T^C = \kappa_T^{dry}$, the cubic polynomial, linear resistivity, and constant TCCs will all produce smaller thermal conductivities relative to the default value. Therefore, for a given heat flux, the change in temperature will be lower for these TCCs compared to the default.

It is apparent that saturating the medium has the effect of widening the κ_T gap between the power law curve and the linear resistivity/cubic polynomial curves. The latter two remain relatively close to each other. It should be noted that this quantitative description will vary depending on how each model is tuned, but qualitatively it is clear that over a large range in temperature, accounting for temperature dependence of thermal conductivity can have a significant impact on heat flux.

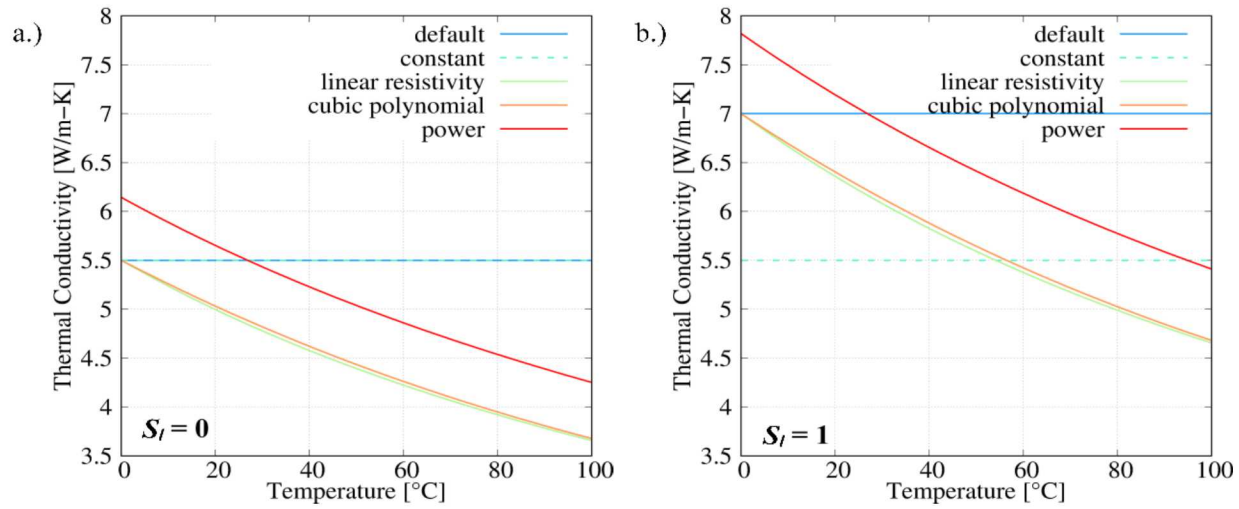

Figure 3-17. Model thermal conductivity function dependencies for a.) unsaturated and b.) saturated cases

3.1.9.4 Conclusions

Thermal characteristic curves imparting temperature-dependent thermal conductivity have been successfully implemented in PFLOTRAN. Unit testing has been implemented to test results among the functions using a parameter space linked by wet and dry thermal conductivities but otherwise varied in the mathematical treatment of temperature dependence.

Continuing work involves incorporating thermal conductivity anisotropy in a manner similar to existing permeability anisotropy. This feature will be an extension of the options for thermal characteristic curves. It will allow for greater versatility in a number of studies, in particular, assessing axial differences in conductivity along repository tunnels. A preliminary demonstration has been performed for a shale host rock repository near-field, single-waste package, high-resolution model. This model compares the resulting temperature profiles between two different thermal characteristic curves; future work will incorporate thermal characteristic curves in a full repository reference case.

3.1.10 AGGREGATE Function for Recording Maximum Concentrations in a Region

In a repository performance assessment, peak concentrations of radionuclides are important indicators of repository performance. For sites (or generic reference cases) where the locations of groundwater wells or springs producing the highest biosphere exposure to radionuclide concentrations cannot be predicted, it can be difficult to determine where to monitor for radionuclide concentrations, especially if there is considerable spatial heterogeneity in permeability in the geologic media between the repository and aquifer location.

A new data-mining capability called the AGGREGATE function was implemented in PFLOTRAN this year to efficiently solve this problem. This functionality tracks an “aggregate metric” of a specific quantity of interest over an arbitrary region of interest inside of a larger model domain. Currently, a maximum value aggregate metric is supported, and support for other metrics is planned for future development. Current aggregate metric functionality is described in detail at www.documentation.pflotran.org.

To illustrate this capability, take as an example a model domain that contains an aquifer where a user is interested in tracking dissolved ^{129}I concentration (e.g. the center, yellow region in Figure 3-18). Instead of monitoring the time evolution of ^{129}I concentration in every cell encompassed by the aquifer region, the

user can monitor the location and magnitude of the maximum value of ^{129}I concentration. This information along with all other state variables requested in the OUTPUT block associated with the location of the aggregate metric are output into a separate -agg.tec space delimited file. Output times correspond to observation times specified in the OUTPUT block. When multiple aggregate metrics are requested for a given region, the number of the aggregate metric is appended to the filename. Headers in the "agg" files indicate the specific aggregate metric to which the file is associated.

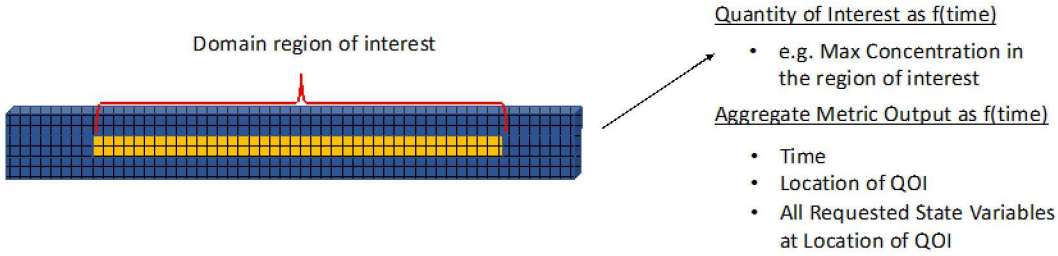

Figure 3-18 Schematic showing a region of interest where an aggregate metric is desired. The location and value of the aggregate value are recorded along with all other state variables at that location.

As an example, in the latest version of PFLOTRAN, the following block can be added to an input deck:

```
OBSERVATION
  REGION aquifer
  AGGREGATE_METRICS
    MAX Total I129
    MAX LIQUID_PRESSURE
    MAX TEMPERATURE
  /
END
```

In this instance, 3 aggregate metrics would be tracked in the aquifer region: maximum aqueous ^{129}I concentration, maximum liquid pressure, and maximum temperature. The associated output file names and headers are described in Table 3-6.

Table 3-6 Aggregate metric output files and associated headers for a sample input deck

Output file name	Header
<simulation_name>-agg-1.tec	Aggregate Metric: Max Total I129
<simulation_name>-agg-2.tec	Aggregate Metric: Max Liquid Pressure
<simulation_name>-agg-3.tec	Aggregate Metric: Max Temperature

The AGGREGATE function is especially useful for the crystalline repository reference case. Realizations of the crystalline host rock surrounding the repository have different stochastically-generated discrete fracture networks (DFNs). Though each DFN has statistically identical fracture density and mean fracture lengths, orientations, and apertures, the resulting locations and connections of the fractures cause peak

radionuclide concentrations in the overlying aquifer to crop up in different locations and at different times.

Figure 3-19 gives an example of how spatially heterogeneous the I-129 plume can be in the overlying aquifer because of the simulated fractures in the host rock. The figure shows that the plume enters the aquifer primarily where major deterministic fracture zones contact the aquifer. Figure 3-31 in Section 3.2.6 shows how the location of the maximum concentration of I-129 in the aquifer can change within a single realization over time. Similar spatial heterogeneity is observed in different DFN realizations but with locations and timing of peaks that can be quite different. Because peak concentration in the aquifer is a valuable indicator of repository performance, it is important to find it in each realization.

The AGGREGATE function is demonstrated in Section 3.2.6. In addition to documenting the maximum concentrations of I-129 in the aquifer and their locations over time, it provides the concentrations of tracers at those locations so that mean travel times of the tracers to those locations can be estimated.

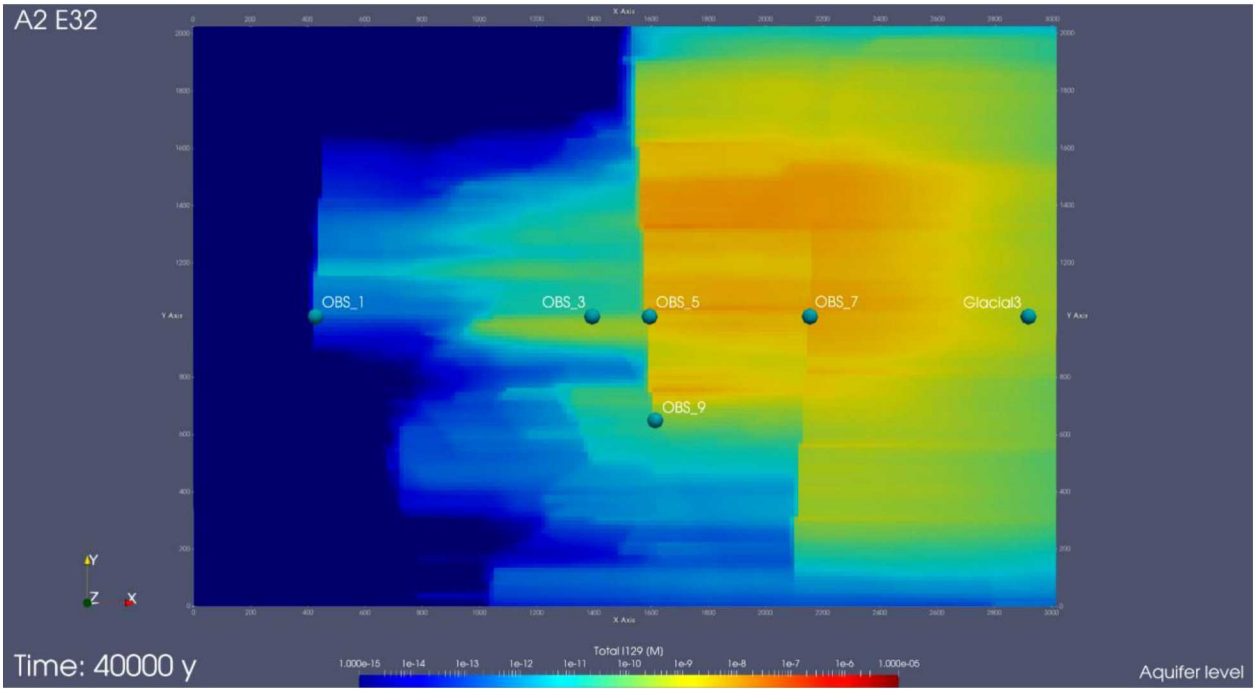

Figure 3-19 Overhead view of the spatial heterogeneity of I-129 concentrations at 40,000 years in the aquifer of a crystalline reference case realization

3.2 Framework Development

In addition to development of the PFLOTRAN code (Section 3.1), there were advances in PA framework and PA methods around the code. These advances include development of:

- Next Generation Workflow graphical interface for GDSA Framework simulations (Section 3.2.1)
- Advanced meshing using VoroCrust (Section 3.2.2)
- Geologic Framework Models for shale and unsaturated alluvium (Section 3.2.3)
- Uncertainty and sensitivity analysis applications and methods (Section 3.2.4)

- Calculations of bulk transport characteristics for stochastically-affected regions (Sections 3.2.5 and 3.2.6)
- Biosphere modeling (Section 3.2.7)
- DECOVALEX-2023 Task F: Performance assessment (Section 3.2.8)
- HPC resources augmentation (Section 3.2.9)

3.2.1 GDSA Framework Graphical Workflow

The GDSA computational framework is largely comprised of two primary computational capabilities: PFLOTRAN and Dakota, as described in Section 2.2. An analysis supporting the performance assessment of a geologic repository involves the development and use of many additional connective computational components beyond these two primary components, including the development of input files, scripts that connect the capabilities of PFLOTRAN and Dakota, scripts to submit calculations to computational resources, capabilities to gather and post-process results, and much more. The collection of these computational components that comprise the complete body of work required to produce results of interest from a computational simulation capability, such as the GDSA framework, is hereafter referred to as an *analysis workflow*. The development of GDSA analysis workflows commonly occurs on an analysis-by-analysis basis and requires the expertise of highly experienced modelers/analysts who are very familiar with the PFLOTRAN code base. These complex analysis workflows involve many manual steps and continuous monitoring of simulations. This can make it difficult to replicate previous analyses, hand-off analyses between analysts, and/or train new analysts to produce analysis workflows as the reproducibility of these analyses depends on how well the modeler/analyst organized and documented what was done.

To improve analysis workflow automation, development, reproducibility, and traceability for repository PA simulations, the GDSA team began developing automated analysis workflows using the Next-Generation Workflow (NGW) capability in FY 2020. The NGW capability is an open source engine that was developed at Sandia National Laboratories to provide analysts with a capability to construct, execute, and communicate end-to-end computational simulation analysis workflows (Orient et al. 2020). This capability is a graphical, node-based interface that includes many pre-programed support functions which are utilized within computational simulation analysis workflows. NGW is available within the Dakota Graphical User Interface (GUI) (Ridgway 2020) and is thus available to the GDSA analysis community.

Development of NGW analysis workflows for the GDSA Framework is focused providing an automated workflow capability with the following objectives:

- Reduce the learning curve for new users to set up and run simulations and analysis workflows
- Speed up analysis workflow execution time
- Eliminate/reduce the need for manual intervention and allow for automated monitoring
- Reduce the potential for the introduction of human errors
- Increase traceability and reproducibility

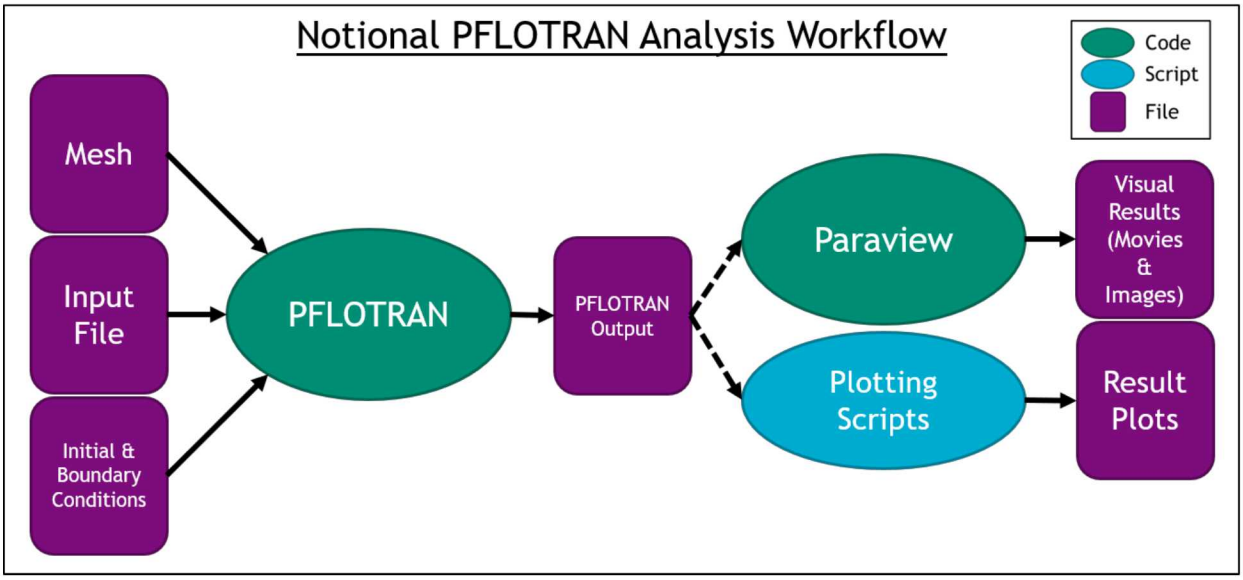

Figure 3-20 Notional deterministic PFLOTRAN analysis workflow

A first step towards developing graphical workflows for GDSA analyses is the development of an understanding of the existing analysis workflow of interest. An example of a basic notional GDSA analysis workflow for a deterministic analysis is shown in Figure 3-20. This example shows the development of analysis results using a PFLOTRAN simulation and subsequent visualization software and plotting scripts.

A graphical workflow was first developed for the geologic disposal example that is available in the materials for the PFLOTRAN short course (Stein 2020). This example demonstrates how to use PFLOTRAN's process models developed for performance assessment simulations of deep geologic nuclear waste repositories. The complete graphical workflow for this example is shown in Figure 3-21 below. This workflow sets parameters of interest, inserts these parameters into the PFLOTRAN input deck, collects input files, runs PFLOTRAN, and develops and runs a post-processing script. This workflow represents the transformation of the notional workflow expressed in Figure 3-20 into the graphical NGW capability.

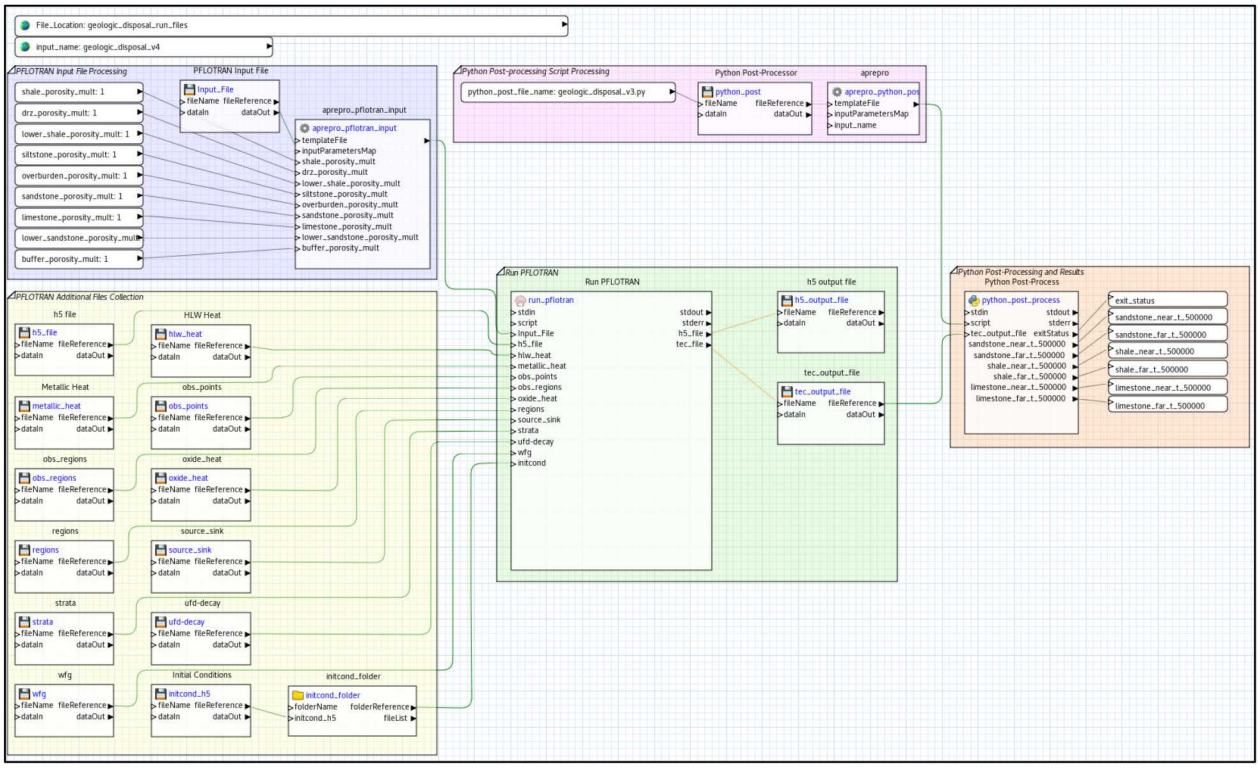

Figure 3-21 Geologic disposal example graphical workflow

A series of NGW analysis workflows for GDSA analysis exemplars, including the short course exercise and the Crystalline Reference Case, were developed in FY 2020 to pilot the use of this capability for the GDSA program. Appendix C details the development of these workflows, provides examples of their use, and proposes a path forward for additional development. The eventual goal of this work is to develop an analysis workflow library that can be made available to the GDSA analysis community.

3.2.2 VoroCrust Meshing

Polyhedral meshing is important for flow and transport codes which include TOUGH2, FEHM, PFLOTRAN, and MODFLOW which are based on the two-point flux discretization. While the solution to flow/transport is stable without an orthogonal mesh, it is not accurate. Geometry conforming Voronoi tessellations are difficult to produce if the geometry is complex. So, if you want orthogonal discretization and you want complex geometry, you need conforming Voronoi tessellations.

VoroCrust is the first provably correct algorithm for conforming Voronoi meshing of non-convex and non-manifold domains with guarantees on the quality of both surface and volume elements. A robust refinement process estimates a suitable sizing field that enables the careful placement of Voronoi seeds across the surface circumventing the need for clipping and avoiding its many drawbacks. The algorithm has the flexibility of filling the interior by either structured or random samples, while all sharp features are preserved in the output mesh. We demonstrate the capabilities of the algorithm on a variety of models and compare against state-of-the-art polyhedral meshing methods based on clipped Voronoi cells establishing the clear advantage of VoroCrust output.

At the beginning of FY 2020, VoroCrust was basically a research C++ code that ran only under Windows. The main focus was to demonstrate that it can automatically handle complex geometries. The algorithm is parallel friendly; however, our implementation was sequential. The code was not optimized and hence it was slow.

The goal of the GDSA funding for VoroCrust is to increase its technical readiness level (TRL) so that it can be deployed in GDSA Framework. In FY 2020, we added new capabilities, and advanced its infrastructure.

The new capabilities added this year include:

- **Eliminating Nearby surface seeds**: VoroCrust Voronoi cells have a bounded aspect ratio. The surface triangles have bounds on angles and aspect ratio. No short edges exist in these triangles. However, the intersection points of the surface sphere triplets could be arbitrarily close to each other. This results in undesired neighbor Voronoi seeds that may cause numerical problems for PFLOTRAN simulations. To address this issue, we implemented an algorithm to detect intersection points that are too close to each other and shrink the associated spheres by introducing random decrease to their radii to move them apart, as illustrated in Figure 3-22. The probability of forming these problematic configurations is low and hence the random sphere shrinkage iterations converge fast. We stop the procedure when with a minimum distance bound of 10% of the smallest associated sphere.

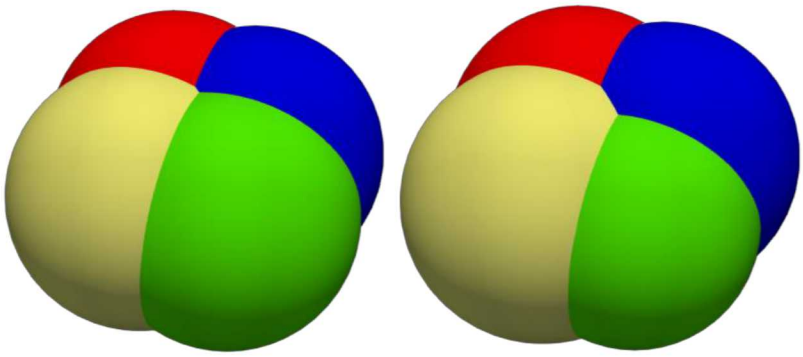

Figure 3-22 Two intersection points of two sphere triplets can be arbitrarily close to each other (left). Shrinking the green sphere resolved this problematic configuration (right).

- **Parallel sphere packing using OpenMP:** VoroCrust starts by covering all the input geometries by solving a maximal sphere packing problem. During this process, VoroCrust selects a random sample from the input geometry, check if it is covered by an existing sphere. If the sampled point is covered by an existing sphere, it is discarded, and another sample is drawn. Otherwise, a new surface sphere is inserted centered on that point. A background grid refinement process helps direct the sampled points toward the uncovered portions of the input geometry. This process can be time-consuming. To improve the speed of this process, we used OpenMP to utilize more than one processor in a shared memory environment so that each processor samples a point to check if it will be inserted or not. The valid samples are then checked against each other sequentially. Moreover, each processor is now in charge of an independent portion of the background grid and hence the grid refinement process is split evenly across processors. The resulting speed up ratio depends on the number of threads involved (which is a user input parameter now). With 12 threads, we recorded speed up ratio of about 8x.
- **Parallel explicit meshing using OpenMP:** After all seeds (near surface and in the interior) are generated, the Voronoi tessellation is uniquely defined by the locations of these seeds. However, PFLOTRAN requires the calculations of the volume and facet areas of each cell. VoroCrust explicitly constructs the Voronoi mesh to be able to calculate these geometric quantities. Since each cell is uniquely defined, each can be constructed independently and hence an OpenMP implementation would have perfect scaling. We simply distribute the cells evenly across

processors and ask each one to construct its assigned cells and estimate the associated geometric quantities for PFLOTRAN.

- **Randomized input:** VoroCrust deploys a random sphere packing problem in the underlying algorithm. We tied the random seed generator with the system clock and now every time VoroCrust runs, it generates a different mesh even if the input geometry did not change. Having multiple meshes for the same geometry is useful in checking the sensitivity of the simulation to the utilized mesh.

In FY 2020 advances were made in the VoroCrust application infrastructure framework for build and testing. We developed a full cross-platform build harness using CMake and we regularly build it on Linux, Windows, and OSX systems.

Regression testing capabilities were added to VoroCrust using the CMake / CTest framework. This enables us to test VoroCrust as we develop new features. This testing framework is undergoing expansion currently to incorporate additional testing capabilities as well as bringing automated nightly testing online.

Quality-of-life improvements to the VoroCrust application were also made this year based on requests from users. The first improvement was to add proper command-line argument processing with proper help messages and best-practices argument handling. We also added in improved output logging to support the user community. This is especially useful when running VoroCrust jobs via batch processing when analysis of the job is done after it has completed.

VoroCrust uses OpenMP to support parallelism but we're working on adding support for additional modes of parallelism. In addition to making OpenMP *optional*, we have also library support for VoroCrust to use the following parallel libraries:

- **MPI** – VoroCrust now supports including MPI headers and code. It does not yet have any algorithms implemented in MPI, but the infrastructure now supports it.
- **Kokkos** – Kokkos is a high-performance parallel library that supports MPI and GPU programming. More information on Kokkos can be found at https://github.com/kokkos/kokkos/wiki

Finally, we developed an official website for VoroCrust which is hosted at https://vorocrust.sandia.gov. The home page is shown in Figure 3-23. The site contains information about the VoroCrust project, provides user documentation, and publication information. Future work on the site includes expanding the user guide and adding a download section to streamline the distribution of the VoroCrust application.

The increased speed of meshing achieved by parallelizing parts of the code was a critical requirement to generating meshes of challenging geometries for PFLOTRAN simulations. VoroCrust meshes are inherently three-dimensional (3D), but all three benchmark problems in LaForce et al. (2020) are comparisons with one- or two-dimensional (1D or 2D) analytical solutions, so the simulation domains must have very high aspect ratios and a large number of cells to mimic 1D or 2D results. For example, the Richards benchmark domain is 100×100×1 m and the tracer benchmark is 0.01×10×0.01 m. The two geological domains simulated in LaForce et al. (2020) also have much greater lateral extent than the vertical thickness between geological surfaces.

Elimination of very close surface seeds has the effect of eliminating some of the small cells and faces in the explicit mesh. This change speeds up PFLOTRAN simulations, as the simulator may need to take very small time steps to resolve fluxes in small cells. Finally, the randomized input allows for push-button generation of multiple meshes of the same problem.

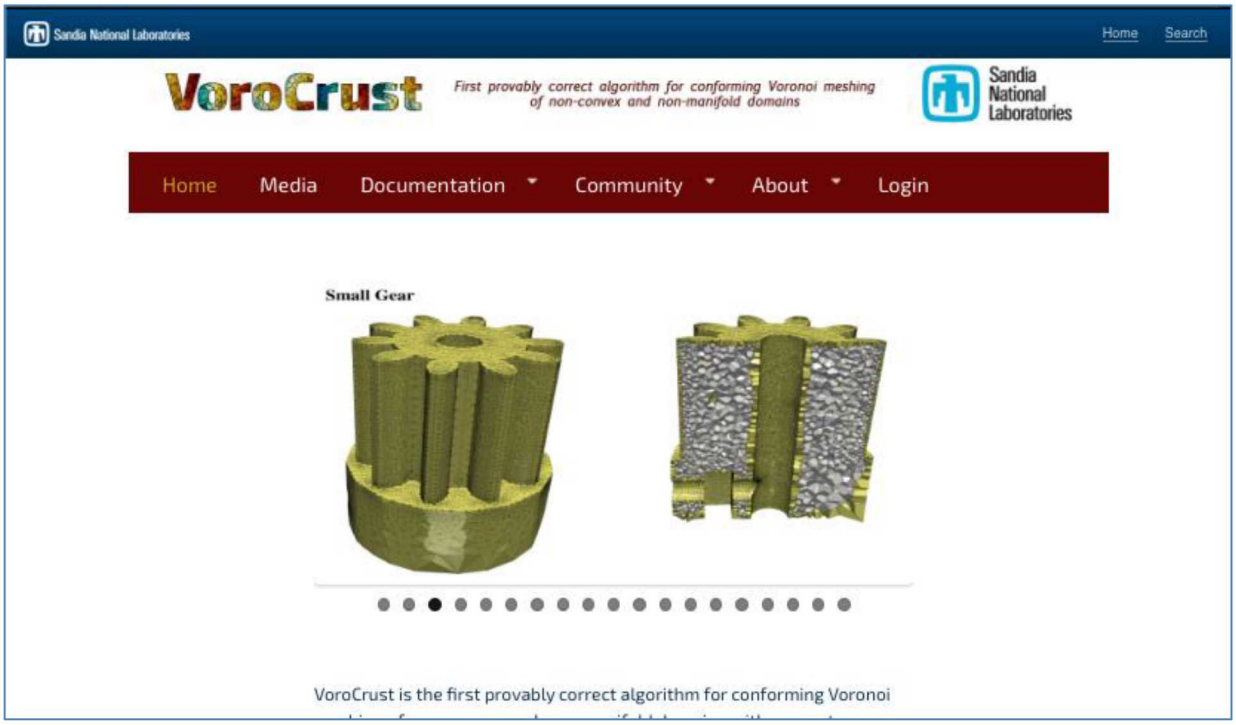

Figure 3-23 VoroCrust website

3.2.3 Geologic Framework Model

3.2.3.1 Overview of Geologic Framework Models

A geologic framework model (GFM) is a quantitative representation of the geologic and hydrologic features of a site or region. For purposes of the GDSA framework, the GFM represents an appropriate volume of rock that surrounds and hosts a generic repository at a scale of a few to several tens of kilometers. Development of a GFM is the first part of a workflow that includes constructing the GFM (based on available data), exporting the relevant geologic features of the GFM for numerical meshing, and using the resulting computational mesh for flow and transport modeling in PFLOTRAN (Sevougian et al. 2019b).

GFMs are being developed for the reference cases to support disposal system modeling of realistic generic geologic systems that are representative of host-rock environments found in the US. Development of this capability began in FY 2019 to support the shale reference case. The region represented in the initial shale GFM was purposely chosen to have a simple geology, with horizontal layers of shale, limestone and sandstone. The simplicity of the geology allowed straightforward testing of the GFM software and the ability to export and mesh the geologic features (Sevougian et al. 2019b; Sevougian et al. 2019c).

A second GFM for an arid unsaturated alluvial basin is being developed at LANL to represent a more complex geologic and hydrologic environment that includes multiple faults and lateral variations in hydrologic properties (Gross et al. 2020). Development of the alluvial basin GFM supports the unsaturated alluvium reference case (LaForce et al. 2020).

3.2.3.2 Geologic Framework Model for the Pierre Shale – A Ductile Sealing Shale

The Pierre Shale and adjacent geologic formations in the northern Great Plains represent a simple layered geologic system with no major tectonic features such as faults. The region represented in the GFM is

relatively large at 69 by 83 km, in order to include a sufficient number of existing borehole datasets to adequately define the stratigraphy of the geologic system. The GFM was gridded at a horizontal resolution of 250 meters and a vertical resolution of 10 meters. Details of development and construction of the GFM are described in Sevougian et al. (2019b) and Sevougian et al. (2019c).

The primary data inputs for the GFM are a digital elevation model, digital geologic maps of the region and borehole data that define the elevations (or depths) of the formation tops across the region. The Pierre Shale in the area of the GFM has a thickness of 450-550 meters. The total thickness of sediments represented in the model is approximately 1500-1800 meters depending on location (Figure 3-1). The stratigraphic sequence is characterized by low-permeability shales that separate major regional aquifers. The upper half of the stratigraphic sequence consists primarily of the Pierre Shale and older shales while the lower half of the sequence consists primarily of carbonate and sandstone aquifers (Figure 3-24). Permeabilities in the sequence range from ~10^{-20} m^2 for shale formations to ~10^{-12} m^2 for the regional carbonate aquifers (Sevougian et al. 2019c). The stratigraphic sequence represented in the GFM, along with permeability values and other hydrologic parameters, were the basis for defining the natural barrier system used in PA simulations for the shale reference case documented in Sevougian et al. (2019c).

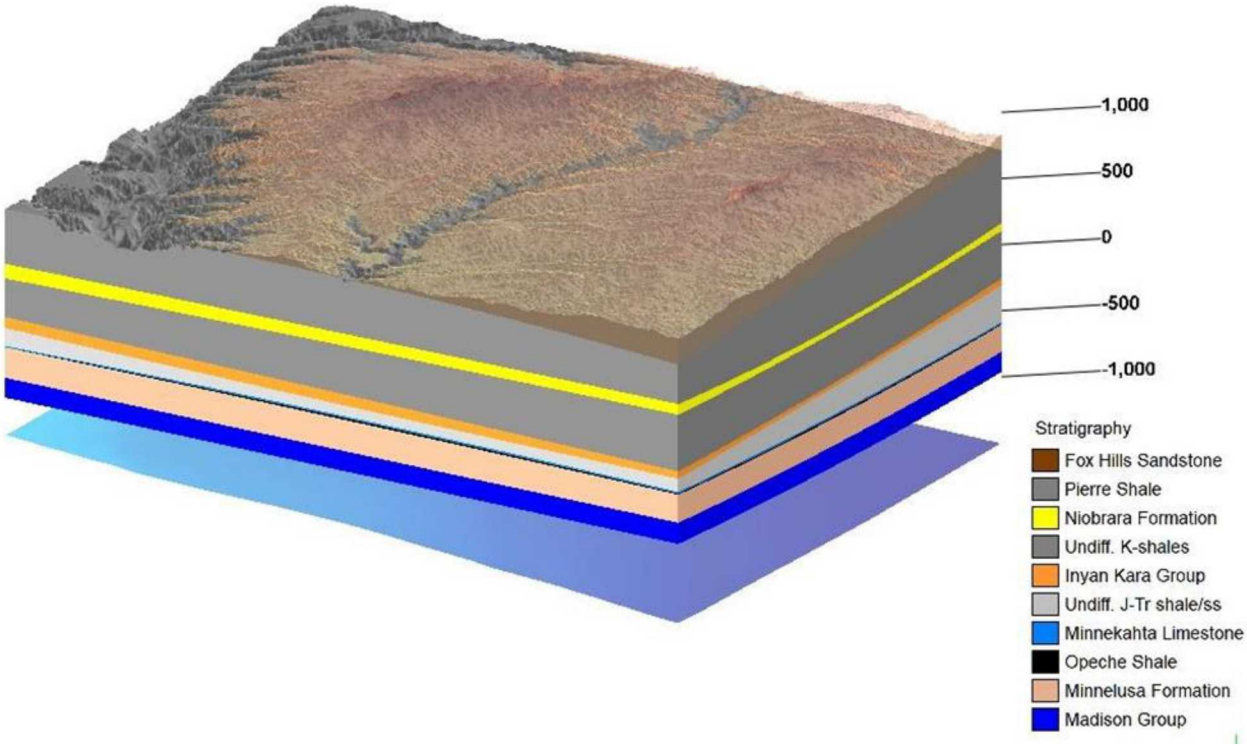

Figure 3-24 Block diagram of the stratigraphy represented in the GFM. View is from the northeast at 15x vertical exaggeration. Vertical scale is elevation in meters relative to sea level. The Fox Hills Formation and parts of the Pierre Shale are at the modern erosional surface. The base of the GFM is the bottom of the Madison Group. The Precambrian surface below the base of the Madison Group is shown for reference but is not part of the GFM.

One of the goals in developing the shale GFM is to demonstrate a workflow that uses the features of the GFM to create a mesh for simulation modeling. Each of the geologic surfaces (formation tops) shown in Figure 3-24 were exported as point cloud data for input into the meshing software. Generating a simulation mesh from the geologic surfaces required a multistep process using python, CUBIT and SCULPT software as described in detail by Sevougian et al. (2019c). The resulting simulation mesh is shown in Figure 3-25.

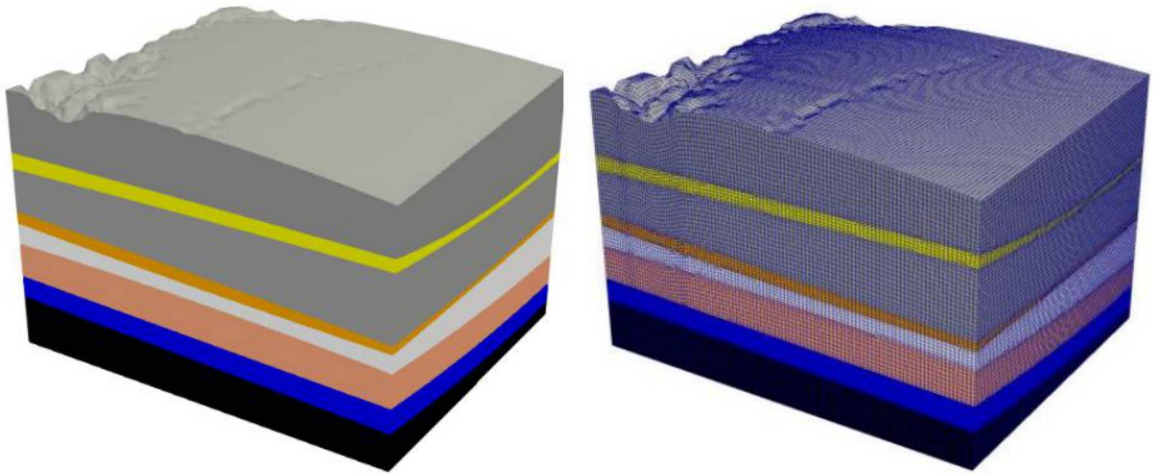

Figure 3-25 Results of the meshing process represented as formation volumes (left) and a hexahedral mesh (right). View is from the northeast at 30x vertical exaggeration.

3.2.3.3 Geologic Framework Model for the Mimbres Basin Unsaturated Zone Alluvial Model

The team at LANL is tasked with building a geologic framework model for a generic unsaturated alluvial basin (Gross et al. 2020). The main focus to date has been developing workflows that incorporate subsurface datasets typically found in alluvial basins, such as seismic and other geophysical surveys, geologic descriptions of deep boreholes, surface geologic maps and shallow water well measurements. The workflow can be applied to build viable GFMs for GDSA and PA analyses.

Alluvial basins in the Basin and Range province are structurally controlled with symmetric grabens or asymmetric half-grabens bounded by master normal faults. Smaller-displacement synthetic and antithetic faults are common and may not intersect the ground surface yet could influence subsurface flow and facies distribution (i.e., physical properties). The alluvial GFM must account for the presence of faults and their impact on sedimentation.

The FY 2020 GFM encompasses a 30 x 20 km area in the Deming sub-basin, which is part of the larger Mimbres Basin of southwestern New Mexico (Gross et al. 2020; Figure 3-26A). The GFM consists of five primary surfaces: three normal faults and two horizons. One horizon is the ground surface and the other the top of bedrock, which corresponds to the base of alluvium where present. For the ground surface we used a point cloud representation of a 10 m resolution digital elevation model resampled to 100m resolution. Structural cross sections (e.g., Figure 3-26B) were used to define the top of bedrock by sampling the contact with synthetic vertical wells at 50m spacing. A three-dimensional (3D) perspective of the GFM is shown in Figure 3-26C. We used the Baker Hughes JewelSuite™ 2019.4 software package to first build the GFM and then apply facies and property modeling parameters.

Once the surfaces are generated in JewelSuite™, the volume is gridded for assigning properties and meshed for computational modeling. Details of the workflow are found in Gross et al. (2020). The meshed volume is shown in Figure 3-27A. The basin-scale 3D grid consists of cells with horizontal dimensions of 200m x 200m and a vertical dimension of 50m. The grid cells are subsequently assigned values of physical properties according to the selected geostatistical modeling method and population parameters. For example, the porosity model in Figure 3-27C was generated using a Sequential Gaussian Simulation (SGS) with a mean of 0.25 and standard deviation of 0.1. It represents an undifferentiated

alluvium (one facies) with isotropic horizontal porosity. In contrast, the SGS permeability model in Figure 3-27D has three stratigraphic layers and a 3:1 horizontal anisotropy aligned parallel to the basin axis. The mean permeability of the middle layer is 1.2 x 10^{-12} m^2. Additional analyses can be performed on the GFM. For example, we generated an alluvial thickness map that shows the geometry and dramatic changes in thickness of the alluvial-fill sediments in the Deming sub-basin (Figure 3-27B). This map can be used to guide the siting of repositories by providing information about geologic buffer thickness and distance from faults.

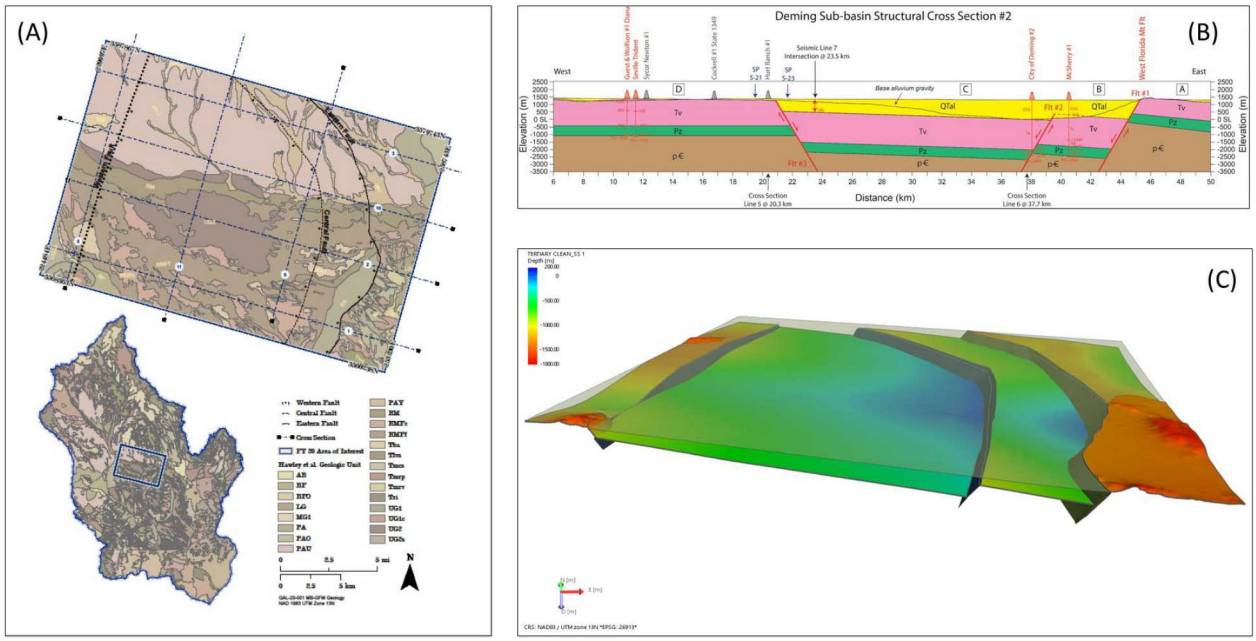

Figure 3-26 (A) Area of interest in the Mimbres Basin, SW New Mexico with geologic map, boundary of GFM and cross section lines used to construct the basin geometry; (B) Example of structural cross section (#2) that was constructed as input for the Unsaturated Alluvial GFM; (C) Surfaces and faults that define the stratigraphic and structural components of the GFM.

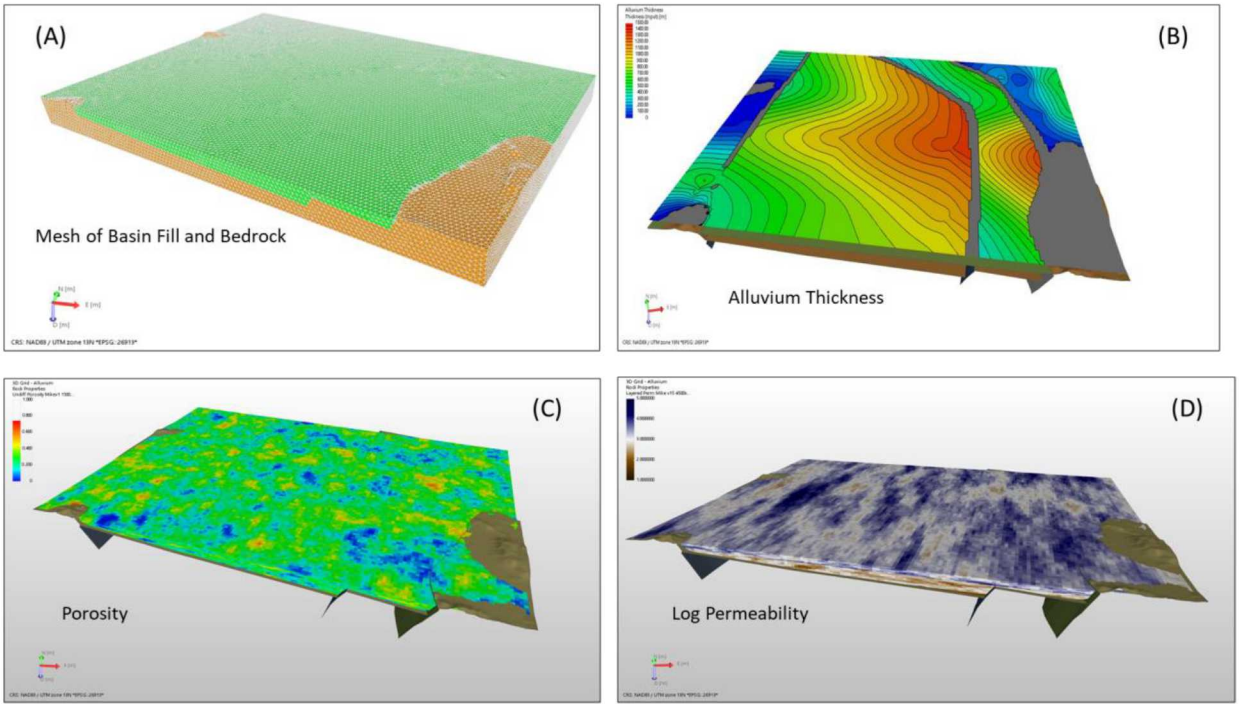

Figure 3-27 (A) Mesh that defines the volume of the Unsaturated Alluvial GFM and subdivision into alluvium (green) and bedrock (brown); (B) Alluvium thickness map derived from the GFM at 100m contour intervals. This type of map provides critical information for repository siting; (C) Geostatistically derived porosity model for undifferentiated alluvium, horizontal isotropic case; (D) Model of geostatistically derived log permeability in mD for layered alluvium, 3x horizontal anisotropic case.

3.2.3.4 Conceptual Model for a Brittle Fractured Shale

The concept of brittle shales as the host rock for the shale reference case was introduced in the Argillite Concepts Workshop as an alternative to the more ductile and sealing shales that have previously been considered (LaForce et al. 2020). Brittle shales are perhaps the most common shale type in the US and occur in most of the major sedimentary basins in the eastern US.

The conceptual model for of a brittle shale, based on the geology of Paleozoic shales in the eastern US, is developed and described in LaForce et al. (2020). Several features and processes inherent in the brittle shale conceptual model distinguish it from the conceptual model for generic ductile shales that was based on the geology of the Pierre Shale. The Pierre Shale has an exceptionally high clay content which dictates several of its properties, including its low mechanical strength and sealing behavior. In contrast, Paleozoic shales have lower clay content (more similar to proposed European shale host rocks) and higher quartz content, which imparts greater mechanical strength, brittle behavior and fracturing.

Interconnected fractures increase the permeability of the shale by several orders of magnitude, from typical values of ~10^{-20} to values of ~10^{-16}, consistent with permeability increases measured in the excavation disturbed zone (EDZ) of European underground research laboratories (URLs). Because most shales have some degree of lithologic layering with different mineralogy and mechanical properties, fracture systems may be organized into a fracture stratigraphy with different fracture characteristic, which has implications for repository siting (LaForce et al. 2020).

3.2.4 Uncertainty Quantification and Sensitivity Analysis

The GDSA Uncertainty Quantification and Sensitivity Analysis work package, SF-20SN01030403, has a Level 3 milestone, M3SF-20SN010304032, to document the advances in uncertainty quantification (UQ) and sensitivity analysis (SA) methods made in the GDSA framework. This year, we focused on four areas:

1. **Further investigation of the crystalline reference case.** This builds from the sensitivity analysis of the crystalline reference case performed in 2019 and documented in SAND2019-13835R, the final report for M2SF-19SN010304031 by Swiler et al. titled "Status Report on Uncertainty Quantification and Sensitivity Analysis Tools in the Geologic Disposal Safety Assessment (GDSA) Framework." As a result of the 2019 investigation, we identified the need for possible indicators of fracture connectivity as well as information about the flow between the repository and the aquifer. These metrics can then be used in SA to help identify why higher peak concentrations happen for certain realizations. To facilitate this, PFLOTRAN added several new quantities of interest that can be reported:

   - Peak concentrations (of I-129 and tracers) in the aquifer at each time step, along with the location of the peaks.
   - Mean travel time from the repository to various locations.
   - Residence time within the repository.
   - Total upward water flux (m^3/yr) from the rock to the aquifer, total water flux (m^3/yr) in the x-direction out the right boundary of the aquifer, and total water flux (m^3/yr) in the x-direction out the right boundary of the crystalline rock. These water fluxes are calculated at each print step.

   The mean travel time metric is documented in Section 3.2.5 and the residence time metric in Section 3.2.6 below. The results of the updated sensitivity analyses with 800 PFLOTRAN runs of the crystalline reference case (20 aleatory samples x 40 epistemic samples) are documented in the M3 milestone report for this year.

2. **Discrete Fracture Networks.** There was a concern that the Discrete Fracture Networks (DFNs) that we had generated using LANL's DFNWorks software were too permeable for the crystalline reference case. As a result, we performed some verification exercises. First, we numerically confirmed the consistency of the number of fractures and fracture area per unit volume in the DFNs with reported numbers from Swedish Nuclear Fuel and Waste Management Company (SKB) of the Forsmark repository site. Then, we performed several calculations to upscale the DFNs to obtain equivalent continuous porous medium (ECPM) results in terms of the hydraulic conductivity tensor values K. We compared the ECPM results for the different K tensor directions that were obtained from upscaling the DFNs with those reported by SKB and found good agreement. The verification exercises we performed are documented in detail in the L3 milestone report for this year.

3. **Multifidelity Uncertainty Quantification.** One significant advance in efficient uncertainty quantification methods for expensive simulations has been a methodology called "multifidelity uncertainty quantification" or MF UQ. The main idea with multifidelity methods is to extract information from a limited number of high-fidelity model evaluations and complement them with a much larger number of a set of lower fidelity evaluations. The final result is an estimator with a much lower variance: a more accurate and reliable estimator can be obtained at lower computational cost. These approaches typically rely on a strong correlation between low and high-fidelity results and the use of control variates. The mathematics behind these approaches can be found in [Geraci, et al.; Giles; Gorodetsky et al.].

Multifidelity approaches can be used in many ways in the *GDSA Framework.* For example, one could have the same PFLOTRAN model but have two different mesh resolutions for it: this would be referred to as a "multilevel" study. Another possibility is to have two codes such as PFLOTRAN and TOUGH2 serving as the high and low fidelity models, respectively. For this year's milestone, we demonstrated the idea of multifidelity UQ on a test problem involving a tank. There were five levels of fidelity according to five mesh discretizations. The results are described in the milestone report.

4. **Uncertainty Quantification Workflow.** UQ workflows are not trivial to define and get running, even when using tools such as Dakota to generate nested studies involving sampling loops over both aleatory and epistemic samples. The analyst has to spend a significant amount of time writing scripts to interface the sample values to PFLOTRAN, extract the results, and put the entire workflow on a high-performance computing platform. Further, as the quantities of interest increase and many vectors of results are generated for each simulation, plotting and aggregating the results in a variety of ways (e.g. averaging over epistemic or aleatory slices as a function of time) becomes very involved. To address this, the GDSA workflow was developed this year. This workflow couples Dakota, PFLOTRAN, and SAW (the Sandia Analysis Workflow software) to present the user with a unified GUI where the actual workflow can be dictated in an easy-to-use graphical format. This workflow also allows greater reproducibility and traceability of the actual files and scripts used for a particular study. This year, we demonstrated the UQ workflow for a GDSA study involving both aleatory and epistemic sampling.

3.2.5 Tracer Method for Quantifying Repository Hydraulic Characteristics

The effective permeability of a repository, or it's resistance to flow, is an example of a repository characteristic potentially affecting repository performance. In PA calculations, however, a simple uncertainty distribution of repository permeability cannot be prescribed because it is a function of many internal features (e.g., buffer, DRZ, layout) and their characteristics, interactions, and uncertainties. Even if we could calculate the permeability of the repository for each realization, it likely would not be a particularly powerful indicator of repository performance because it is not a direct indicator of how long it would take a conservative radionuclide like I-129 to migrate beyond the DRZ after waste package breach. That measure is additionally affected by buffer porosity, hydraulic gradients, and the permeability of the surrounding host rock.

A more direct method for determining such characteristics is to inject a tracer and measure what happens. A stable conservative tracer is injected into the repository region at the beginning of the simulation. The total mass of tracer remaining in the region is then tracked over time. This allows time-series calculations of the mean residence time (MRT) of the injected tracer in the repository and the net mass flux (NMF) of the tracer out of the repository. The inverse of MRT is the replacement rate or flush rate. If the MRT is high, the flush rate is low.

For the crystalline repository PA model, the residence time of a solute in the repository region can vary significantly between realizations because the stochastically-generated discrete fracture networks (DFNs) are different for each aleatoric realization. Also, the permeabilities and porosities of the buffer and DRZ are different for each epistemic realization. In the current GDSA crystalline repository reference case, the overall DFN characteristics (e.g., fracture densities and distributions of apertures, sizes, and orientations) are designed to be identical among the DFN realizations; however, for each DFN realization the fractures that connect to the DRZ are in different locations, the number and sizes of fractures that connect to the DRZ are different, and the connections of these fractures to faults and other fractures in the host rock are different. Therefore, by random chance, some realizations have repositories with stronger hydraulic connections to nearby faults.

The cumulative MRT of an initial tracer of a model region is calculated by tracking the total mass of the tracer in the region over time (t) using the following equation

$$\mathrm{MRT}(t) = \int F(t)\, dt \tag{29}$$

$F(t)$ is the fraction of initial pulse remaining, calculated from

$$F(t) = \frac{N(t) - N_b}{N_o - N_b} \tag{30}$$

$N(t)$ is the total mass of the tracer in the region at a given time, N_o is the initial total mass of the tracer in the region, and N_b is the total background mass of the tracer in the region.

The cumulative MRT will increase with time until essentially all the tracer pulse is flushed from the region. If the simulation does not provide sufficient time for essentially complete flushing, the temporally-independent MRT property of the region cannot be calculated. For this reason, it may be better to calculate the median residence time, i.e., the time required for half of the tracer to exit the region.

The MRT is directly related to the volume of water in the region. Consequently, if the porosity of the region is uncertain, then the variation in MRT between realizations will largely be due to porosity uncertainty. Uncertainty in other factors affecting the MRT, such as water fluxes at the boundary of the region, may be swamped by uncertainty in porosity.

The net mass flux, NMF (kg yr^{-1}), of the tracer out of the region is calculated from

$$\mathrm{NMF}(t) = \frac{dN(t)}{dt} \tag{31}$$

Compared to MRT, NMF provides a more direct measure of the hydraulic connection of the repository to the host rock mainly because it is not as sensitive to the volume of water in the repository.

A set of 20 aleatoric realizations of the crystalline repository reference case was used to calculate the MRT and NMF characteristics of the repository region for sensitivity analyses. A conservative tracer was initiated in the repository at a concentration of 0.1 M. The repository region was defined as a rectangular box that tightly encompassed the repository and DRZ. The MASS_BALANCE_FILE option of PFLOTRAN was used to calculate the mass remaining in the repository at eight different simulation times.

Figure 3-28 plots the cumulative MRT for each realization. The mass of remaining initial tracer in the repository over time is plotted in Figure 3-29. In general, approximately half of the initial tracer is gone in these simulations after about 50,000 years, and more than 80% of the mass is gone after one million years. At one million years, the cumulative MRT calculations range from 230,000 years to 360,000 years. The primary reason for this variability is the variability in the porosity of the buffer (Swiler et al. 2020).

Figure 3-30 plots the NMF of initial tracer for each realization. This variable is much less affected by the volume of water in the region. Consequently, the variability observed in the NMF is primarily due to random realization of fracture sizes, orientations, locations, and connections in the DFNs.

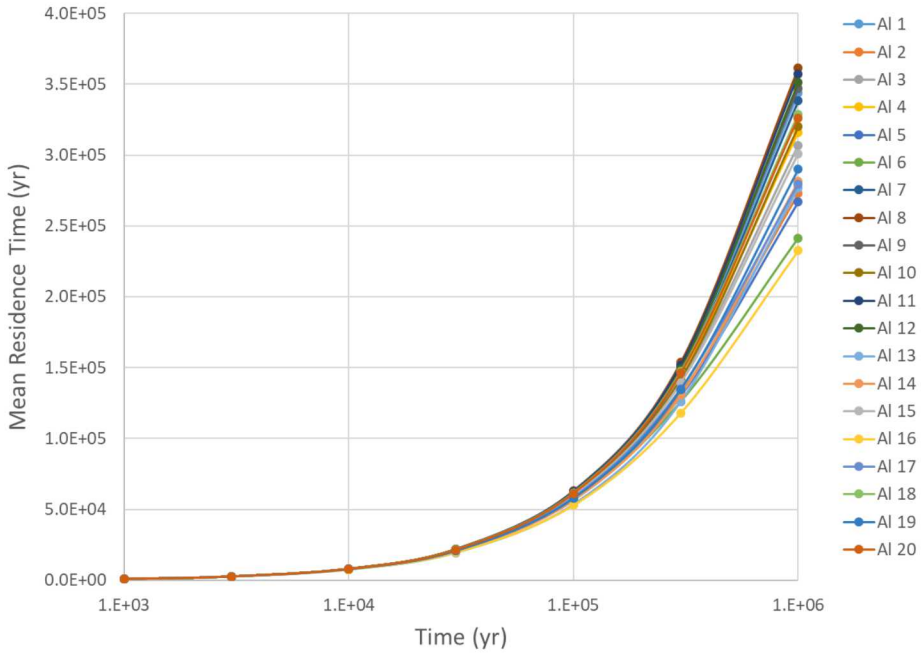

Figure 3-28 Cumulative mean residence time (MRT) of a conservative tracer in the repository region for 20 aleatory (Al) realizations of the crystalline repository reference case

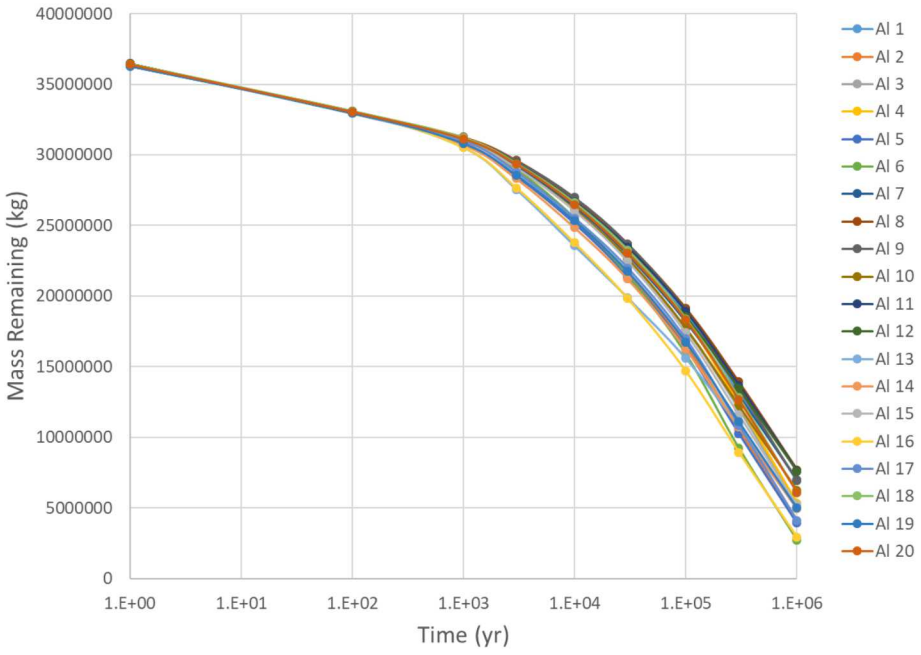

Figure 3-29 Mass of conservative tracer remaining in the repository region over time for 20 aleatory (Al) realizations of the crystalline repository reference case

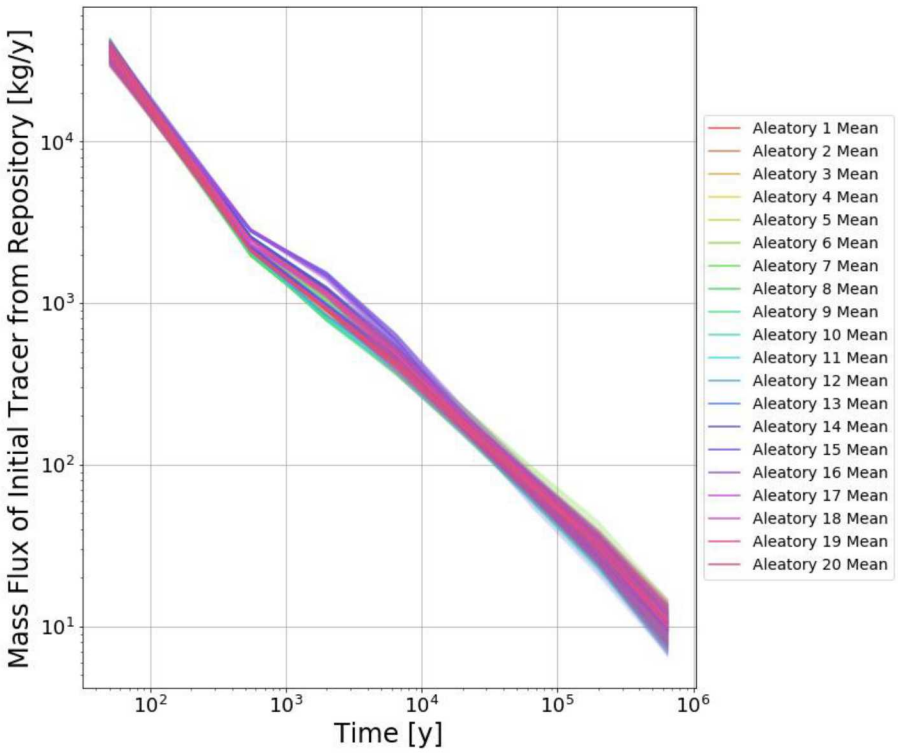

Figure 3-30 Net mass flux (NMF) of initial conservative tracer out of the repository region over time for 20 aleatory realizations of the crystalline repository reference case

3.2.6 Tracer Method for Quantifying Mean Travel Time

Like repository mean residence time (MRT) (Section 3.2.5), mean travel time from the repository to an aquifer is a bulk characteristic that can have an important effect on repository performance. The ability to measure mean travel time and its variability in a PA calculation allows quantification of the extent that mean travel time contributes to uncertainty in repository performance.

In the case of crystalline rock, mean travel time from the repository through the host rock to an aquifer is affected by the various sizes, orientations, and connections of fractures and fracture zones along the flow path. These features can vary significantly from one DFN realization to the next. This variability, as explained in some depth in Section 3.2.5, occurs because the stochastically-generated DFNs in the crystalline host rock are different for each aleatoric realization. In addition, because a portion of the tracer at the receptor location likely migrates through parts of the aquifer, the mean travel time is also affected by characteristics of the aquifer, e.g., aquifer permeability.

Mean travel time, like mean residence time, can be directly measured using tracers. Identical concentrations of two conservative tracers are artificially and continuously injected at a constant rate at the starting point. The only difference between the two tracers is that one of them decays or ingrows exponentially over time since injection. Because the movement of these tracers within the domain is identical, the difference in concentration at a distant location is solely due to the mean time since tracer injection. This measure of time is considered the mean travel time (MTT) of these tracers.

Exponential decay (or ingrowth) is described by the equation:

$$C(t) = C_o e^{-rt} \tag{32}$$

where C is the concentration at time t, C_o is the initial concentration, and r is the rate of the reaction. The rate can be calculated from the half-life $t_{1/2}$ using the equation:

$$r = \frac{\ln(2)}{t_{1/2}} \tag{33}$$

For ingrowth, $t_{1/2}$ and r are negative. Solving for t gives:

$$t = \frac{-\ln\left({}^{C(t)}/_{C_o}\right)}{r} \tag{34}$$

In terms of MTT, C_o is analogous to the concentration of stable tracer C_s, and $C(t)$ is analogous to the concentration of unstable (decaying or ingrowing) tracer C_u. Thus, MTT is estimated from the equation:

$$\text{MTT} = \frac{-\ln\left({}^{C_u}/_{C_s}\right)}{r} \tag{35}$$

This equation assumes that initial background concentrations of these tracers, the ingrowing concentrations of an unstable background tracer, and trace concentrations of these tracers flowing into the domain from flux boundaries are negligible compared to the concentrations observed at the monitor location.

Figure 3-31 provides an example of MTT over time for tracers migrating from the repository to the overlying aquifer for one realization of the crystalline repository reference case. In this example, the tracers are injected evenly and continuously throughout the repository at a volumetric rate of 1 mL yr^{-1}, each at a concentration of 0.01 M. A very low volumetric rate is set to prevent significant effects on pressure and flow. The unstable tracer is set to ingrow at a half-life of -100,000 yr. At that rate, a tracer concentration, if its initial concentration were contained in a cell, would increase by a factor of 1024 (i.e., 2^{10}) in one million years. The monitor location in this example moves around in the overlying aquifer based on the location of the maximum I-129 concentration at each time step. The maximum I-129 concentrations and their locations over time were monitored and recorded using the new PFLOTRAN aggregate function described in Section 3.1.10.

As shown in Figure 3-31, MTT increases with time in this application. At 10,000 years, it is approximately 3,600 years, and at one million years it is around 690,000 years. These MTT values correspond to 36% and 69% of simulation time, respectively. The lower percentage at 10,000 years is due to a larger proportion of the tracer masses at the monitor location taking a faster flow path. At late times, there is enough time for slower pathways to contribute to tracer masses at the location of maximum I-129. This type of information is expected to be useful in sensitivity analyses to help identify and quantify contributions to repository performance metrics.

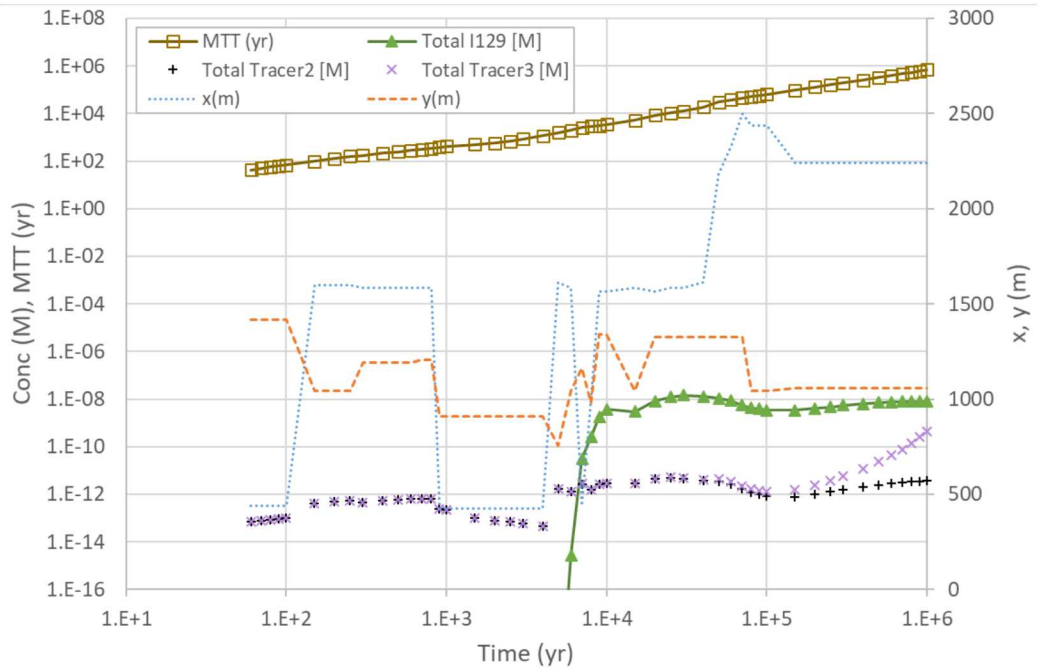

Figure 3-31 Mean travel time (MTT) of stable (Tracer2) and ingrowing (Tracer3) conservative tracers from the repository region to the location (x, y) of maximum I-129 concentration in the aquifer for a single realization of the crystalline repository reference case

3.2.7 Biosphere

Over the years, the GDSA team has developed repository reference cases for different host rocks. The performance of a reference case has primarily been assessed using peak concentrations of radionuclides in aquifers. Because reference case development has generally focused on improving simulation of features and processes in the EBS and geosphere, peak aquifer concentrations have served adequately in sensitivity analyses to quantify the effects of these features and processes on performance (e.g., Swiler et al. 2019).

The ultimate measure of performance for a nuclear waste repository, however, is the effect on the biosphere, especially on human health. Currently, the GDSA Framework biosphere model consists of an ingestion dose model from drinking contaminated well water (Mariner et al. 2017, Section 3.2.3). That model can be used to simulate Example Reference Biospheres (ERBs) 1A and 1B of the International Atomic Energy Agency (IAEA 2003). In addition, it can account for the dose effects of short-lived unsupported radionuclides such as radon-222. Unsupported radionuclides are those not explicitly simulated in PFLOTRAN flow and transport. Inclusion of the unsupported radionuclides in the dose calculations is based on the model of (Olszewska-Wasiolek and Arnold 2011).

In FY 2020, a new GDSA work package at Pacific Northwest National Laboratory (PNNL) was created to develop a requirements document and implementation plan for a comprehensive biosphere model for GDSA Framework. This model will be open source, will be coupled to PFLOTRAN, and will be consistent with international recommendations and guidance for such models built for deep geological repositories.

Figure 3-32 shows a schematic diagram of the various pathways planned for inclusion in the biosphere model. These pathways cover a large number of biosphere FEPs. A detailed description of the plans for the model is documented in Condon et al. (2020).

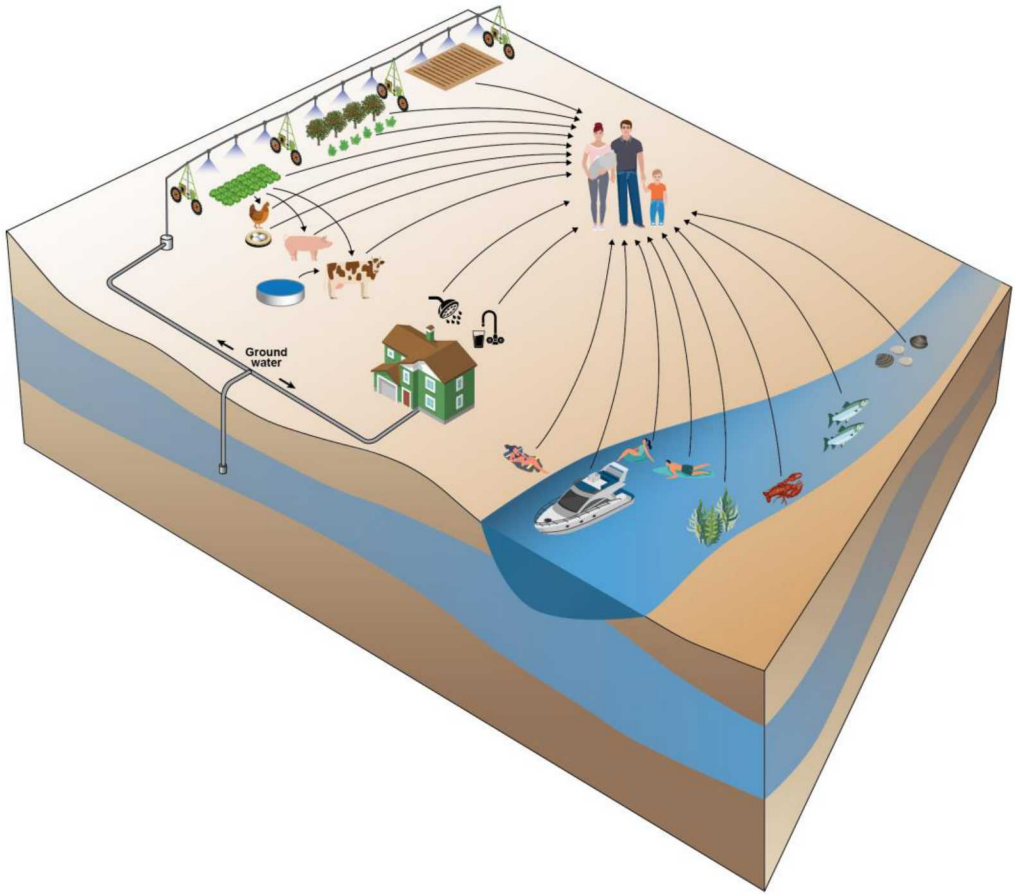

Figure 3-32 Schematic diagram of pathways to be included in new biosphere model being developed for GDSA Framework (graphic from Condon et al. 2020)

3.2.8 DECOVALEX-2023 Task F, Performance Assessment

The DECOVALEX project is an international research and model comparison collaboration for advancing the understanding and modeling of coupled thermo-hydro-mechanical-chemical (THMC) processes in geological systems (decovalex.org). Task F of DECOVALEX-2023 is a new task that will focus on comparison of models and methods used for post-closure performance assessment. Members of the GDSA team at SNL are leading this effort.

Two hypothetical repositories will be modeled in Task F, one in crystalline rock and the other in salt. Over the next four years, this task promises to provide numerous opportunities for learning new modeling approaches, developing new models for use in PA simulations, testing uncertainty and sensitivity analysis methods, comparing PA methods, and networking with modelers in other programs. Additional information on the plans and status of this work is documented in LaForce et al. (2020).

3.2.9 Computing Resources

The GDSA team purchased 16 nodes (36 cores/node, 192 GB RAM/node) on the new SNL HPC cluster Boca this year. As queue times for the shared Skybridge SNL HPC cluster get longer and longer, this purchase promises to improve GDSA PA productivity for years to come. All modules on Skybridge are available on Boca. Ownership of these nodes ensures that they will always be available to the GDSA group. In addition, the GDSA team has access but not exclusivity to the free nodes on Boca.

3.3 User Group

GDSA Framework is being developed for DOE and its subcontractors. Many of the software components of GDSA Framework are open source, including PFLOTRAN, Dakota, and dfnWorks. These codes are utilized by a community of users from around the world for work related to, and unrelated to, repository performance assessment (e.g., Hammond and Lichtner 2010, Chen et al. 2013, de Vries et al. 2013, Karra et al. 2014, Gardner et al. 2015, Kumar et al. 2016, Zachara et al. 2016, Avasarala et al. 2017, Trinchero et al. 2017, Shuai et al. 2019)

This section reviews the open source strategy, the PFLOTRAN user community, and how investment in GDSA Framework development is benefitting not only nuclear waste repository performance assessment, but the entire field of subsurface simulation.

3.3.1 Open Source

Open source software licensing governs the free distribution of source code and/or binaries among a group of software developers and users. PFLOTRAN utilizes the GNU LGPL (lesser general public license) which states that the code may be distributed and modified as desired, but any changes to the original source code must be free and publicly available. On the other hand, LGPL allows anyone to link a proprietary third-party library to the code or develop a graphical user interface on top of the code for profit. Further details are provided in Mariner et al. (2019, Section 2.3.4.1).

There are many benefits to open source collaboration, especially when taxpayer funds support much of the code development. First, it encourages collaboration among a diverse team of developers. This collaboration pushes the code to the masses who can help test and debug the code while providing feedback regarding user interaction. Open source provides transparency that exposes implementation details that are often critical for scientific reproducibility and quality assurance. These details are often deliberately or unintentionally omitted from user documentation, journal publications and reports. From a financial standpoint, open source allows developers to pool funds across a diverse set of projects funded in academia, government laboratories or the private sector. In addition, funding that would be spent on licensing fees can be redirected towards development. Finally, although the most fit codes can survive under any licensing option, open source may provide a more level playing field for natural selection to run its course.

PFLOTRAN development is currently supported by multiple developer groups from around the world. DOE is perhaps the largest proponent of PFLOTRAN development through its national laboratories funded by the DOE Offices of Environmental Management, Nuclear Energy, and Science. In addition, private sector companies such as OpenGoSim (opengosim.com) have invested development in support of oil and gas and carbon sequestration efforts, while Amphos21 has developed PFLOTRAN capability for nuclear waste disposal (e.g., de Vries et al. 2013, Iraola et al. 2019).

3.3.2 International User Community

PFLOTRAN's open source licensing and accessible distribution facilitate collaboration amongst a broader U.S. and international community. This broad user community enhances the development of PFLOTRAN by sharing conceptual models, incorporating novel physicochemical algorithms, optimizing code performance, debugging problematic issues, and generating grass-roots publicity, all of which benefit DOE in return.

The PFLOTRAN website at www.pflotran.org directs interested parties to the online documentation and the Bitbucket repository (including source code and documentation build status and code coverage). Developer and user mailing lists are managed through Google Groups.

Estimating the size and extent of the PFLOTRAN user community is relatively difficult due to the inability to track downloads on Bitbucket. However, through Google Analytics, the hits on the PFLOTRAN website are tracked which provides a qualitative estimate (Figure 3-33) and demonstrates that the PFLOTRAN user base is multi-national.

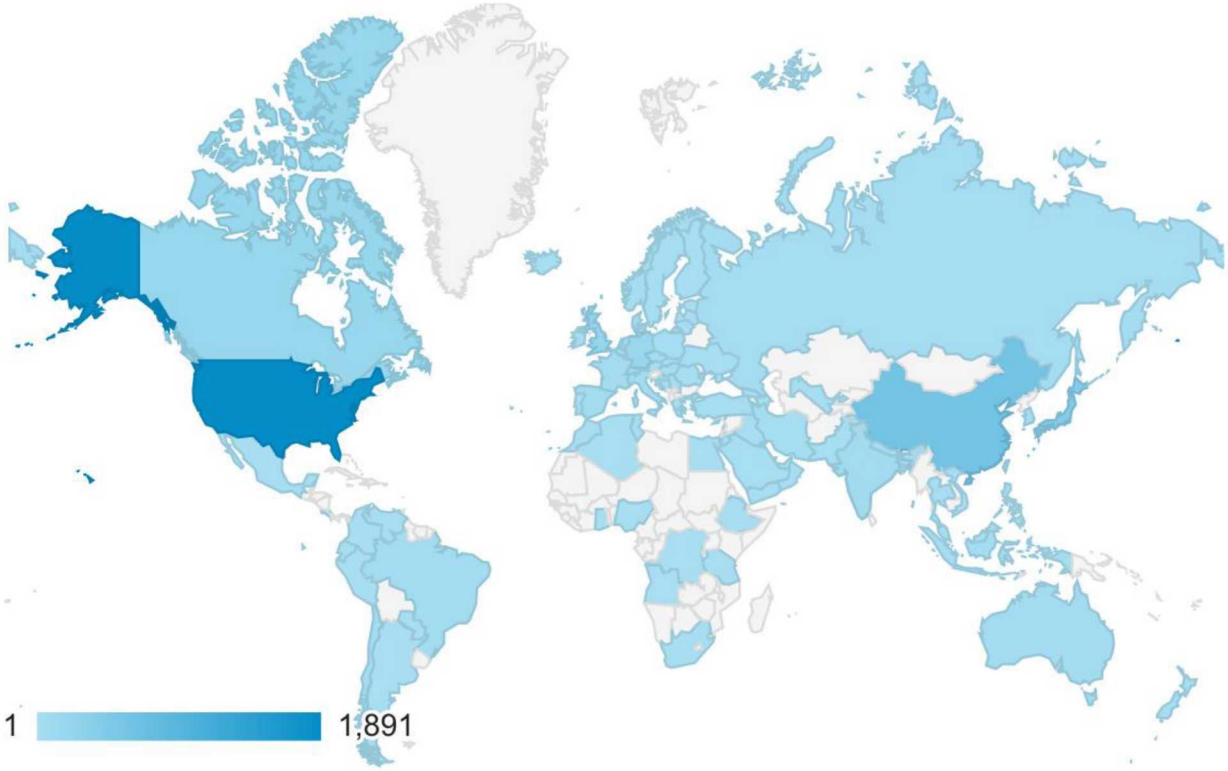

Figure 3-33 User count on the PFLOTRAN website around the world between August 1, 2019 and August 1, 2020, colored by country

3.3.3 GDSA Framework Website

The GDSA team continues to support and develop the GDSA Framework website at pa.sandia.gov. This website is publicly available. The home page is shown in Figure 3-34.

The purpose of the website is to:

- Describe GDSA Framework, its capabilities, and the objectives behind its development
- Provide recent reports for downloading
- Provide links to software used in GDSA Framework (e.g., PFLOTRAN, Dakota, dfnWorks)
- Identify collaborators involved in GDSA Framework development
- Announce upcoming events (e.g., PFLOTRAN short courses)
- Provide contact information

Figure 3-34 GDSA Framework website (pa.sandia.gov)

3.3.4 SFWST Document Archive

The GDSA team continues to improve and maintain the SFWST Document Archive (SDA). The SDA is a restricted-access SharePoint website that serves as a document repository for reports generated in:

- NE 81, Office of SFWST
  - Disposal Research (DR)
  - Storage and Transportation (S&T)
- NE 82, Office of Integrated Waste Management (IWM)
- 2019 SFWD Annual Meeting in Las Vegas

The SDA contains copies of both UUR (unclassified unlimited release) and unclassified limited release (ULR) deliverable documents and concise information about their pedigree (e.g., "downloaded from OSTI," "best available draft from author," etc.) and their release status (e.g., "ULR," "internal use only, do not cite or release," etc.). The archive is a searchable and sortable resource for SFWD participants; however, "Non-Public" archives are restricted as needed. The "Public" archives are available to all SFWD staff, DOE employees, and contractors.

In FY 2020, the search tools were improved for the Public NE 81 archive. Two search tools were developed, one to search for strings in the content of the documents and one to search the metadata. The metadata search tool includes a filter app that allows for further search refinement, as shown in Figure

3-35. Metadata fields include fiscal year of publication, first author, milestone identification number, lab, file type, and others.

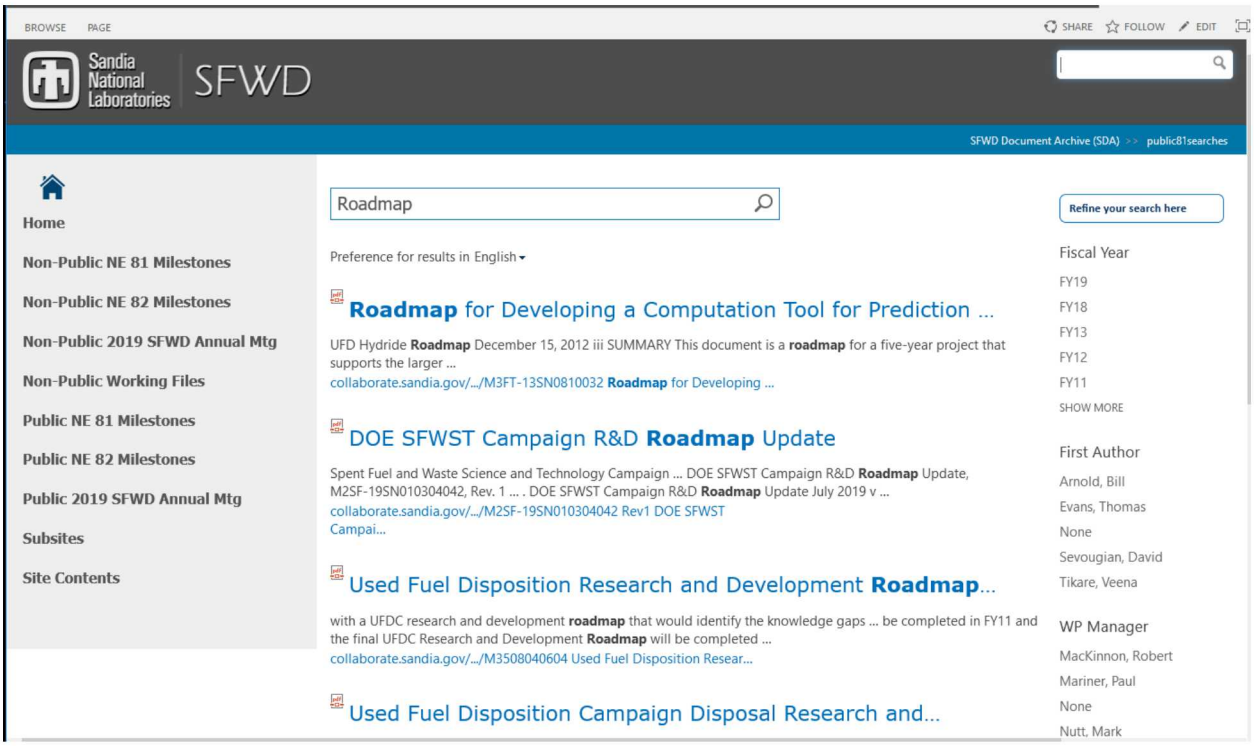

Figure 3-35 Demonstration of the new metadata search and filter tool for the SFWST Document Archive

4. DISPOSAL RESEARCH R&D ROADMAP

The 2019 update of the Disposal Research R&D Roadmap evaluated the progress, priorities, and remaining gaps in disposal research R&D activities (Sevougian et al. 2019a). Section 4.1 summarizes ongoing (and gap) GDSA PA activities in the Roadmap Database, and Section 4.2 identifies the FY 2020 GDSA efforts related to those PA activities.

4.1 Findings of the 2019 Roadmap Update for GDSA

Activities defined and tracked in the Roadmap Database are a collection of specific disposal research objectives focused on improving our knowledge of FEPs and how they affect repository performance. These activities include:

- Collecting and measuring the properties of features (e.g., radionuclides, waste forms, waste package, buffer, DRZ, repository layout, host rock, etc.) and their associated uncertainties
- Identifying and modeling important processes (e.g., flow of heat and groundwater, waste package degradation, waste form degradation, radionuclide adsorption, buffer evolution, etc.) at small scale and/or in repository simulations
- Estimating the magnitudes, consequences, and probabilities of events that might affect repository performance (e.g., criticality, disruptive events)
- Developing tools and processes to propagate uncertainties in repository performance calculations and to enhance sensitivity analysis

A total of 17 activities were defined for GDSA PA in the 2019 Roadmap update exercise (Sevougian et al. 2019a). They are listed in Table 4-1.

Table 4-1 GDSA PA activities in the Roadmap Database of the 2019 Disposal R&D Roadmap update

Activity	*Gap	Name
P-01		*CSNF repository argillite reference case*
P-02		*CSNF repository crystalline reference case*
P-03		*CSNF repository bedded salt reference case*
P-04		*CSNF repository unsaturated zone (alluvium) reference case*
P-05		*Disruptive events*
P-06		*(Pseudo) colloid-facilitated transport model*
P-07		*Intrinsic colloid model*
P-08	*	*Other missing FEPs (processes) in PA-GDSA*
P-09		*Surface processes and features*
P-10		*Uncertainty and sensitivity analysis*
P-11	*	*Pitzer model*
P-12		*WP degradation model framework*
P-13	*	*Full representation of chemical processes in PA*
P-14		*Generic capability development for PFLOTRAN*
P-15	*	*Species and element properties*
P-16	*	*Solid solution model*
P-17	*	*Multi-component gas transport*

4.2 Alignment of FY 2020 GDSA Efforts with 2019 Roadmap Activities

As indicated in Section 3, there were many advances in GDSA PA capabilities in FY 2020. In addition to those advances, there was planning for the near term and longer term, building of infrastructure, and integration across SFWST Disposal Research R&D. This section examines how GDSA efforts in FY 2020 align with the GDSA PA activities identified in the 2019 Roadmap update and how several of the FY 2020 GDSA efforts go beyond the Roadmap activities to support development of the GDSA framework.

The PA activities in the Disposal R&D Roadmap Database (Table 4-1) provide objectives for improving the simulation of physical processes in GDSA Framework. Table 4-2 lists the major GDSA efforts in FY 2020 and maps most of them to the PA activities in the Roadmap Database. This mapping indicates that a large number of the PA activities in the Roadmap Database received attention in multiple FY 2020 GDSA efforts. Those that received little or no attention in FY 2020 were colloids (P-06, P-07), Pitzer modeling (P-11), and solid solution modeling (P-16).

Not all FY 2020 GDSA efforts listed in Table 4-2 were aimed at addressing GDSA PA activities in the Roadmap Database. Several of them advanced the GDSA framework in other ways. They include advances in workflow processes, code development infrastructure, HPC resources, and planning for future GDSA Framework development. Those advances directly facilitate the ability of the GDSA development team to address the various GDSA PA objectives.

In addition to listing and mapping the various FY 2020 GDSA efforts to specific GDSA PA activities in the Roadmap Database, Table 4-2 attempts to identify the major parties that participated in the FY 2020 GDSA efforts. GDSA activities commonly require careful integration between SNL GDSA work packages and other parties. Table 4-2 also maps the FY 2020 GDSA efforts to the newly developed 5-Year Plan thrusts. The planned GDSA thrusts are discussed in Section 5.

Table 4-2 FY 2020 GDSA efforts mapped to GDSA Roadmap activities and 5-Year Plan GDSA thrusts

FY 2020 GDSA Efforts	FY 2020 Participants	Roadmap Database PA Activity	Near-Term GDSA Thrusts
5-Year disposal research R&D plan (Section 5.1)	SNL	-	All
Agile and Jira code management system (Section 3.1.1)	SNL	-	G03
Biosphere modeling (Section 3.2.7)	PNNL, SNL	P-08	G01, G04
Buffer and DRZ evolution (Section 3.1.8)	SNL	P-14	G01
Calculation of bulk transport characteristics for stochastically-affected regions (Sections 3.2.5 and 3.2.6)	SNL	P-02, P-10	G01, G02
Crystalline reference case development (Swiler et al. 2020)	SNL	P-02, P-10	G02, G04
DECOVALEX-2023 Task F: Performance assessment (Section 3.2.8)	SNL, LBNL, LANL, International	P-02, P-03, P-05, P-12	G02, G04
dfnWorks integration (Swiler et al. 2020)	SNL, LANL	P-02, P-10, P-14	G01, G02
Dynamic K_D / smart K_D modeling (Section 3.1.5)	SNL, LBNL	P-13, P-15	G01
Fuel matrix degradation (Section 3.1.7)	SNL, ANL	P-13, P-14	G01
Geologic Framework Model (Section 3.2.3)	SNL, LANL, INL	P-01, P-04, P-09	G03, G04, G05
High-temperature concepts for shale repository (Stein et al. 2020)	SNL, LANL, LBNL, ORNL	P-01, P-12	G04
High-temperature reference case modeling (LaForce et al. 2020)	SNL, ORNL	P-08, P-12, P-13, P-14	G01
HPC resources augmentation (Section 3.2.9)	SNL	-	G03
Next Generation Workflow graphical interface for GDSA Framework simulations (Section 3.2.1)	SNL	-	G02, G03
PFLOTRAN convergence (Section 3.1.4)	SNL	P-01, P-02, P-03, P-04, P-17	G01
Process model coupling requirements, guidelines (Section 3.1.3)	SNL	-	G03
QA toolbox and test suite development (Section 3.1.2)	SNL	-	G03
Release of PFLOTRAN version 3.0 (Section 3.1.1)	SNL	-	G03
Salt reference case development (LaForce et al. 2020)	SNL	P-03	G04
SFWST Document Archive improvements (Section 3.3.4)	SNL	-	G03
Spatially-observant performance metric (AGGREGATE function) (Section 3.1.10)	SNL	P-02, P-10	G02
Temperature-dependent thermal conductivity (Section 3.1.9)	SNL	P-14	G01, G04
Uncertainty and sensitivity analysis (UQ/SA) (Section 3.2.4)	SNL	P-02, P-10	G02
UQ/SA international (Swiler et al. 2020)	SNL, International	P-01, P-02, P-10	G02
VoroCrust meshing (Section 3.2.2)	SNL	P-01, P-02, P-03, P-04, P-09	G01, G04
Waste package degradation (Section 3.1.6)	SNL	P-12, P-13	G01

5. FIVE-YEAR PLAN FOR DISPOSAL RESEARCH R&D

5.1 5-Year Plan

In FY 2020, DOE requested development of a 5-year plan for high priority activities of the SFWST Campaign Disposal Research (DR) R&D activities. As requested, this plan was prepared and delivered to DOE. The cover is shown in Figure 5-1. For each DR R&D technical area, evaluation and prioritization of current and planned activities are discussed and schedules are outlined. This plan will be revised each year to align with changes in objectives and funding.

For GDSA, five primary thrusts were identified for the near term (1-2 years):

- Advanced coupled process simulation capabilities,
- State-of-the-art uncertainty and sensitivity analysis,
- Traceable, user-friendly workflow for GDSA Framework,
- Repository systems analysis for various disposal concepts and selected host rocks, and
- Development of geologic models with interactive, web-based visualization.

Longer term (3-5 years) thrusts include multi-fidelity modeling, in-package chemistry, gas flow in the EBS, cement seal evolution, new repository designs, and preparation for site applications. A more detailed description of the near-term thrusts is provided in Appendix D. Section 5.2 addresses how current efforts and Roadmap activities align with these near-term thrusts.

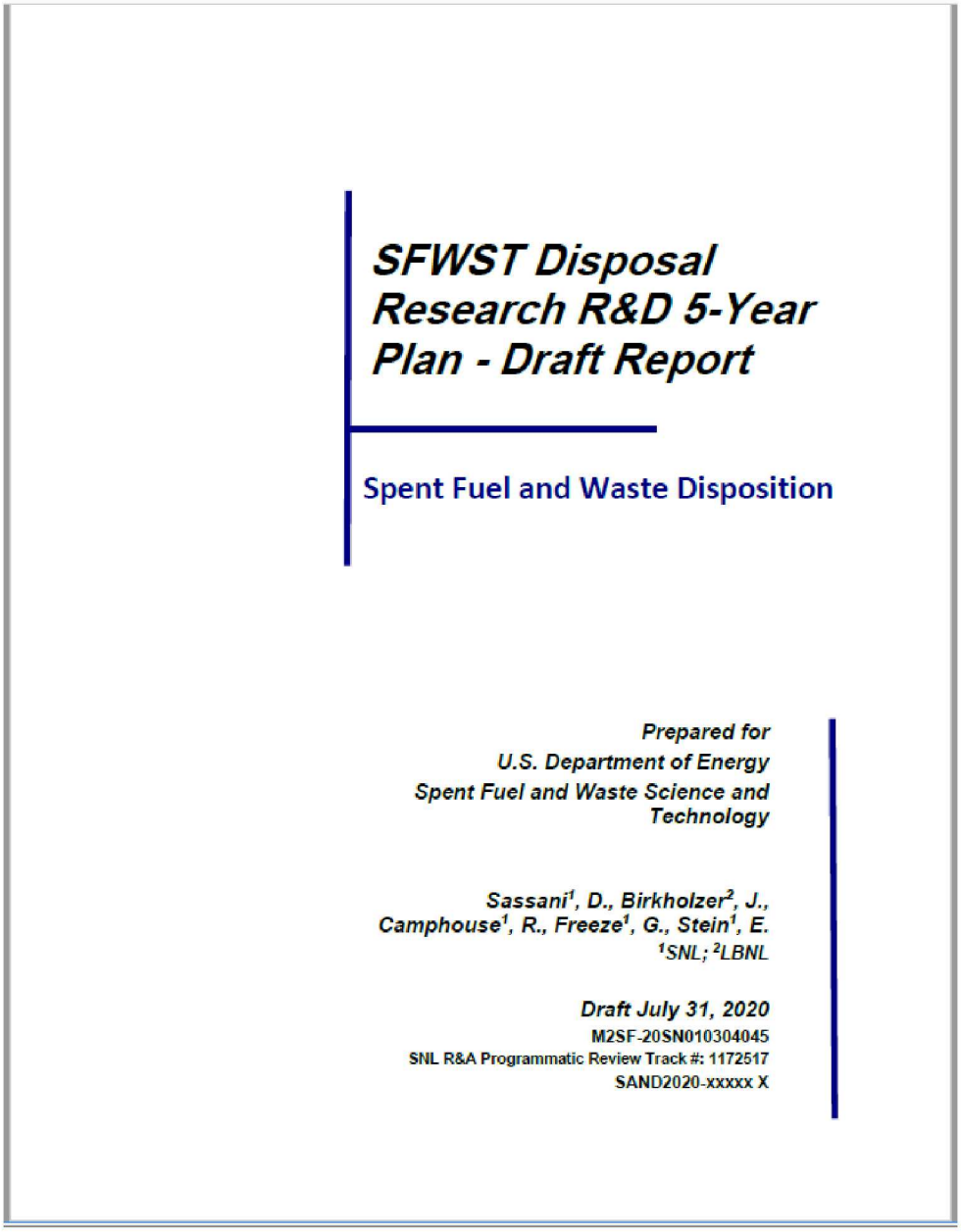

SFWST Disposal Research R&D 5-Year Plan - Draft Report

Spent Fuel and Waste Disposition

Prepared for
U.S. Department of Energy
Spent Fuel and Waste Science and Technology

Sassani[1], D., Birkholzer[2], J., Camphouse[1], R., Freeze[1], G., Stein[1], E.
[1]SNL; [2]LBNL

Draft July 31, 2020
M2SF-20SN010304045
SNL R&A Programmatic Review Track #: 1172517
SAND2020-xxxxx X

Figure 5-1 SFWST Disposal Research R&D 5-Year Plan (Sassani et al. 2020)

5.2 Alignment of the Near-Term GDSA Thrusts of the 5-Year Plan with FY 2020 GDSA Efforts and GDSA Roadmap Activities

To evaluate the coverage of the GDSA thrusts of the 5-Year Plan by FY 2020 GDSA efforts, the near-term thrusts were linked to FY 2020 GDSA efforts in Table 4-2. Each major thrust was given a name and unique identifier as shown in Table 5-1. The thrust identifier was linked to the FY 2020 GDSA effort in the last column of Table 4-2 if the effort aligned with the thrust.

As indicated in Table 4-2 each thrust was addressed to some degree in FY 2020. To link the FY 2020 GDSA infrastructure efforts to a thrust, a broader interpretation of the G03 Workflow thrust was used. Certainly, it should be noted that while each of the thrusts garnered some attention in FY 2020, there was no attempt to quantify how much of the scope of each thrust was addressed in FY 2020.

To evaluate the linkages between the GDSA thrusts of the 5-Year Plan and GDSA Roadmap activities, each activity was evaluated for its ability to address a GDSA thrust. As shown in Appendix E, each near-term thrust was found to have at least one GDSA Roadmap activity linked to it, and each GDSA Roadmap activity was linked to at least one GDSA thrust. Several GDSA thrusts, especially those involving the development of new modeling capability, were linked to a large number of GDSA Roadmap activities. The near-term GDSA thrusts with the fewest linked GDSA Roadmap activities included G02 and G03; however, there is no reason to correlate the number of linkages with the importance of the thrust or the resources needed to address the thrust.

At this early stage of the 5-Year Plan, it is unclear how much the mapping of efforts, Roadmap activities, and thrusts (e.g., Table 4-2 and Appendix E) can help guide planning and production efforts in the years ahead. However, this type of mapping does provide a fairly organized way to better understand how each thrust and Roadmap activity is being addressed.

Table 5-1 Near-term thrusts in the new 5-year plan for GDSA. Descriptions are provided in Appendix D

Thrust	Description	Tech. Area	Term
	Geologic Disposal Safety Assessment		
G01	*Advanced simulation capability*	*GDSA*	*Near*
G02	*Uncertainty and sensitivity analysis*	*GDSA*	*Near*
G03	*Workflow*	*GDSA*	*Near*
G04	*Repository systems analysis*	*GDSA*	*Near*
G05	*Geologic modeling*	*GDSA*	*Near*

6. CONCLUSIONS

This report describes FY 2020 advances of the Geologic Disposal Safety Assessment (GDSA) Framework and PFLOTRAN development groups of the Spent Nuclear Fuel and Waste Science and Technology (SFWST) Campaign. The common mission of these groups is to develop a geologic disposal system modeling capability for nuclear waste that can be used to probabilistically assess the performance of disposal options and generic sites. The capability is a framework called GDSA Framework that employs HPC-capable codes PFLOTRAN and Dakota.

The FY 2020 advances in GDSA PA modeling capabilities are substantial. They allow for emulation of fuel matrix degradation (FMD) processes (e.g., radiolytic oxidation) at each waste package in a repository simulation, simulation of changes to buffer and DRZ properties over time, improved simulation of heat flow, improved PFLOTRAN convergence for multiphase systems, and improved assessment of performance using a new function that finds the highest concentrations of radionuclides in a region. New quantitative methods allow for characterization of regions affected by stochastically-generated discrete fracture networks, e.g., in terms of mean or shortest travel time from the repository to an aquifer and mean residence time of an initial tracer in the repository region. In addition, new modeling approaches under development in FY 2020 include advanced meshing capabilities, a new approach for dynamically simulating adsorption as affected by changing local conditions, new concepts for simulating waste package degradation, and advanced biosphere modeling. Progress in simulation workflow, QA workflow, process model coupling workflow, and other forms of supporting infrastructure in FY 2020 was also extensive and is expected to greatly facilitate continued model development, user-friendliness, and user adoption going forward.

An important responsibility of the GDSA team is to integrate with disposal R&D activities across the SFWST Campaign to ensure that R&D activities support the portions of generic safety cases being developed. In FY 2020, the GDSA team participated with other scientists and engineers at ORNL, LANL, DOE, and SNL in the development of a new high-temperature shale reference case. That effort resulted in new reference case designs, new options for waste package materials and other EBS components, and new conceptual process models. Other activities involved integration with LANL, ANL, LBNL, and PNNL including development of dfnWorks for the crystalline reference case, Geologic Framework Modeling for the unsaturated alluvium reference case, FMD model integration, DECOVALEX-2023 Task F performance assessment, and planning for the development of an advanced biosphere model.

Another important accomplishment in FY 2020, at the request of DOE, was the preparation of a 5-year plan for high priority activities of the Disposal Research R&D of the SFWST Campaign. In the prepared plan, evaluation and prioritization of current and planned activities for each technical area in Disposal Research R&D are discussed, and schedules are outlined (Sassani et al. 2020). This plan will be revised each year to align with changes in objectives and funding.

Each year, GDSA Framework improves as additional modelers and programmers from around the world use, apply, and contribute to its development. GDSA Framework is accessible to everyone because the primary codes, PFLOTRAN and Dakota, are open source, available for free download, and have supporting documentation online. The GDSA team has worked to increase the number of users and participants by (1) maintaining a collaborative web site (pa.sandia.gov), (2) expanding online documentation of verification testing, generic reference cases, and code features, (3) developing quality assurance documentation and a user manual, (4) conducting PFLOTRAN short courses, (5) presenting papers and posters on GDSA Framework capabilities at international forums, and (6) engaging in international collaborations such as DECOVALEX. Outreach and collaborations support a primary objective of the GDSA work package by facilitating testing of, and feedback on, PFLOTRAN and GDSA Framework and by increasing the likelihood outside users will contribute directly to code development in the future.

The ability to simulate increasingly complex repository reference cases continues to affirm that HPC-capable codes can be used to simulate important multi-physics couplings directly in a total system safety assessment demonstration. The generic repository systems modeled to date indicate that PFLOTRAN and its coupled codes can simulate complex coupled processes in a multi-kilometer domain while simultaneously simulating sub-meter-scale coupled behavior in the repository. Continued development is needed to ensure GDSA Framework is ready for application to potential sites that may be selected in the future. The challenge is to address the remaining needs using available resources. Meeting this challenge will require close integration with technical teams across the SFWST Campaign.

7. REFERENCES

Adams, B. M., K. R. Dalbey, M. S. Eldred, L. P. Swiler, W. J. Bohnhoff, J. P. Eddy, D. M. Vigil, P. D. Hough and S. Lefantzi (2012). DAKOTA, A Multilevel Parallel Object-Oriented Framework for Design Optimization, Parameter Estimation, Uncertainty Quantification, and Sensitivity Analysis: Version 5.2+ User's Manual. Albuquerque, New Mexico, Sandia National Laboratories.

Adams, B. M., M. S. Ebeida, M. S. Eldred, J. D. Jakeman, L. P. Swiler, W. J. Bohnhoff, K. R. Dalbey, J. P. Eddy, K. T. Hu, D. M. Vigil, L. E. Baumann and P. D. Hough (2013). Dakota, a Multilevel Parallel Object-Oriented Framework for Design Optimization, Parameter Estimation, Uncertainty Quantification, and Sensitivity Analysis, Version 5.3.1+ Theory Manual. Albuquerque, New Mexico, Sandia National Laboratories.

Avasarala, S., P. C. Lichtner, A. M. S. Ali, R. Gonzalez-Pinzon, J. M. Blake and J. M. Cerrato (2017). "Reactive Transport of U and V from Abandoned Uranium Mine Wastes." Environmental Science & Technology 51(21): 12385-12393.

Balay, S., J. Brown, K. Buschelman, V. Eijkhout, W. D. Gropp, D. Kaushik, M. G. Knepley, L. Curfman McInnes, B. F. Smith and H. Zhang (2013). PETSc Users Manual. Argonne, Illinois, Argonne National Laboratory.

Bennett, D. G. and R. Gens (2008). "Overview of European concepts for high-level waste and spent fuel disposal with special reference waste container corrosion." Journal of Nuclear Materials 379(1-3): 1-8.

Birch, A. F., & Clark, H. (1940). The thermal conductivity of rocks and its dependence upon temperature and composition. *American Journal of Science*, *238*(8), 529-558.

Blanton, T.L. and J.E. Olson (1999), Stress magnitudes from logs: Effects of tectonic strains and temperature, SPE Reservoir Eval. & Eng., 2(1):62-68.

Blesch, C. J., Kulacki, F. A., & Christensen, R. N. (1983). *Application of integral methods to prediction of heat transfer from a nuclear waste repository* (No. ONWI-495). Ohio State Univ. Research Foundation, Columbus (USA).

Bustin R.M., A.M.M. Bustin, X. Cui, D.J.K. Ross, and V.S.M. Pathi (2008), Impact of shale properties on pore structure and storage characteristics, SPE 119892-MS.

Chen, D., Pan, Z.J., and Ye Z.H. (2015), Dependence of gas shale fracture permeability on effective stress and reservoir pressure: model match and insights, Fuel, 139:383-392.

Chen, X., G. Hammond, C. Murray, M. Rockhold, V. Vermeul and J. Zachara (2013). "Applications of ensemble-based data assimilation techniques for aquifer characterization using tracer data at Hanford 300 area." Water Resources Research 49: 7064-7076.

Chen, X., H. Murakami, M. Hahn, G. E. Hammond, M. L. Rockhold, J. M. Zachara and Y. Rubin (2012). "Three-Dimensional Bayesian Geostatistical Aquifer Characterization at the Hanford 300 Area using Tracer Test Data." Water Resources Research 48.

Condon, C. A., B. A. Napier, S. Ghosh, W. C. Weaver and C. B. Varnum-Lowry (2020). GDSA Biosphere Model Software Requirements Document. Richland, Washington, Pacific Northwest National Laboratory.

de Vries, L. M., J. Molinero, H. Ebrahimi, U. Svensson, P. Lichtner and E. Abarca (2013). Regional Scale HPC Reactive Transport Simulation of Nuclear Spent Fuel Repository in Forsmark, Sweden. Joint 8th International Conference on Supercomputing in Nuclear Applications (SNA) / 4th Monte Carlo Meeting (MC), Paris, France.

Dewhurst D.N., A.C. Aplin, and J.-P. Sarda (1999), Influence of clay fraction on pore-scale properties and hydraulic conductivity of experimentally compacted mudstones, Journal of Geophysical Research, 104:29261-29274.

DOE (2011). Used Fuel Disposition Campaign Disposal Research and Development Roadmap. Washington, DC, Fuel Cycle Technologies, Office of Nuclear Energy, US Department of Energy.

DOE (2013). Strategy for the Management and Disposal of Used Nuclear Fuel and High-Level Radioactive Waste, January 2013. Washington, DC. http://energy.gov/downloads/strategy-

management-and-disposalused-nuclear-fuel-and-high-level-radioactive-waste, U.S. Department of Energy.

Dong, J.J., J.Y. Hsu, W.J. Wu, T. Shimamoto, J.H. Hung, E.C. Yeh et al. (2010), Stress dependence of the permeability and porosity of sandstone and shale from TCDP Hole-A, International Journal of Rock Mechanics and Mining Science, 47:1141-1157.

Flynn, D. R. and T. W. Watson (1969). Measurements of the thermal conductivity of soils to high temperatures Washington, DC, National Bureau of Standards.

Frederick, J.M. 2018. PFLOTRAN QA Test Suite. Retrieved July 28, 2020 from qa.pflotran.org.

Freeze, G., M. Voegele, P. Vaughn, J. Prouty, W. M. Nutt, E. Hardin and S. D. Sevougian (2013b). Generic Deep Geologic Disposal Safety Case. Albuquerque, New Mexico, Sandia National Laboratories.

Freeze, G., P. E. Mariner, J. A. Blink, F. A. Caporuscio, J. E. Houseworth and J. C. Cunnane (2011). Disposal System Features, Events, and Processes (FEPs): FY11 Progress Report. Albuquerque, New Mexico, Sandia National Laboratories.

Freeze, G., W. P. Gardner, P. Vaughn, S. D. Sevougian, P. Mariner, V. Mousseau and G. Hammond (2013a). Enhancements to the Generic Disposal System Modeling Capabilities. Albuquerque, New Mexico, Sandia National Laboratories.

Gardner, W. P., G. Hammond and P. Lichtner (2015). "High Performance Simulation of Environmental Tracers in Heterogeneous Domains." Groundwater 53: 71-80.

Gilliam, T. M., & Morgan, T. M. (1987). Shale: Measurement of Thermal Properties (No. ORNL/TM-10499). *Oak Ridge National Lab., TN (USA). Oak Ridge, Tennessee*.

Gross, M., Miller, E., Milazzo, D., Miller, T.A., Lavadie-Bulnes, A., Swanson, E., Hayes-Rich, N., Roback R., Stauffer, P.H., LaForce, T. and M.S. Ebeida (2020). Geologic Framework Models for the Alluvial Basin Reference Case. Los Alamos, New Mexico, Los Alamos National Laboratory.

Gross, M., P. H. Stauffer, T. A. Miller, E. Miller, E. Swanson, N. Hayes-Rich, A. Lavadie-Bulnes, D. Milazzo and R. Roback (2020). Geologic Framework Models for the Alluvial Basin Reference Case. Los Alamos, New Mexico, Los Alamos National Laboratory.

Hammond, G. E. and P. Lichtner (2010). "Field-scale modeling for the natural attenuation of uranium at the Hanford 300 area using high performance computing." Water Resources Research 46.

Hammond, G. E., P. C. Lichtner and M. L. Rockhold (2011b). "Stochastic simulation of uranium migration at the Hanford 300 Area." Journal of Contaminant Hydrology 120-121: 115-128.

Hammond, G. E., P. C. Lichtner, C. Lu and R. T. Mills (2011a). PFLOTRAN: Reactive Flow and Transport Code for Use on Laptops to Leadership-Class Supercomputers. Groundwater Reactive Transport Models. F. Zhang, G. T. Yeh and J. Parker, Bentham Science Publishers.

Hammond, G. E., P. C. Lichtner, R. T. Mills and C. Lu (2008). "Toward petascale computing in geosciences: application to the Hanford 300 Area." Journal of Physics Conference Series 125: 12051-12051.

Hammond, G., P. Lichtner and C. Lu (2007). "Subsurface multiphase flow and multicomponent reactive transport modeling using high performance computing." Journal of Physics: Conference Series 78: 1-10.

IAEA (2003). "Reference Biospheres" for Solid Radioactive Waste Disposal. Vienna, Austria, International Atomic Energy Agency.

IAEA (2006). Geological Disposal of Radioactive Waste. Safety Requirements No. WS-R-4. Vienna, Austria, International Atomic Energy Agency.

Iraola, A., P. Trinchero, S. Karra and J. Molinero (2019). "Assessing dual continuum method for multicomponent reactive transport." Computers & Geosciences 130: 11-19.

Jerden, J., E. Lee, V. K. Gattu and W. Ebert (2019). Fuel Matrix Degradation Model Development Update: Alloy Corrosion Rates and Hydrogen Generation. Illinois, Argonne National Laboratory.

Jerden, J., G. Hammond, J. M. Copple, T. Cruse and W. Ebert (2015b). Fuel Matrix Degradation Model: Integration with Performance Assessment and Canister Corrosion Model Development. Washington, DC, US Department of Energy.

Jerden, J., J. M. Copple, K. E. Frey and W. Ebert (2015a). Mixed Potential Model for Used Fuel Dissolution - Fortran Code. O. o. U. N. F. Disposition. Washington, DC, US Department of Energy.

Jerden, J., V. K. Gattu and W. Ebert (2018). Update on Validation and Incorporationof a New Steel Corrosion Module into Fuel Matrix Degradation Model. Illinois, Argonne National Laboratory.

Jove-Colon, C. et al. (2020). Evaluation of Nuclear Spent Fuel Disposal in Clay-Bearing Rock - Process Model Development and Experimental Studies. M2SF-20SN010301051. Sandia National Laboratories. Albuquerque, New Mexico.

Jung, Y., G.S.H. Pau, S. Finsterle, R.M. Pollyea (2017), TOUGH3: A new efficient version of the TOUGH suite of multiphase flow and transport simulators, Computers and Geosciences, 108: 2-7.

Karra, S., S. L. Painter and P. C. Lichtner (2014). "Three-phase numerical model for subsurface hydrology in permafrost-affected regions (PFLOTRAN-ICE v1.0)." Cryosphere 8(5): 1935-1950.

King, F. and M. Kolar (2019). "Lifetime Predictions for Nuclear Waste Disposal Containers." Corrosion 75(3): 309-323.

Kuhlman, K., M. Mills, R. Jayne, E. Matteo, C. Herrick, M. Nemer, J. Heath, Y. Xiong, C. Choens, P. Stauffer, H. Boukhalfa, E. Guiltinan, T. Rahn, D. Weaver, B. Dozier, S. Otto, J. Rutqvist, Y, Wu, M. Hu, S. Uhlemann, J. Wang (2020). FY20 Update on Brine Availability Test in Salt, M2SF-20SN010303032. Sandia National Laboratories. Albuquerque, New Mexico.

Kumar, J., N. Collier, G. Bisht, R. T. Mills, P. E. Thornton, C. M. Iversen and V. Romanovsky (2016). "Modeling the spatiotemporal variability in subsurface thermal regimes across a low-relief polygonal tundra landscape." Cryosphere 10(5): 2241-2274.

Kwon, O., A.K. Kronenberg, and A.F. Gangi (2001), Permeability of Wilcox shale and its effective pressure law, Journal of Geophysical Research, 106(B9): 19339-19353.

LaForce, T., K. W. Chang, F. V. Perry, T. S. Lowry, E. Basurto, R. Jayne, S. Jordan, E. Stein, R. Leone and M. Nole (2020). GDSA Repository Systems Analysis FY 2020 Update Albuquerque, New Mexico, Sandia National Laboratories.

Li, B., & Tchelepi, H. A. (2015, February). Numerical Trust Region Newton Solver for Multiphase Transport in Porous Media Based on Detailed Nonlinear Analysis. In *SPE Reservoir Simulation Symposium*. Society of Petroleum Engineers.

Lichtner, P. C. and G. E. Hammond (2012). Quick Reference Guide: PFLOTRAN 2.0 (LA-CC-09-047) Multiphase-Multicomponent-Multiscale Massively Parallel Reactive Transport Code. Los Alamos, New Mexico, Los Alamos National Laboratory.

Liu, H.-H., J. Rutqvist, and J.G. Berryman (2009), On the relationship between stress and elastic strain for porous and fractured rock, International Journal of Rock Mechanics and Mining Science, 46:289-296.

Lu, C. and P. C. Lichtner (2007). "High resolution numerical investigation on the effect of convective instability on long term CO2 storage in saline aquifers." Journal of Physics Conference Series 78: U320-U325.

Mariner, P. E., E. R. Stein, J. M. Frederick, S. D. Sevougian and G. E. Hammond (2017). Advances in Geologic Disposal System Modeling and Shale Reference Cases. Albuquerque, New Mexico, Sandia National Laboratories.

Mariner, P. E., E. R. Stein, J. M. Frederick, S. D. Sevougian, G. E. Hammond and D. G. Fascitelli (2016). Advances in Geologic Disposal System Modeling and Application to Crystalline Rock. Albuquerque, New Mexico, Sandia National Laboratories.

Mariner, P. E., E. R. Stein, S. D. Sevougian, L. J. Cunningham, J. M. Frederick, G. E. Hammond, T. S. Lowry, S. Jordan and E. Basurto (2018). Advances in Geologic Disposal Safety Assessment and an Unsaturated Alluvium Reference Case. Albuquerque, New Mexico, Sandia National Laboratories.

Mariner, P. E., L. A. Connolly, L. J. Cunningham, B. J. Debusschere, D. C. Dobson, J. M. Frederick, G. E. Hammond, S. H. Jordan, T. C. LaForce, M. A. Nole, H. D. Park, F. V. Perry, R. D. Rogers, D.

T. Seidl, S. D. Sevougian, E. R. Stein, P. N. Swift, L. P. Swiler, J. Vo and M. G. Wallace (2019). Progress in Deep Geologic Disposal Safety Assessment in the U.S. since 2010. Albuquerque, New Mexico, Sandia National Laboratories.

Mariner, P. E., T. M. Berg, K. W. Chang, B. J. Debusschere, R. C. Leone and D. T. Seidl (2020). Surrogate Model Development of Spent Fuel Degradation for Repository Performance Assessment Albuquerque, New Mexico, Sandia National Laboratories.

Mariner, P. E., W. P. Gardner, G. E. Hammond, S. D. Sevougian and E. R. Stein (2015). Application of Generic Disposal System Models. Albuquerque, New Mexico, Sandia National Laboratories.

McKee C.R., A.C. Bumb, and R.A. Koenig (1988), Stress-dependent permeability and porosity of coal and other geological formations, SPE Form Evaluation, 3:81-91.

Meacham, P. G., D. R. Anderson, E. J. Bonano and M. G. Marietta (2011). Sandia National Laboratories Performance Assessment Methodology for Long-Term Environmental Programs: The History of Nuclear Waste Management. Albuquerque, New Mexico, Sandia National Laboratories.

Mills, R., C. Lu, P. C. Lichtner and G. Hammond (2007). Simulating subsurface flow and transport on ultrascale computers using PFLOTRAN. 3rd Annual Scientific Discovery through Advanced Computing Conference (SciDAC 2007), Boston, Journal of Physics Conference Series.

Navarre-Sitchler, A., R. M. Maxwell, E. R. Siirila, G. E. Hammond and P. C. Lichtner (2013). "Elucidating geochemical response of shallow heterogeneous aquifers to CO2 leakage using high-performance computing: implications for monitoring CO2 sequestration." Advances in Water Resources 53: 44-55.

Neuzil (2019), Permeability of clay and shales, Ann. Rev. Earth Planet. Sci., 47:247-273.

OECD (2004). Post-Closure Safety Case for Geological Repositories Nature and Purpose. Paris, France, Organisation for Economic Co-Operation and Development, Nuclear Energy Agency.

Olszewska-Wasiolek, M. A. and B. W. Arnold (2011). Radioactive Disequilibria in the Saturated Zone Transport Model and the Biosphere Model for the Yucca Mountain Repository — The Case of Radon-222. International High-Level Radioactive Waste Management Conference, Albuquerque, New Mexico.

Orient, G., R. Clay, E. Friedman-Hill and E. Hoffman (2020). Next Generation Workflow – an Open Source Software System for Computational Modeling to Support Agile VVUQ. ASME V&V Symposium, May 20-22, 2020.

Rechard, R. P. (1995). Performance Assessment of the Direct Disposal in Unsaturated Tuff of Spent Nuclear Fuel And High-Level Waste Owned by US Department of Energy. Albuquerque, New Mexico, Sandia National Laboratories. 1, 2, and 3.

Rechard, R. P. (2002). General approach used in the performance assessment for the Waste Isolation Pilot Plant. Scientific Basis for Nuclear Waste Management XXV, Boston, Massachussetts, Materials Research Society.

Rechard, R. P. and C. T. Stockman (2014). "Waste degradation and mobilization in performance assessments of the Yucca Mountain disposal system for spent nuclear fuel and high-level radioactive waste." Reliability Engineering and System Safety 122(2): 165-188.

Rechard, R. P. and M. S. Tierney (2005). "Assignment of probability distributions for parameters in the 1996 performance assessment for the Waste Isolation Pilot Plant, Part 1: Description of process." Reliability Engineering and System Safety 88(1): 1-32.

Ridgway, E. M. (2020). Dakota. GUI Version 6.12 User Manual – Next-Gen Workflow. https://dakota.sandia.gov/content/next-gen-workflow. Accessed August 5, 2020.

Rutqvist, J., Davis, J., Zheng, L., Vilarrasa, V., Houseworth, J., and Birkholzer, J. (2014a) Investigation of Coupled THMC Processes and Reactive Transport: FY14 Progress. Prepared for U.S. Department of Energy, Used Fuel Disposition, FCRD-UFD-2014-000497, Lawrence Berkeley National Laboratory, LBNL-6720E (2014a).

Rutqvist, J., Guglielmi, Y., Xu, H., Tian, Y., Zarzycki, P., Deng, H., Li, P., Hu, M., Nico, P., Borglin, S., Fox, P., Sasaki, T., Birkholzer, J. (2020). Investigation of Coupled Processes in Argillite Rock:

FY20 Progress (LBNL-2001324). Lawrence Berkeley National Lab. (LBNL), Berkeley, CA (United States).

Rutqvist, J., Ijiri, Y., & Yamamoto, H. (2011), Implementation of the Barcelona Basic Model into TOUGH–FLAC for simulations of the geomechanical behavior of unsaturated soils. Computers & Geosciences, 37(6), 751-762.

Rutqvist, J., L. Zheng, F. Chen, H.-H. Liu, and J. Birkholzer (2014b), Modeling of coupled thermo-hydro-mechanical processes with links to geochemistry associated with bentonite-backfilled repository tunnels in clay formations, Rock Mech. Rock Eng., 47:167-186.

Sassani, D., J. Birkholzer, R. Camphouse, G. Freeze and E. Stein (2020). SFWST Disposal Research R&D 5-Year Plan - Draft Report. Albuquerque, New Mexico, Sandia National Laboratories.

Sevougian, S. D., E. R. Stein, T. LaForce, F. V. Perry, T. S. Lowry, L. J. Cunningham, M. Nole, C. B. Haukwa, K. W. Chang and P. E. Mariner (2019b). GDSA Repository Systems Analysis Progress Report. Albuquerque, New Mexico, Sandia National Laboratories.

Sevougian, S. D., E. R. Stein, T. LaForce, F. V. Perry, T. S. Lowry, M. Nole and K. W. Chang (2019c). GDSA Repository Systems Analysis FY 2019 Update. Albuquerque, New Mexico, Sandia National Laboratories.

Sevougian, S. D., G. A. Freeze, P. Vaughn, P. Mariner and W. P. Gardner (2013). Update to the Salt R&D Reference Case. Albuquerque, New Mexico, Sandia National Laboratories.

Sevougian, S. D., G. A. Freeze, W. P. Gardner, G. E. Hammond and P. E. Mariner (2014). Performance Assessment Modeling and Sensitivity Analyses of Generic Disposal System Concepts. Albuquerque, New Mexico, Sandia National Laboratories.

Sevougian, S. D., P. E. Mariner, L. A. Connolly, R. J. MacKinnon, R. D. Rogers, D. C. Dobson and J. L. Prouty (2019a). DOE SFWST Campaign R&D Roadmap Update, Rev. 1. Albuquerque, New Mexico, Sandia National Laboratories.

Shi, J.Q. and S. Durucan (2016), Near-exponential relationship between effective stress and permeability of porous rocks revealed in Gangi's phenomenological models and application to gas shales, International Journal of Coal Geology, 154-155: 111-122.

Shuai, P., X. Y. Chen, X. H. Song, G. E. Hammond, J. Zachara, P. Royer, H. Y. Ren, W. A. Perkins, M. C. Richmond and M. Y. Huang (2019). "Dam Operations and Subsurface Hydrogeology Control Dynamics of Hydrologic Exchange Flows in a Regulated River Reach." Water Resources Research 55(4): 2593-2612.

Steefel, C. (2009), CrunchFlow. Software for modeling multicomponent reactive flow and transport. User's Manual, Lawrence Berkely National Laboratory, Berkeley, CA, USA.

Stein, E. R. (2020). PFLOTRAN Short Course Geologic Disposal Example. https://bitbucket.org/pflotran/pflotran/src/master/shortcourse/exercises/geologic_disposal/. Accessed April 2, 2020.

Stein, E. R., D. C. Dobson, R. Rogers and Y. Wang (2020). (in progress) High Temperature Argillite Reference Case. Albuquerque, New Mexico, Sandia National Laboratories.

Swiler, L. P., E. Basurto, D. M. Brooks, A. C. Eckert, P. E. Mariner, T. Portone and E. R. Stein (2020). Status Report on Uncertainty Quantification and Sensitivity Analysis Tools in the Geologic Disposal Safety Assessment (GDSA) Framework Albuquerque, New Mexico, Sandia National Laboratories.

Swiler, L. P., J. C. Helton, E. Basurto, D. M. Brooks, P. E. Mariner, L. M. Moore, S. Mohanty, S. D. Sevougian and E. R. Stein (2019). Status Report on Uncertainty Quantification and Sensitivity Analysis Tools in the Geologic Disposal Safety Assessment (GDSA) Framework. Albuquerque, New Mexico, Sandia National Laboratories.

Trangenstein, J. A., & Bell, J. B. (1989). Mathematical structure of the black-oil model for petroleum reservoir simulation. SIAM Journal on Applied Mathematics, 49(3), 749-783.

Trinchero, P., I. Puigdomenech, J. Molinero, H. Ebrahimi, B. Gylling, U. Svensson, D. Bosbach and G. Deissmann (2017). "Continuum-based DFN-consistent numerical framework for the simulation

of oxygen infiltration into fractured crystalline rocks." Journal of Contaminant Hydrology 200: 60-69.

Vosteen, H. D., & Schellschmidt, R. (2003). Influence of temperature on thermal conductivity, thermal capacity and thermal diffusivity for different types of rock. *Physics and Chemistry of the Earth, Parts A/B/C*, *28*(9-11), 499-509.

Wang, Y., Y. Xiong, T. Hadgu, E. Kalinina, M. M. Mills, A. C. Sanchez, J. Jerden, S. Thomas, E. Lee, V. K. Gattu, W. Ebert, H. Viswanathan, S. Chu, A. R. Hoinville, J. Hyman, S. Karra, N. Makedonska, K. Telfeyan, Y. Guglielmi, C. Chang, P. Cook, P. Dobson, F. Soom, S. Nakagawa, C.-F. Tsang, S. Borglin, C. Doughty, L. Zheng, M. Zavarin, E. Balboni, C. Atkins-Duffin, W. Bourcier, S. F. Carle, K. Smith and C. Booth (2020). Process Model Development and Experimental Investigation for Spent Fuel Disposal in Crystalline Rocks: FY 2020 Report. Albuquerque, New Mexico, Sandia National Laboratories.

Zachara, J. M., X. Y. Chen, C. Murray and G. Hammond (2016). "River stage influences on uranium transport in a hydrologically dynamic groundwater-surface water transition zone." Water Resources Research 52(3): 1568-1590.

Zheng, J., L. Zheng, H.-H. Liu, and Y. Ju (2016), Relationships between permeability, porosity and effective stress for low-permeability sedimentary rock, International Journal of Rock Mechanics & Mining Sciences, 78: 304-318.

Zoback, M. D. (2010). Reservoir geomechanics. Cambridge University Press.

Appendix A. DYNAMIC K_D – A REDUCED-ORDER SORPTION MODEL

DYNAMIC K_D – A REDUCED-ORDER SORPTION MODEL

Introduction

Within the computational geosciences, there has been a recent concerted effort to adopt machine learning and artificial intelligence to reduce complexity and speedup simulator performance (or enlarge problem size). Reduced-order representations of relatively mechanistic biogeochemical process models have been proposed (e.g. Stockmann et al., 2017), but how effective are these reduced-order models at replicating the relatively mechanistic biogeochemical process models that they replace? What computational speedups (measured by shorter wall clock times) are realized when utilizing these simplified process models? How do these speedups compare to those enabled through the use of high-performance computing (HPC) and simplified coupling schemes (e.g., loosely coupled operator splitting in place of the fully coupled global implicit approach)?

This research investigates the application of a reduced-order, dynamic K_D approach to modeling U(VI) surface complexation at the Hanford Site in southeastern Washington state. The study compares both solution accuracy and speedup enabled by the dynamic K_D model in combination with HPC and operator splitting. Numerous researchers have demonstrated that the degree to which U(VI) sorbs to soil grains at the Hanford 300 Area is largely proportion to the fraction of Columbia River water within the underlying aquifer (Hammond and Lichtner, 2010; Zachara et al., 2020).

Tab. A-1 summarizes the river and groundwater chemistry at Hanford 300 Area based on previous geo-chemical transport modeling at the site using PFLOTRAN (Hammond and Lichtner, 2010). The geochemical conceptual model considers 13 primary species (primary dependent variables), 88 secondary aqueous complexes, one mineral (calcite) and two U(VI) surface complexes. The Columbia River water has a higher pH and a lower ionic strength (due to lower concentrations of major cations and anions) relative to the groundwater beneath the site, and U(VI) sorbs more strongly in the presence of river water.

The dimensionless $\mathcal{K}_D$ is a measure of the ratio of mass in the sorbed to that in the aqueous phase

$$\mathcal{K}_D = \frac{\Psi_S}{1000\phi s_l \Psi} \quad \text{(A-1)}$$

with total sorbed concentration Ψ_S [mol/m_{bulk}^3], total aqueous concentration Ψ [mol/L_{water}], porosity ϕ [m_{pore}^3/m_{bulk}^3], liquid saturation s_l [m_{water}^3/m_{pore}^3], and 1000 liters per m^3 water. $\mathcal{K}_D$ is over an order of magnitude larger for river water than ground water. The proposed dynamic K_D model leverages existing knowledge of water chemistry and U(VI) surface complexation at the site to develop a simplified representation for U(VI) sorption.

Tab. A-1 Simulated total component concentrations of major cations and anions at Hanford 300 Area

Parameter	Hanford 300 Area Groundwater†	Columbia River Water†
pH	7.6	7.8
Ionic Strength	6.88e-3	2.01e-3
Ca^{2+}	1.21e-3	4.50e-4
Mg^{2+}	5.10e-4	1.82e-4
HCO_3^-	2.57e-3	1.13e-3
K^+	1.55e-4	1.90e-5
Na^+	1.34e-3	5.12e-5
$\mathcal{K}_D$	5.56	62.37
Equilibrating Mineral	Calcite	N/A

†equilibrated with sediment, $\mathcal{K}_D$ = ratio of sorbed to aqueous mass [dimensionless K_D]

Methodology

A simple mixing model was developed using mixtures of the end-member groundwater and river water geochemistry presented in Tab. A-1. Based on a specified river water fraction, mixtures of river and groundwater were re-equilibrated within PFLOTRAN using equilibrium surface complexation, and the resulting nonlinear distribution of $\mathcal{K}_D$ is plotted in red as a function of river water fraction in Tab. A-1. A reduced-order dynamic K_D model was then developed to replicate this distribution of U(VI) $\mathcal{K}_D$ based on the equation

$$\mathcal{K}_D = \mathcal{K}_{D\,groundwater} + \left(\mathcal{K}_{D\,river} - \mathcal{K}_{D\,groundwater}\right)\chi_{river}^{\beta_{\mathcal{K}_D}} \quad \text{(A-2)}$$

with river water fraction χ_{river}, exponent $\beta_{\mathcal{K}_D}$ (fitting parameter), and end-members $\mathcal{K}_{D\,groundwater}$ and $\mathcal{K}_{D\,river}$. Note that all these parameters are unitless. Fig. A-1 demonstrates that the dynamic K_D model, calibrated with $\beta_{\mathcal{K}_D}$ = 3.26, fits the $\mathcal{K}_D$ generated from the surface complexation model well.

The main benefit to using the reduced-order dynamic K_D model is smaller problem size. As discussed earlier, surface complexation requires simulating 13 primary species, 88 aqueous complexes, two minerals and two surface complexes. PFLOTRAN must solve for the 13 primary species as primary dependent variables at each grid cell. The dynamic K_D model requires only two primary variables (river tracer and U(VI)) and a single linear K_D reaction (i.e., no aqueous complexation, mineral precipitation-dissolution or surface complexation). The smaller problem size greatly accelerates simulator performance.

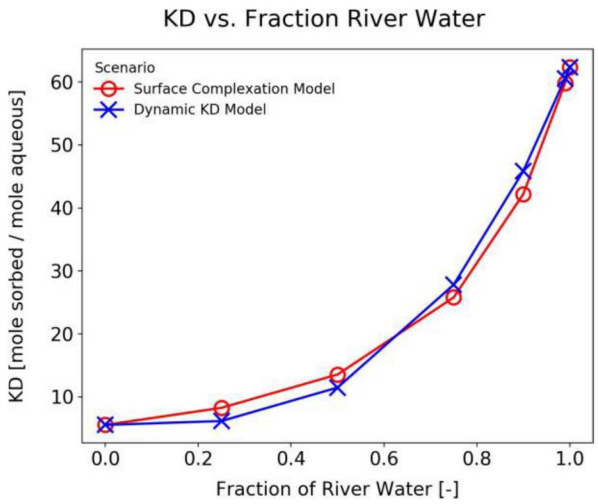

Fig. A-1 **Comparison of dimensionless $\mathcal{K}_D$ function of the fraction of river water: surface complexation versus the dynamic $\mathcal{K}_D$**

Governing Equations

This section presents the numerical methods employed within PFLOTRAN to simulate biogeochemical transport, the understanding of which provides better context for comparing simulator accuracy and performance. PFLOTRAN utilizes the finite volume method to discretize the governing mass conservation equations for groundwater flow and reactive transport. Newton's method is employed to solve the resulting implicit (in time) nonlinear systems of partial differential equations.

Groundwater Flow

The governing mass conservation equation for variably-saturated groundwater flow is solved using the Richards equation and has the form

$$\frac{\delta}{\delta t}(\phi s \rho) + \nabla \cdot \rho q = Q \tag{A-3}$$

with porosity ϕ, liquid saturation s, liquid density ρ and the source term Q. The Darcy flux q is defined as

$$q = \frac{k k_r}{\mu} \nabla (p - \rho g z) \tag{A-4}$$

with intrinsic permeability k, relative permeability k_r, viscosity μ, liquid pressure p and acceleration due to gravity g.

Reactive Transport

The governing mass conservation equation for multicomponent biogeochemical transport of chemical species j has the form

$$\frac{\delta}{\delta t}\left(\phi s \Psi_j + \Psi_{s,j}\right) + \nabla \cdot \Omega_j = -\sum I_j \tag{A-5}$$

with total aqueous component concentration Ψ, total sorbed concentration Ψ_S, kinetic reaction rate I and the advective-dispersive flux term Ω

$$\Omega_j = (q - \phi s \tau D \nabla)\Psi_j \tag{A-6}$$

τ is tortuosity and D is the hydrodynamic dispersion coefficient. The total sorbed concentration is calculated by rearranging Eq. A-1 as

$$\Psi_S = \mathcal{K}_D 1000 \phi s_l \Psi \tag{A-7}$$

Coupling of Transport and Reaction

PFLOTRAN employs the fully coupled global implicit or loosely coupled operator split approaches to solve Eq. A-5. The global implicit approach entails the solution of one large nonlinear system of equations of size (number of grid cells number of chemical species). The operator split approach decouples transport from reaction. Total component concentrations are transported individually using the linear advection-dispersion equation

$$\frac{\delta}{\delta t}\left(\phi s \Psi_j\right) + \nabla \cdot \Omega_j = 0 \tag{A-8}$$

while nonlinear biogeochemical reaction is solved locally at each grid cell

$$\frac{\delta}{\delta t}\left(\phi s \Psi_j + \Psi_{S,j}\right) = -\sum I_j \tag{A-9}$$

Consider a single time step for the reactive transport scenario depicted in Fig. A-2 with nine grid cells and three chemical components. The global implicit approach requires the solution of a large nonlinear system of equations with a Jacobian composed of 27 rows and columns. At least one Newton iteration is required. The operator split approach requires the solution of three linear systems for transport (transport matrices with 9 rows/columns) and nine nonlinear systems for reaction (Jacobian matrices with 3 rows/columns). For reactive transport problems composed of large numbers of species and complex (highly nonlinear) chemistry, the global implicit approach can require significantly more time than operator splitting. The tradeoff is accuracy. Operator spitting is known to introduce splitting error into the solution (Valocchi and Malmstead, 1992).

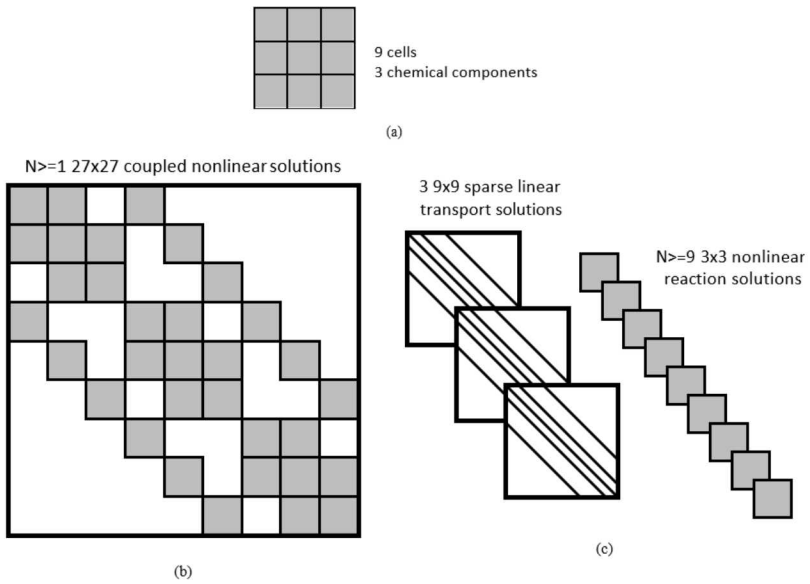

Fig. A-2 **Schematic of a hypothetical reactive transport problem with 9 grid cells arrayed in a 2D 3 3 configuration with 3 chemical components (a). Global implicit Jacobian with fill pattern (b). Three transport matrices and 9 reaction Jacobians matrices for operator splitting (c). Each shaded block represents the 3×3 block for geochemical coupling at each grid cell.**

Results

Problem Scenario

A test problem representative of Hanford 300 Area groundwater-river water dynamics and geochemistry was developed to compare the performance of the dynamic K_D model. As illustrated in Fig. A-3, the 256 × 256 × 16 m domain is gridded at 1 m resolution. The domain is bounded by groundwater on three sides with river water to the east. The 16 × 16 × 8 m source zone has an origin of <128, 96, 4>.

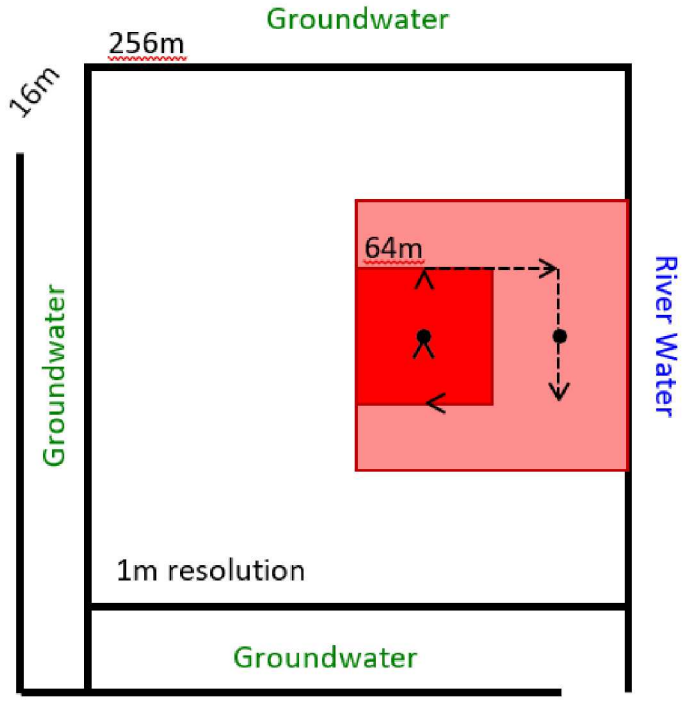

Fig. A-3 **Schematic of test problem motivated by Hanford 300 Area flow and chemistry. The 64m square plume is transported over the course of a year in a clockwise pattern in the directions indicated.**

Two flow regimes are considered for the 10-year simulations. In the first flow regime, flow velocities are prescribed within a homogeneous porous medium. Solely reactive transport is considered with a uniform pore water velocity of 64 m/yr assigned in the four principle directions of north, east, south and west over the course of a year. In the second regime, PFLOTRAN solves for flow within a heterogeneous porous medium. A hydraulic gradient of 2×10^{-4} is assigned in the same four directions and the resulting velocity field is utilized for reactive transport. These two flow regimes provide a test bed for bounding computational performance and process model accuracy by comparing solely reactive transport (with uniform velocities prescribed) to a more sophisticated coupling of reactive transport to PFLOTRAN's RICHARDS flow process model (with a heterogeneous permeability field).

Comparison of Simulation Results

Tab. A-2 outlines the scenarios simulated for this comparison. PFLOTRAN results are compared for four sorption process models, two flow regimes and two coupling schemes. The flow regimes, coupling and K_D conceptual model are defined above. The constant K_D sorption model is identical to the dynamic K_D but for a constant $\mathcal{K}_D$. An in-depth discussion of equilibrium and kinetic multi-rate surface complexation is provided by Hammond and Lichtner (2010).

For all comparisons, the equilibrium surface complexation results are considered the most correct as it is assumed that this sorption model is the most mechanistic. It is possible that the kinetic multi-rate model is more accurate than the equilibrium formulation. However, since the constant and dynamic K_D models are

equilibrium-based (i.e. not kinetic), equilibrium surface complexation should be the standard metric. The primary purpose for including kinetic multi-rate surface complexation was more to assess computational performance than compare accuracy as the multi-rate formulation is more expensive to calculate than equilibrium. For multi-rate surface complexation, the kinetic rate and site fraction distributions employed are from Hammond and Lichtner (2010); they have not been altered. As the mean of the kinetic rate distribution approaches infinity, the multi-rate formulation results will converge to those generated by equilibrium surface complexation.

Tab. A-2 Matrix of problem scenarios for comparison

Sorption Model	Prescribed Uniform Flow		Heterogeneous Flow Field	
Constant K_D	Operator Split	Global Implicit	Operator Split	Global Implicit
Dynamic K_D	Operator Split	Global Implicit	Operator Split	Global Implicit
Equilibrium Surface Complexation	Operator Split	Global Implicit	Operator Split	Global Implicit
Kinetic Multirate Surface Complexation	Operator Split	Global Implicit	Operator Split	Global Implicit

Snapshots in Time

Fig. A-4 through Fig. A-7 illustrate cross-sectional snapshots of total aqueous and sorbed U(VI) concentrations at 5 and 10 years simulation time, respectively. At 5 and 10 years, the constant K_D model in the upper left corner appears to be immobile since the images are plotted at the same time each year. The plume actually moves at a retarded rate (due to sorption) in the clockwise pattern shown earlier. This is evident when shown in an animation. The dynamic K_D and equilibrium surface complexation models demonstrate relatively good agreement, while the kinetic multi-rate surface complexation model shows significant discrepancies.

Since desorption with the multi-rate surface complexation model is kinetically limited (unlike the three other equilibrium formulations), most of the multi-rate U(VI) mass remains in the source zone while the aqueous U(VI) mixes rapidly with neighboring groundwater, resulting in a diffuse aqueous plume. At 10 years, a third of the multi-rate U(VI) remains sorbed in the source zone. It should be noted that in addition to location, the shapes of the dynamic K_D and equilibrium surface complexation models are very similar. This suggests that the dynamic K_D model captures many higher-order, nonlinear characteristics of the surface complexation model better than the constant K_D and kinetic multi-rate models.

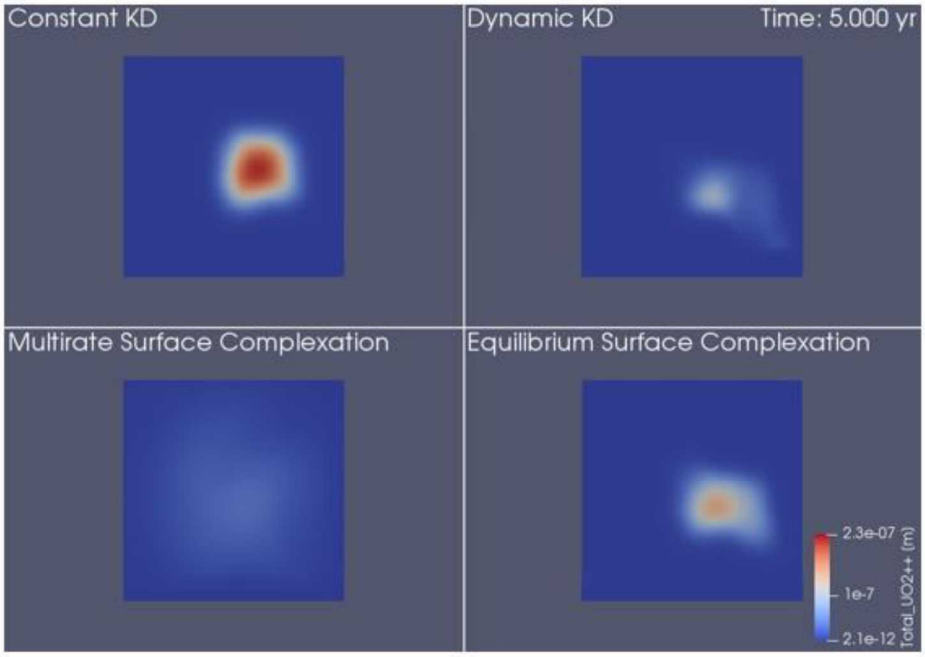

Fig. A-4 **Total aqueous U(VI) at 5 years simulation time for each of the four sorption models using global implicit reactive transport with heterogeneous flow**

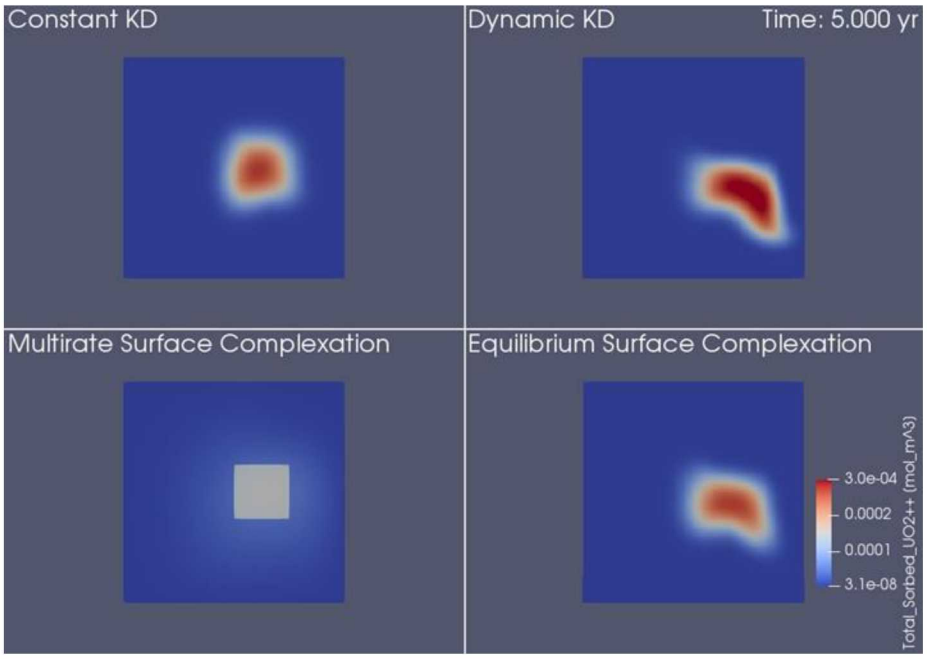

Fig. A-5 **Total sorbed U(VI) at 5 years simulation time for each of the four sorption models using global implicit reactive transport with heterogeneous flow**

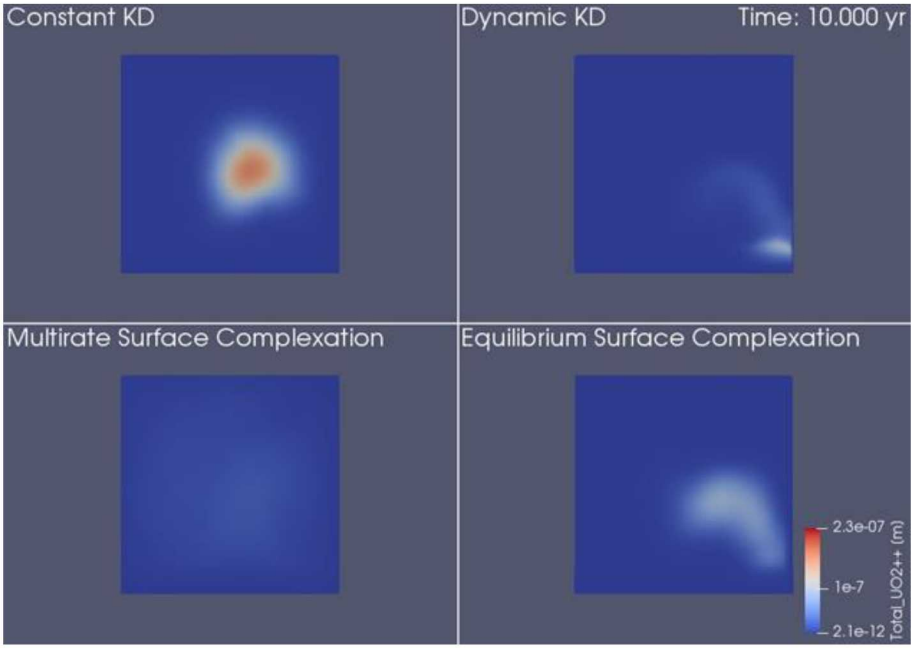

Fig. A-6 **Total aqueous U(VI) at 10 years simulation time for each of the four sorption models using global implicit reactive transport with heterogeneous flow**

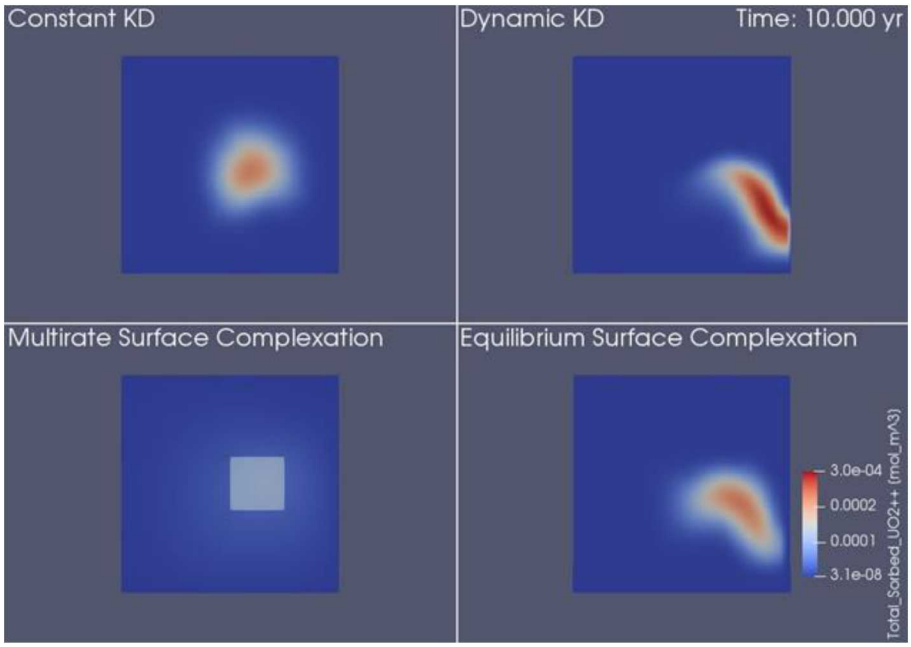

Fig. A-7 **Total sorbed U(VI) at 10 years simulation time for each of the four sorption models using global implicit reactive transport with heterogeneous flow**

Breakthrough at Observation Points

The breakthrough of simulated aqueous and sorbed U(VI) and River Tracer was monitored at observation points placed at the center of the source (<160, 128, 8>, West Observation Point) and 64 m to the east (<224, 128, 8>, East Observation Point). Fig. A-8 illustrates these concentrations over the ten-year simulation. As river water intrudes the site during high river stage, both aqueous and sorbed U(VI) is displaced. This is particularly evident at the eastern observation point. Over time, U(VI) concentrations in both phases increase at the eastern observation point and decrease within the source zone (the western observation point). Relative to equilibrium surface complexation, the dynamic K_D model underpredicts aqueous and sorbed U(VI) concentrations in the source zone while the constant K_D model overestimates U(VI) concentrations. It is unclear which of the K_D-based models is more accurate to the west, except that the dynamic K_D model undulates more similarly to the equilibrium surface complexation model.

At the eastern observation point, all three equilibrium sorption models overlap rather well in the aqueous phase. This is likely due to the dominance of river water and chemistry in this near-river location. The dynamic K_D and equilibrium surface complexation models exhibit the closest match in the sorbed phase.

Fig. A-9 illustrates $\mathcal{K}_D$ at the two observation points. The dynamic K_D model is well correlated with river tracer concentration, as would be expected since it is a function of normalized river tracer concentration. However, the maximum $\mathcal{K}_D$ for the dynamic K_D model far surpasses that of the equilibrium surface complexation model at both observation points. It is important to recall that the $\mathcal{K}_D$ is a measure of distribution (i.e., the ratio of aqueous to sorbed mass) not a concentration itself. In addition, a linear scale is used for $\mathcal{K}_D$ in this figure while a log scale was used in Fig. A-8. Thus, Fig. A-9 will tend to accentuate differences between the sorption models.

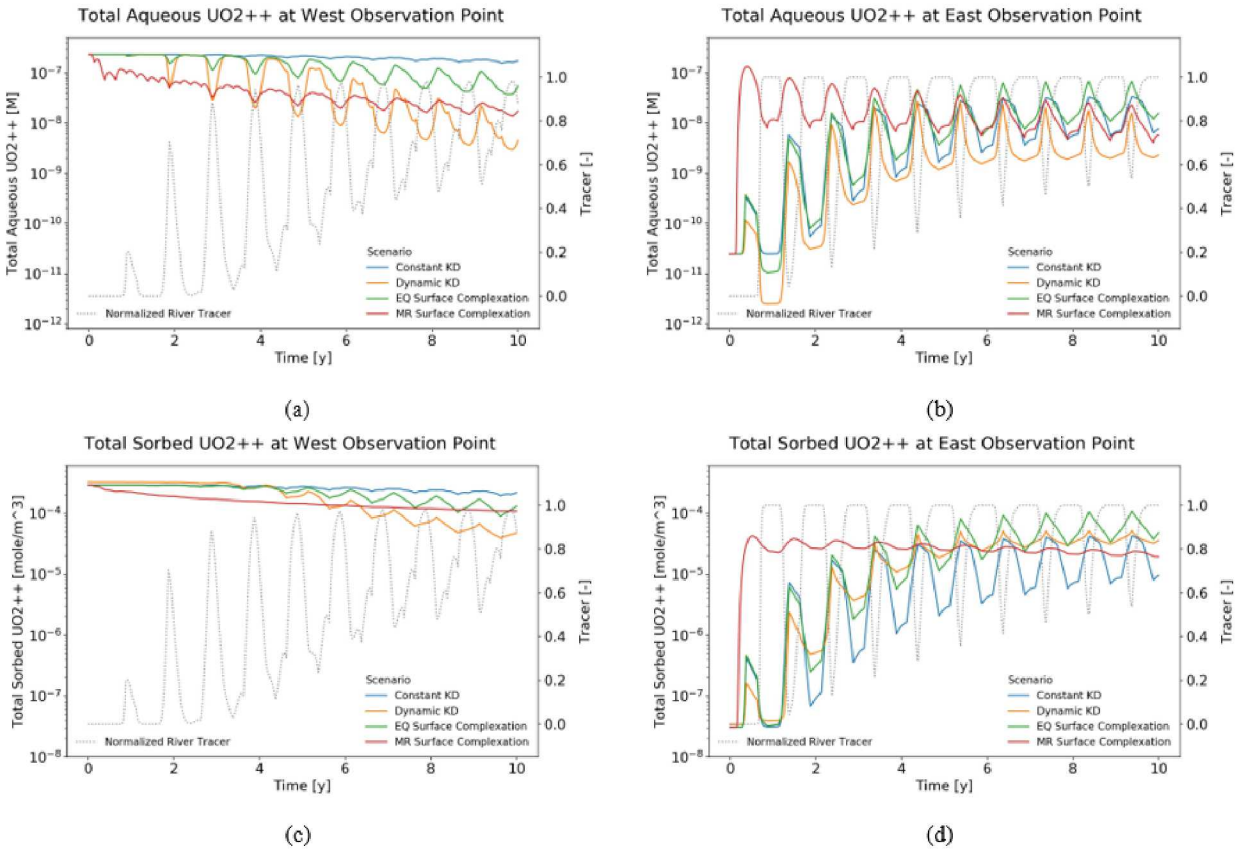

Fig. A-8 **Breakthrough of total aqueous U(VI), total sorbed U(VI) and river tracer concentrations at west and east observation points**

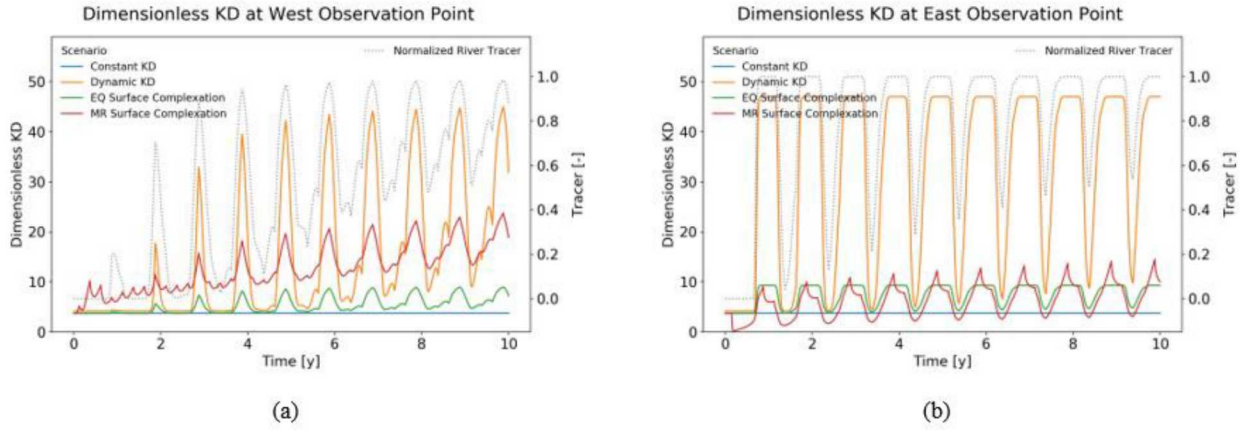

Fig. A-9 **Observed dimensionless K_D at the west and east observation points**

Comparison of Computational Performance

This section presents a comparison of computational performance for the matrix of problem scenarios presented in Tab. A-2 executed on 16–1024 processes on the Skybridge supercomputer at Sandia National Laboratories. Overall, 116 simulations were executed in the comparison:

- 4 sorption models: constant K_D, dynamic K_D, equilibrium surface complexation, kinetic multirate surface complexation 2 coupling schemes: global implicit (GIRT), operator split (OSRT)
- 2 flow fields: prescribed uniform, heterogeneous
- 7 process configurations: 16, 32, 64, 128, 256, 512, 1024
- $4 \times 2 \times 2 \times 7 = 112$.

Fig. A-10 describes the format in which results are plotted in the figures that follow. Lines in the plot define run time versus the number of processes employed for each scenario in Tab. A-2. Both axes are in $\log_{10}$ scale. The dashed gray line represents the slope of ideal parallel performance. Line slope steeper than ideal exhibits super-linear performance, while shallower is sub-linear. For ideal parallel performance, a scenario will run 64× faster on 1024 processes than 16 (1024/16 = 64).

Multiple scenarios are plotted in each figure for comparison purposes. The vertical distance between lines for specified process counts reflects the algorithmic speedup provided by one scenario over another. For instance, the constant K_D sorption model run with a specified uniform velocity field executed in operator split mode on 1024 processes should run much faster than kinetic multi-rate surface complexation run with heterogeneous flow and global implicit coupling for each of the process configurations (16–1024). In all aspects, the computational or algorithmic demand of the first scenario is less than the second. Therefore, the vertical distance between the lines is considered algorithmic speedup, or the speedup enabled by using alternative algorithms.

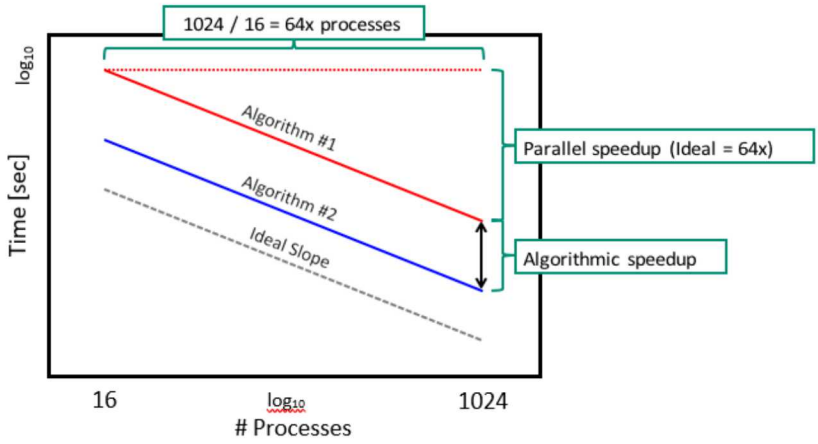

Fig. A-10 Description of performance plots where the curves represent the performance of each scenario executed on 16–1024 processes. The Ideal Slope line is provided as a reference for ideal performance.

Performance of Flow Solution

Eight of the scenarios utilized a heterogeneous flow solution where the RICHARDS flow process model within PFLOTRAN solves for single-phase variably-saturated groundwater flow within a heterogeneous permeability field. The resulting flow field is identical for all scenarios, but the run time may differ due to random artifacts on the supercomputer (e.g., layout of processes, communication congestion, disk read/write access, OS jitter). This is to be expected. Fig. A-11 shows these times for the eight scenarios that employed heterogeneous flow. Note the deviation of performance at high processes counts which suggests that one or more of the artifacts mentioned above affected communication time (the time spent

transferring information from one process to others in the parallel algorithms). For the most part, these flow results overlap up to 64 processes. Hammond et al. (2014) demonstrated that for flow problems composed of one degree of freedom per grid cell, which is the case in these scenarios, parallel performance tends to degrade below 10 thousand degrees of freedom (dofs) per process as time spent in parallel communication becomes excessive compared to time in floating point calculations. At 128 processes, the number of dofs per process is 8192 and degradation in performance is to be expected. Fig. A-12 is the same as Fig. A-11 with the average time spent in flow superimposed in solid black. This solid "Flow Average" line is used later to illustrate the cost of flow relative to the reactive transport process models.

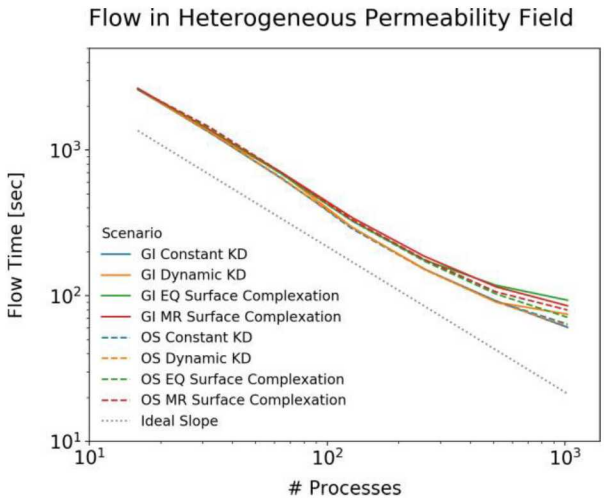

Fig. A-11 Run time performance of flow process model for scenarios employing heterogeneous flow

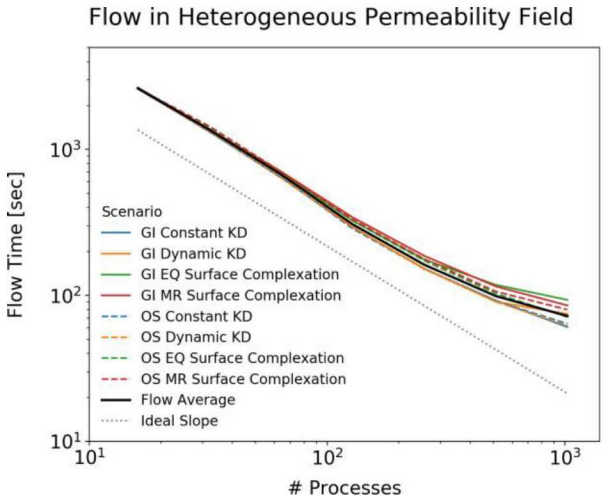

Fig. A-12 Flow solutions times with the average superimposed

Speedup Results

Fig. A-13 plots the wall clock times for the four sorption process models run with specified uniform flow (a) and heterogeneous flow (b). The parallel scalability for all eight algorithms is very similar as the algorithmic speedup (the vertical distance between the lines) is similar for all process counts. The slight deviation from ideal speedup at high process counts applies to all scenarios.

The parallel speedup for 1024 processes relative to 16 lies between 42–46 for all scenarios. The two K_D models are 21 and 7 times faster than the surface complexation models for the uniform and heterogeneous flow scenarios, respectively. The slightly larger time required for the dynamic K_D model (relative to constant K_D) is attributable to the solution of two transport dofs per grid cell instead of one.

The global implicit results plotted in Fig. A-14 demonstrate similar behavior, but all wall clock times are shifted upward (relative to Fig. A-13). Since the global implicit approach fully couples all primary dependent variables in the reactive transport problem, the linear system of equations solved in Newton's method is much larger, and the embedded chemistry can be highly nonlinear. Thus, more time is spent within the linear and nonlinear solvers for global implicit coupling.

The surface complexation model times are nearly identical, though kinetic multi-rate is still slower. This is expected since the kinetic multi-rate calculation is essentially equilibrium surface complexation with 50 mass transfer calculations appended (see Hammond and Lichtner, 2010). The expense of calculating heterogeneous flow combined with surface complexation is minimal as the overall run time is similar to specified uniform flow (compare "MR Surface Complexation" in (a) and (b) in Fig. A-14).

Fig. A-15 shows the distribution of time between transport and chemical reaction for each of the operator split scenarios run with uniform flow. Both surface complexation models require significantly more time for reaction than transport (2–6 times as much) while the reaction portions of the K_D scenarios are much more efficient. In fact, transport requires 2–3 times as much time as reaction for the K_D scenarios. These results demonstrate that any further effort expended to reduce reaction times will provide minimal improvement to the overall wall clock times for these process models, as the transport portion of the calculation is the bottleneck.

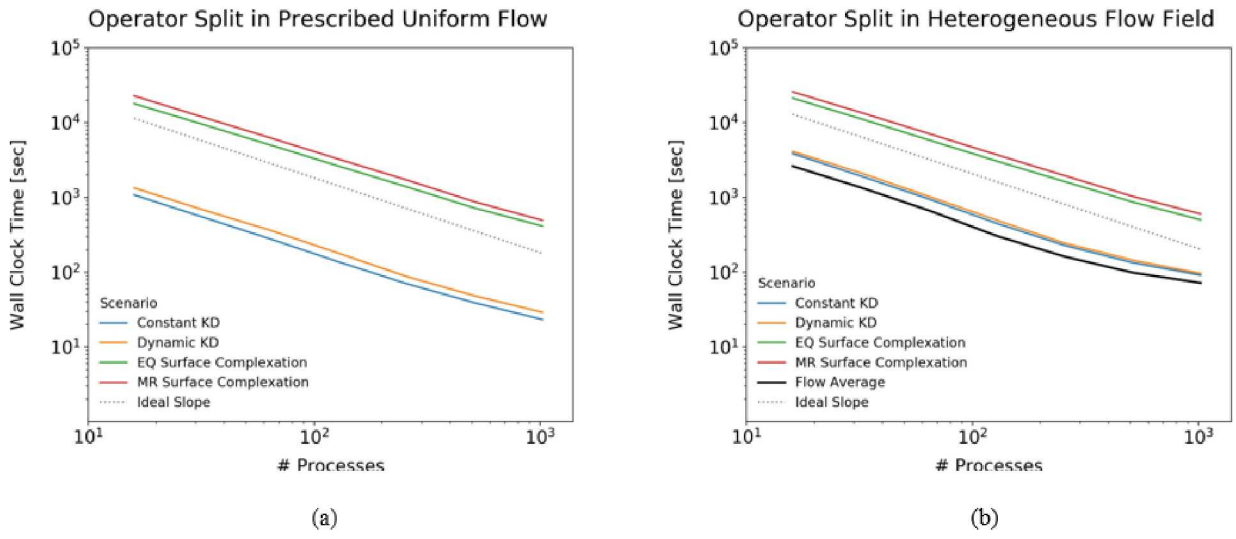

Fig. A-13 Operator split wall clock times with uniform (left) and heterogeneous (right) flow

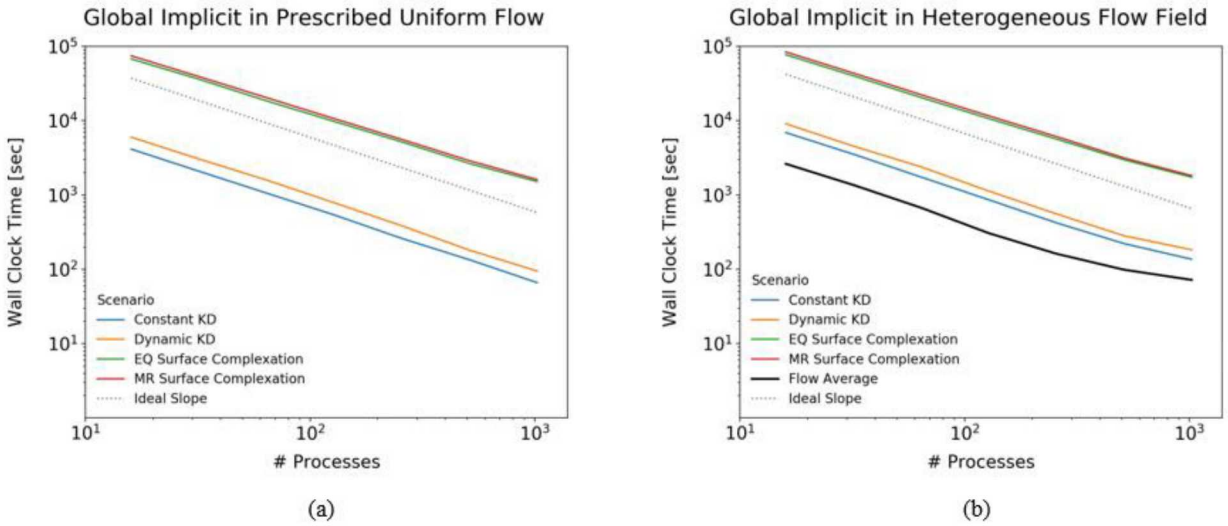

Fig. A-14 Global implicit wall clock times with uniform (left) and heterogeneous (right) flow

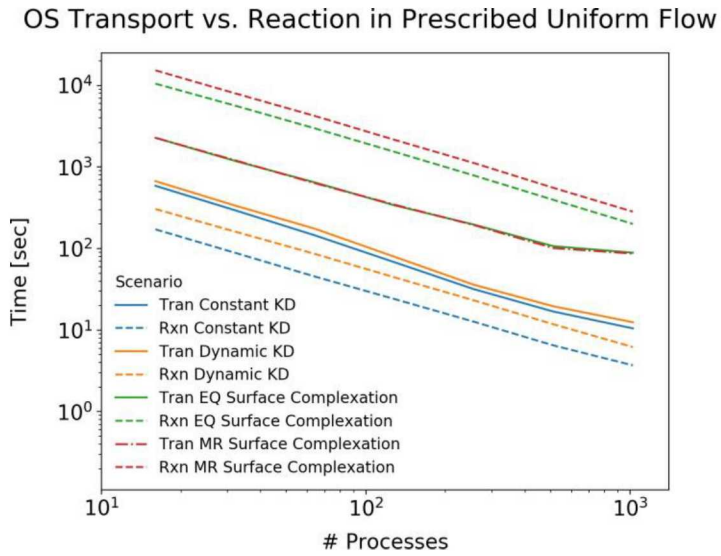

Fig. A-15 Comparison of transport versus reaction time for operator split reactive transport in uniform flow field

Discussion

Tab. A-3, Tab. A-4, and Tab. A-5 present the maximum speedups enabled by operator splitting, parallel processing and simplification of sorption chemistry, respectively. These results are specific to the Hanford 300 Area problem described above being run on Sandia's Skybridge supercomputer using PFLOTRAN. It is possible that these maximum speedups will differ on other problem scenarios and supercomputers.

As discussed above, the use of operator splitting can speedup reactive transport modeling by reducing the size of the linear and nonlinear systems of equations being solved. Table 3 lists the maximum speedup of operator splitting over the global implicit approach for all parallel process configurations for each sorption model and flow configuration. In other words, the speedup of 3.9 listed for Specified Uniform and Constant K_D is the maximum speedup observed when operator splitting was compared to global implicit using the same number of processes over the test range of 16–1024 processes. For all sorption models, the speedup is lower for the heterogeneous flow scenarios since the flow process model experiences no performance gain due to operator splitting. The flow regime has less of an impact on operator splitting speedup for the surface complexation models as they are more computational expensive overall (see Fig. A-13 and Fig. A-14) and the flow process model consumes less of the overall wall clock time.

Tab. A-4 shows the maximum speedups (and efficiencies) provided by parallel processing on the Skybridge supercomputer. These relative speedups are calculated by dividing the wall clock times for simulations run on 1024 processes by the corresponding times on 16 processes. Results are not split out amongst the K_D-based (constant and dynamic) and surface complexation (equilibrium and kinetic multi-rate) sorption models as there was little difference in run times. As there is more computation required for the global implicit solution, the higher efficiencies on the right two columns are expected. Note that the efficiency of the global implicit K_D-based runs is nearly perfect for uniform flow.

Tab. A-5 presents the maximum speedups provided by the simplified K_D-based chemistry models relative to the surface complexation models. These speedups are calculated by dividing the surface complexation model's time by the K_D model's time for the same number of parallel processes and same flow regime. The K_D-based sorption models clearly outperform the full surface complexation, especially for specified uniform flow. It should be noted that the computational expense of using the dynamic instead of the constant K_D model (measured as % increase in wall clock time) was on average 26% (24–31%) and 8% (5–10%) for uniform and heterogeneous flow, respectively. These costs are small relative to the accuracy gained through using the dynamic K_D sorption model (compare constant vs dynamic K_D in Fig. A-4 through Fig. A-9). Although the maximum speedups due to using simplified chemistry alone top out at 10–20, the combined effect of using parallel processing and operator splitting increases these speedups by a factor of 100. This can be demonstrated as follows.

The results demonstrate that the dynamic K_D sorption model best matches the equilibrium surface complexation model. Using the speedups provided in Tab. A-3, Tab. A-4, and Tab. A-5, one may determine maximum speedup for each of the two flow scenarios based on a combination of (1) operator split instead of global implicit coupling, (2) parallel processing (1024 instead of 16 processes) and (3) simplified chemistry (dynamic K_D model in place of equilibrium surface complexation). The wall clock times and projected speedups are listed in Tab. A-6, where the dynamic K_D model experiences a combined speedup of 2314 and 802 for uniform and heterogeneous flow, respectively.

Tab. A-3 Maximum speedup due to operator split instead of global implicit coupling

Flow Field	Constant K_D	Dynamic K_D	Equilibrium Surface Complexation	Kinetic Multirate Surface Complexation
Specified Uniform	3.9	4.5	3.8	3.3
Heterogeneous	1.9	2.3	3.6	3.2

Tab. A-4 Maximum speedup (efficiency) due to parallel processing

	Operator Split		Global Implicit	
Flow Field	K_D-based	Surface Complexation	K_D-based	Surface Complexation
Specified Uniform	46.3 (72%)	46.2 (72%)	63.1 (99%)	46.2 (72%)
Heterogeneous	43.0 (67%)	42.9 (67%)	50.5 (79%)	46.1 (72%)

Tab. A-5 Maximum speedup due to simplified chemistry

Flow Field	Operator Split	Global Implicit
Specified Uniform	~21	~18
Heterogeneous	~7	~12

Tab. A-6 Projected speedup due to operator split solution, parallel processing and simplified chemistry

Flow Field	Operator Split/ Dynamic K_D/1024	Global implicit/Equilibrium Surface Complexation/16	Speedup
Specified Uniform	29.2 sec	67556.0 sec	2314
Heterogeneous	96.2 sec	77117.0 sec	802

Conclusions

This study demonstrates the benefits of reduced-order sorption models for simulating U(VI) transport at the Hanford 300 Area. The research demonstrates the improved accuracy of a dynamic K_D model over the constant K_D model and the superior performance of the dynamic K_D model over equilibrium surface complexation. The dynamic K_D model was calibrated to maximum and minimum ratios of sorbed to aqueous U(VI) based on batch geochemistry generated from a more mechanistic surface complexation model and concentrations from representative groundwater and river water at the site. The superior accuracy of the dynamic K_D model was shown, e.g., in Fig. A-7, where the dynamic K_D model matched equilibrium surface complexation much better than the constant K_D model. The speedup results presented above demonstrate that by using the dynamic K_D model alone, a speedup of ~10–20 can be achieved over the surface complexation models depending on whether a flow process model is included in the simulation. In addition, parallel processing and the decoupling of transport and reaction through operator splitting can further enhance simulator performance by 100-fold with speedups ranging ~800–2300, again, depending on whether a flow process model is included in the simulation.

References

Hammond, G. E. and Lichtner, P. C.: Field-scale model for the natural attenuation of uranium at the Hanford 300 Area using high-performance computing, Water Resources Research, 46, https://doi.org/10.1029/2009WR008819, https://agupubs.onlinelibrary.wiley.com/doi/abs/10.1029/2009WR008819, 2010.

Hammond, G. E., Lichtner, P. C., and Mills, R. T.: Evaluating the performance of parallel subsurface simulators: An illustrative example with PFLOTRAN, Water Resources Research, 50, 208–228, https://doi.org/10.1002/2012WR013483, https://agupubs.onlinelibrary.wiley.com/doi/abs/10.1002/2012WR013483, 2014.

Stockmann, M., Schikora, J., Becker, D.-A., FlÃ¼gge, J., Noseck, U., and Brendler, V.: Smart Kd-values, their uncertainties and sen- sitivities - Applying a new approach for realistic distribution coefficients in geochemical modeling of complex systems, Chemo- sphere, 187, 277 – 285, https://doi.org/https://doi.org/10.1016/j.chemosphere.2017.08.115, http://www.sciencedirect.com/science/article/pii/S0045653517313395, 2017.

Valocchi, A. J. and Malmstead, M.: Accuracy of operator splitting for advection-dispersion-reaction problems, Water Resources Research, 28, 1471–1476, https://doi.org/10.1029/92WR00423, https://agupubs.onlinelibrary.wiley.com/doi/abs/10.1029/92WR00423, 1992.

Zachara, J. M., Chen, X., Song, X., Shuai, P., Murray, C., and Resch, C. T.: Kilometer-Scale Hydrologic Exchange Flows in a Gravel Bed River Corridor and Their Implications to Solute Migration, https://doi.org/10.1029/2019WR025258, https://agupubs.onlinelibrary.wiley.com/doi/abs/10.1029/2019WR025258, e2019WR025258 2019WR025258, 2020.

(This page is intentionally blank.)

Appendix B. FUEL MATRIX DEGRADATION MODELING IN FORTRAN

APPENDIX B. FUEL MATRIX DEGRADATION MODELING IN FORTRAN

Introduction

Surrogate models for the FMD (Fuel Matrix Degradation) process model provide significant improvements in speed for high throughput modeling of various reference cases. These models are trained on data produced by the FMD process model; bootstrapping the surrogate models to the data on which they were trained. If the underlying process model is updated, due to new experimental data, the surrogate models necessarily have to be retrained. The current implementation of the FMD process model is slow, has convergence issues, and produces discontinuities in outputted fluxes. Therefore, improving the efficiency and reliability of the FMD process model is crucial. Herein we will describe current and on-going efforts to identify computational bottlenecks in the FMD process model and the refactoring process. A brief overview of the model will be provided, efforts to refactor the code from scratch will be described, and a computational bottleneck with potential solution will be identified.

FMD Physical Model

We will provide a brief summary of the key features of the FMD model, however the model has been described in much greater detail in several references (Jerden, et al., 2012; Jerden, et al., 2018) The FMD model seeks to predict the degradation rate of UO_2 using a Mixed Potential Model approach, originally based on the Canadian Mixed Potential Model of Shoesmith, King, and Kolar (Shoesmith, et al., 2003). The Mixed Potential Approach works on two assumptions: (1) electrochemical reactions can be broken into partial oxidation/reduction reactions, and (2) no net accumulation of charge is observed (Wagner and Traud, 1938). Electrochemical reactions are observed at the fuel surface; catalyzed by noble metal particles and uncatalyzed, and at the steel surface. In addition to the electrochemical reactions, the following capabilities are included

- Hydrogen generated from steel corrosion
- Alpha radiolysis and oxidant generation from fuel burn-up
- Precipitation of UO_2 creating a porous layer that affects diffusion
- Arrhenius temperature dependence of reaction rates
- One-dimensional diffusion

The chemical processes included in the FMD model are shown in Fig. B-1. The 1D reaction column is divided into three regions; namely the fuel surface, the solution region, and the steel surface. In practice each region can be discretized into several grid cells.

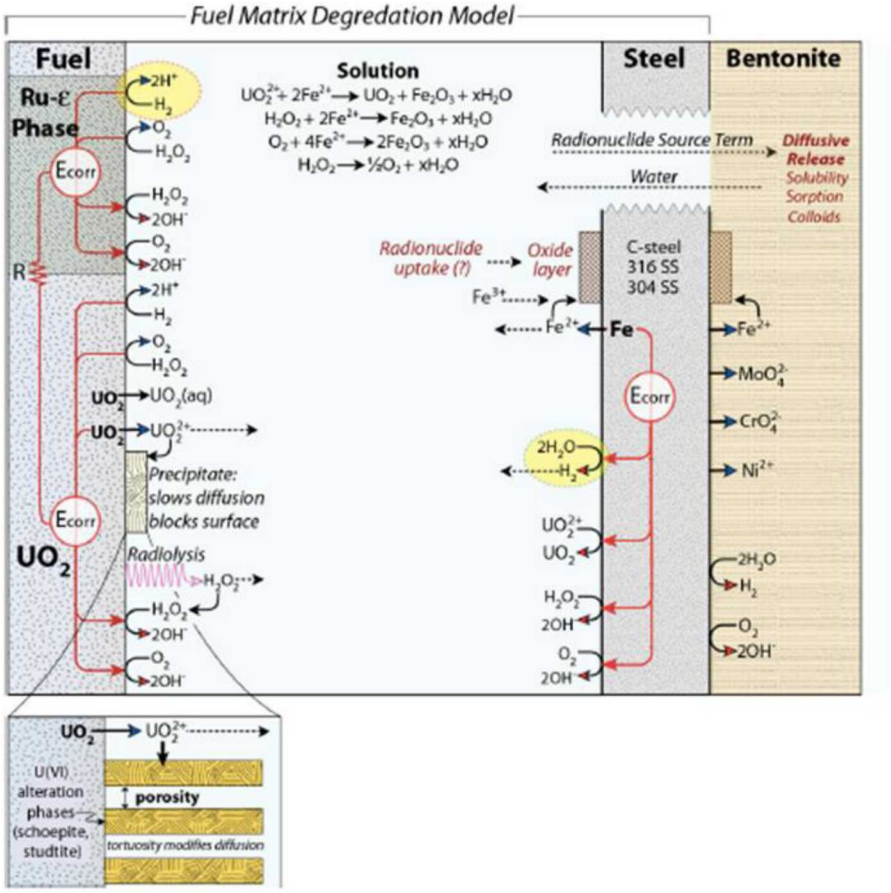

Fig. B-1 **Schematic depicting the physical model described by the FMD model. Three regions are included; fuel surface, bulk solution, and steel surface. Electrochemical reactions are observed in the fuel and steel regions, where noble metal particles (Ru-ε) can catalyze these reactions at the fuel surface. Fuel (UO_2) dissolves, via chemical dissolution or oxidation, to form UO_2^{2+} which diffuses to the breached steel surface and becomes the radionuclide source term. UO_2^{2+} can also reprecipitate in the form of shoepite, forming a porous barrier and slowing diffusion to the fuel surface.**

The bulk solution reactions depicted in Fig. B-1 are implemented by discretizing the system in space and time and solving the partial differential equations using a nonlinear solver. In the Mixed Potential Model approach, the electrochemical reactions at the fuel and steel surface are implemented by calculating the mass loss according to the current density as described by Faradays Law.

$$\frac{dFuel}{dt} = \frac{i_{corr}^{fuel} MW_{fuel}}{nF} \tag{B.1}$$

where i_{corr}^{fuel} is the corrosion current density, MW_{fuel} is the molecular weight of the fuel, n is the number of transferred electrons, and F is Faraday's constant. A current density for each reaction can be defined and is shown in Tab. B-1. A particular challenge exists where the current densities depend on both the concentrations and the corrosion potential for a particular surface ($E_{corr}^{fuel}/E_{corr}^{steel}$). In the current

implementation these unknowns are solved sequentially; first solving for the corrosion potential with a given concentration, and then solving for the new concentration given the calculated corrosion potential.

H_2O_2 is the primary oxidant included in the FMD model. This species is produced via alpha radiolysis. Radiolysis is incorporated into the FMD model via a straightforward analytical function which describes the production of H_2O_2 as a function of space and time (Buck, et al., 2013). It is given by

$$Molar\ Yield\ of\ H_2O_2(x,t) = \left[G_{H_2O_2}\right](H_2, O_2) * [Dose\ Rate](x,t) * g(x) \quad \text{(B.2)}$$

where $g(x)$ is a geometrical factor that alters the diffusion of aqueous species through the tortuosity of precipitated UO_2.

Tab. B-1 **Electrochemical reactions and parameters included in the FMD model where i is the current density for a given reaction, k is the half reaction rate constant, α is the charge transfer coefficient, E^0 is the standard potential, and dT is temperature factor given by $dT = \left(\frac{1}{298} - \frac{1}{T}\right)/R$ where T is the current temperature and R is the gas constant. There are 3 surfaces (fuel, fuel/NMP, and steel) and each surface has a corrosion potential, E_{corr}, which must be determined at each timestep.**

Surface	Reactions	Equation	k	α	E° (V)
Fuel	$UO_2 \rightarrow UO_2^{2+} + 2e^-$	$i^{UO_2,1} = nF\varepsilon k_{UO_2,1} exp\left[\frac{\alpha_{UO_2,1}F}{RT}\left(E_{corr}^{UO_2} - E_{UO_2,1}^0\right)\right]$	$5.0x10^{-8}exp[6.0x10^4 \cdot dT]$	0.96	0.169
	$UO_2 + 2CO_3^{2-} \rightarrow UO_2CO_3^{2-} + 2e^-$	$i^{UO_2,2} = nF\varepsilon k_{UO_2,2}[CO_3^{2-}]^{\frac{2}{3}} \exp\left[\frac{\alpha_{UO_2,2}F}{RT}\left(E_{corr}^{UO_2} - E_{UO_2,2}^0\right)\right]$	$1.3x10^{-8}exp[6.0x10^4 \cdot dT]$	0.82	.173
	$UO_2 \rightarrow UO_{2,(aq)}$	$i^{UO_2,3} = nF\varepsilon k_{UO_2,3} \exp\left[\frac{\alpha_{UO_2,3}F}{RT}\left(E_{corr}^{UO_2} - E_{UO_2,3}^0\right)\right]$	$2.0x10^{-14}exp[6.0x10^4 \cdot dT]$	0.00	0.000
	$H_2 + 2OH^- \rightarrow 2H_2O + 2e^-$	$i^{H_2} = nF\varepsilon k_{H_2}[H_2] exp\left[\frac{\alpha_{H_2}F}{RT}\left(E_{corr}^{UO_2} - E_{H_2}^0\right)\right]$	$3.6x10^{-12}exp[6.0x10^4 \cdot dT]$	0.50	0.584
	$H_2O_2 + 2OH^- \rightarrow O_2 + 2H_2O + 2e^-$	$i^{H_2O_2,1} = nF\varepsilon k_{H_2O_2,1}[H_2O_2] exp\left[\frac{\alpha_{H_2O_2,1}F}{RT}\left(E_{corr}^{UO_2} - E_{H_2O_2,1}^0\right)\right]$	$7.4x10^{-8}exp[6.0x10^4 \cdot dT]$	0.41	-0.098
	$H_2O_2 + 2e^- \rightarrow 2OH^-$	$i^{H_2O_2,2} = nF\varepsilon k_{H_2O_2,2}[H_2O_2] exp\left[\frac{\alpha_{H_2O_2,2}F}{RT}\left(E_{corr}^{UO_2} - E_{H_2O_2,2}^0\right)\right]$	$1.2x10^{-12}exp[6.0x10^4 \cdot dT]$	-0.41	0.973
	$O_2 + 2H_2O + 4e^- \rightarrow 4OH^-$	$i^{O_2} = nF\varepsilon k_{O_2}[O_2] exp\left[\frac{\alpha_{O_2}F}{RT}\left(E_{corr}^{UO_2} - E_{O_2}^0\right)\right]$	$1.4x10^{-12}exp[6.0x10^4 \cdot dT]$	-0.50	0.157
Fuel, NMP	$H_2 + 2OH^- \rightarrow 2H_2O + 2e^-$	$i^{H_2} = nF\varepsilon k_{H_2}[H_2] exp\left[\frac{\alpha_{H_2}F}{RT}\left(E_{corr}^{NMP} - E_{H_2}^0\right)\right]$	$5.0exp[6.0x10^4 \cdot dT]$	0.50	0.584
	$H_2O_2 + 2e^- \rightarrow 2OH^-$	$i^{H_2O_2,1} = nF\varepsilon k_{H_2O_2,1}[H_2O_2] exp\left[\frac{\alpha_{H_2O_2,1}F}{RT}\left(E_{corr}^{NMP} - E_{H_2O_2,1}^0\right)\right]$	$1.2x10^{-12}exp[6.0x10^4 \cdot dT]$	-0.40	0.973
	$H_2O_2 + 2OH^- \rightarrow O_2 + 2H_2O + 2e^-$	$i^{H_2O_2,2} = nF\varepsilon k_{H_2O_2,2}[H_2O_2] exp\left[\frac{\alpha_{H_2O_2,2}F}{RT}\left(E_{corr}^{UO_2} - E_{H_2O_2,2}^0\right)\right]$	$5.0x10^{-12}exp[6.0x10^4 \cdot dT]$	0.41	-0.098
	$O_2 + 2H_2O + 4e^- \rightarrow 4OH^-$	$i^{O_2} = nF\varepsilon k_{O_2}[O_2] exp\left[\frac{\alpha_{O_2}F}{RT}\left(E_{corr}^{UO_2} - E_{O_2}^0\right)\right]$	$1.4x10^{-12}exp[6.0x10^4 \cdot dT]$	-0.50	0.157
Steel	$Fe \rightarrow Fe^{2+} + 2e^-$	$i^{steel} = nF\varepsilon k_{steel} exp\left[\frac{\alpha_{steel}F}{RT}\left(E_{corr}^{steel} - E_{steel}^0\right)\right]$	$1.0x10^{-6}exp[1.0x10^4 \cdot dT]$	0.20	0.203
	$2H_2O + 2e^- \rightarrow H_2 + 2OH^-$	$i^{H_2O} = nF\varepsilon k_{H_2O} exp\left[\frac{\alpha_{H_2O}F}{RT}\left(E_{corr}^{steel} - E_{H_2O}^0\right)\right]$	$1.0x10^{-6}exp[1.0x10^4 \cdot dT]$	-0.48	-1.072

FMD Implementation

Currently the most frequently updated and used implementation of the FMD model is a MATLAB version. While a stand-alone Fortran version exists (Jerden, et al., 2015), it is a simply a copy of the MATLAB version into a new programming language. The MATLAB implementation exists as a main program and several subroutines and functions that make use of multiple built-in MATLAB functionalities. A flow chart for the MATLAB version of the FMD model is depicted in Fig. B-2. A main program (AMP_main) launches the simulation and drives the loop over time points. A function (`AMP_solve`) is called at each time point which runs the standard Newton Raphson (NR) iteration process to solve for new concentrations. For each NR iteration the Jacobian and Residual are calculated in three stages using AMP_reactFuel, AMP_reactCani, AMP_reactBulk which calculates the components to each at the fuel surface, canister surface, and bulk reaction regions. However, the concentration of several components are dependent upon the corrosion potential, therefore for each new concentration solve the corrosion potential at both surfaces must be solved using a separate NR process.

The number of NR iterations needed to solve for the new concentrations at each time point, from a representative FMD simulation, are shown in Fig. B-3; roughly 5-10 iterations are needed. For *each* of these iterations the number of iterations needed to solve for the corrosion potentials at the fuel and steel surface are shown in Fig. B-4. We note the number of NR iterations needed to solve for the new concentrations at the second time point is 11. Therefore, we would expect 11 separate points at the second time point in Fig. B-4. However, the number of iterations needed to solve for the corrosion potentials are often identical and therefore several points are overlapping, therefore only 3 distinct points are observed.

It is clear from this analysis that significant computing time is spent sequentially iterating over dependent processes (new concentrations and corrosion potentials). And, in fact, a timing test was performed and noted that ~30% of the computational time is spent solving for the corrosion potentials. *We hypothesize that we can couple the NR solves for the new concentration and corrosion potentials.* Similar to the evolution of reactive-transport modeling from sequential reaction and transport iterations to the global implicit approach where a fully-coupled nonlinear system of equations for both reaction and transport are included in the Jacobian, we believe that a significant speed up will be observed by reducing the overall number of iterations needed.

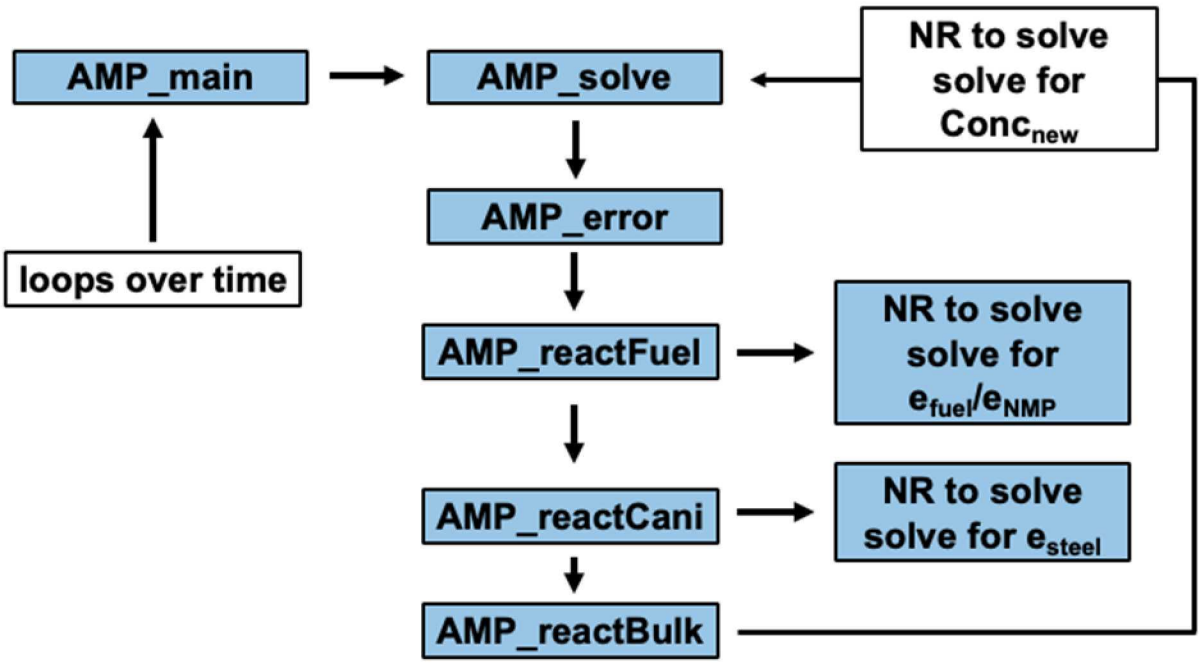

Fig. B-2 **Flow chart for the FMD model implemented in MATLAB. AMP_main starts the simulation and iterates over time. AMP_solve runs the standard Newton Raphson (NR) iteration to solve for the new concentrations. Within each NR iteration, the corrosion potential at the fuel surface (AMP_reactFuel) and canister surface (AMP_reactCani) are solved iteratively using a separate NR process.**

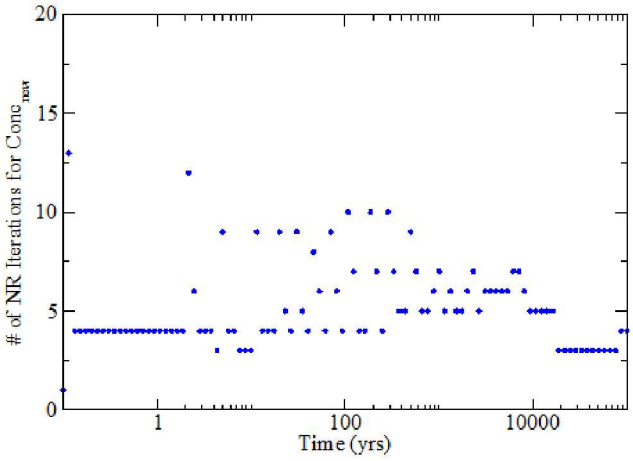

Fig. B-3 **The number of Newton Raphson (NR) iterations needed at each time point throughout the simulation to solve for the new concentrations.**

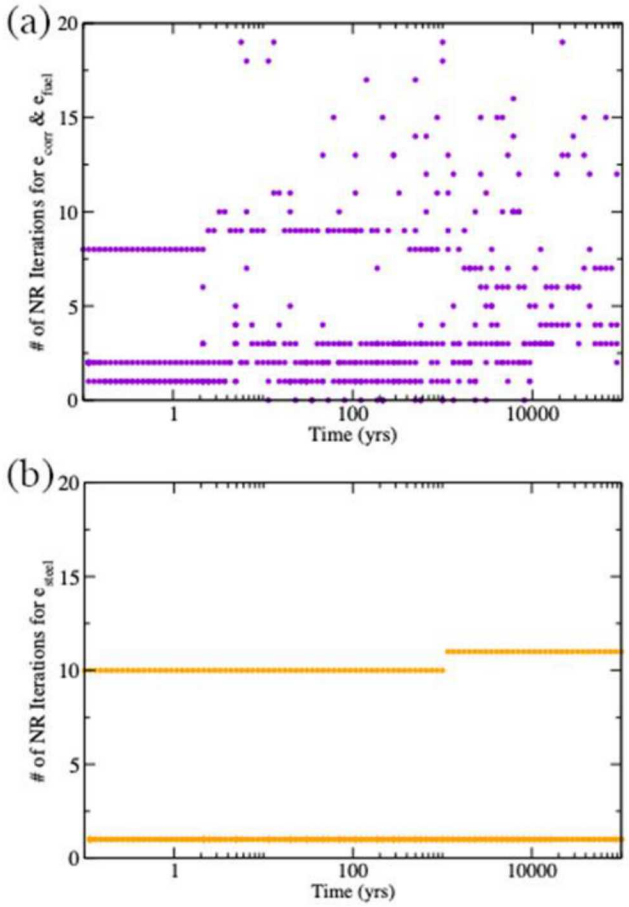

Fig. B-4 **Number of Newton Raphson (NR) iterations needed to solve for the corrosion potential at the fuel surface (a) and canister surface (b). Note that for each time point a NR solve is performed to update the concentrations, and for each of those NR iterations, the number of iterations shown in (a) and (b) are performed. The identical number of iterations is often needed and leads to overlapping points on this figure.**

We will briefly describe the hypothetical approach that will be pursued in future efforts. Imagine a 1D reactive-transport system that incorporates 3 species (A, B, and C). The standard residual is given by

$$f\left(c^{k+1,p}\right) = \frac{c^{k+1,p} - c^{k}}{\Delta t} + L\left(c^{k+1,p}\right) - R(c^{k+1,p}) \tag{B.3}$$

where c is the concentration of a given species, L is the diffusion operator, and R is the kinetic rate expression. We will now introduce a fictitious function for the fuel corrosion potential ($g(E_{corr}^{fuel})$). In the interest of simplicity, we introduce a single function, however the FMD model currently has two corrosion potential functions. Assuming the corrosion potential function only depends on the corrosion potential and the concentration of A, (E_{corr}^{fuel}, c^{A}), the residual is transformed to

$$f\left(c^{k+1,p}\right) = \frac{c^{k+1,p} - c^{k}}{\Delta t} + L\left(c^{k+1,p}\right) - R\left(c^{k+1,p}\right) + g\left(E_{corr}^{fuel}, c^{A}\right). \tag{B.4}$$

The derivative can then be computed to determine the Jacobian. New concentrations and corrosion potentials are updated using the standard NR approach. In matrix form this has the effect of adding an

additional row (new equation) and additional column (new unknown) to the usual submatrices. However, we note that this *only* applies to the grid cells in which the corrosion potential plays a role (e.g., the fuel surface region). Moreover, the corrosion potential variable (E_{corr}^{fuel}) appears in no other functions, therefore most of the new entries in the Jacobian will be 0. And lastly, in this example, we have assumed the corrosion potential function is solely a function of the corrosion potential (E_{corr}^{fuel}) and the concentration of species A (c^A), therefore there will only be nonzero entries in the columns in which the derivatives with respect to these variables are performed. Note, in practice, there could be multiple corrosion potential functions which could depend on the concentrations of several species.

Current Efforts

Given the identification of the computational bottleneck, our approach is to refactor the FMD algorithm, with the philosophy of creating a stand-alone Fortran version that could be (1) more easily used and updated by external collaborators, and (2) be modified for other potential corrosion applications. In this vein we seek to develop, from scratch, a 1D reactive-transport code that implements the FMD model described above. What follows describes that current effort.

Diffusion is implemented by discretizing the system in space and time using the finite volume approach. Imagine a 1D column with 3 grid cells and 1 diffusing species. The resulting discretized governing equation is given by (ignoring advection, kinetic reaction, and the source term)

$$V\frac{(\phi C)_i^{k+1}-(\phi C)_i^k}{\Delta t}-\left(\phi AD\frac{C_i-C_{i-1}}{\Delta x}\right)_{i-\frac{1}{2}}^{k+1}+\left(\phi AD\frac{C_{i+1}-C_i}{\Delta x}\right)_{i+\frac{1}{2}}^{k+1}=0=f(C^{k+1,i}) \qquad \text{(B.5)}$$

where k and k+1 are the current and new time step, V is the volume, ϕ is the porosity, C_i is the concentration in the ith grid cell, Δt is the time step, Δx is the distance between grid point centers, A is the area, and D is the diffusion coefficient. In this 1D case we will assume Δy and Δz are 1 and therefore V = Δx and A = 1. We will also assume a *full* grid cell exists at the boundaries. Concentrations are updated using the NR approach while a linear solver is used to solve the equation

$$J\delta C=-f(C^{k+1,i}) \qquad \text{(B.6)}$$

In matrix form this looks like

$$\begin{bmatrix} \frac{V\phi}{\Delta t}-\frac{\phi 2AD}{\Delta x} & \frac{\phi AD}{\Delta x} & 0 \\ \frac{\phi AD}{\Delta x} & \frac{V\phi}{\Delta t}-\frac{\phi 2AD}{\Delta x} & \frac{\phi AD}{\Delta x} \\ 0 & \frac{\phi AD}{\Delta x} & \frac{V\phi}{\Delta t}-\frac{\phi 2AD}{\Delta x} \end{bmatrix}\begin{bmatrix}\delta C_1\\ \delta C_2\\ \delta C_3\end{bmatrix}=\begin{bmatrix}-f\left(C_1^{k+1}\right)\\ -f\left(C_2^{k+1}\right)\\ -f\left(C_3^{k+1}\right)\end{bmatrix} \qquad \text{(B.7)}$$

Adding reactivity to this matrix transforms this matrix into a large (N_c * N_{grid}) × (N_c * N_{grid}) where N_c is the number of components and N_{grid} is the number of grid cells.

Currently we have coded all bulk solution reactions. Our initial diffusion approach mirrored Patankar's implementation which was less general than desired (Patanker, 1980). The finite volume approach briefly described here has now been implemented and bulk solution reactions are being added sequentially. Our workflow for adding a new reaction involves testing it in isolation (turning all other reactions off) and without diffusion, then turning diffusion on, and finally coupling the new reaction with all other previously tested reactions. The code is maintained in a GitLab repository.

A representative batch reaction/no diffusion result is shown in Fig. B-5. In this example we are simulating the bulk reaction of $UO_2^{2+} + 2OH^- + H_2O \rightarrow UO_3 \cdot 2H_2O$ governed by $\frac{d[UO_2^{2+}]}{dt} = -\frac{d[UO_3 \cdot 2H_2O]}{dt} = -k[UO_2^{2+}]$. As a test we have increased the initial concentration of $UO_3 \cdot 2H_2O$ from small (dashed) to large (dotted) while maintaining the initial concentration of UO_2^{2+}. We observe that over identical simulation time, identical amounts of UO_2^{2+} are converted to $UO_3 \cdot 2H_2O$ as; i.e., all black curves are identical. This is expected as the rate of change in the concentration is independent of the $UO_3 \cdot 2H_2O$ concentration. The shape of the red curves are identical and are simply shifted vertically by the difference in the initial concentration.

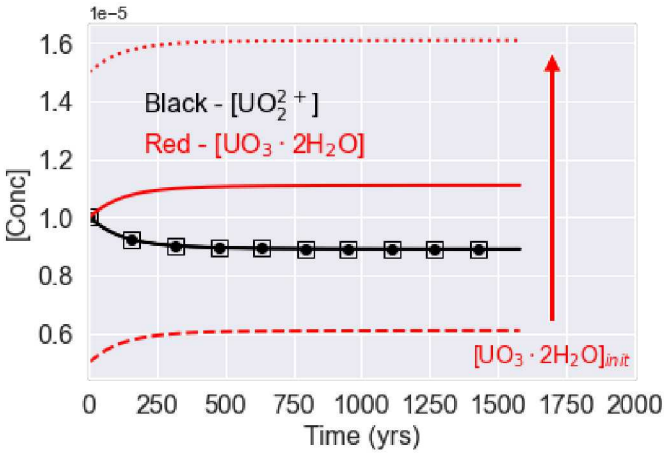

Fig. B-5 **UO_2^{2+} (black) and $UO_3 \cdot 2H_2O$ concentrations as a function of time for the bulk solution reaction given by $O_2^{2+} + 2OH^- + H_2O \rightarrow UO_3 \cdot 2H_2O$. The initial concentration of UO_2^{2+} is the same while the initial concentration of $UO_3 \cdot 2H_2O$ is varied from small (dashed) to larger (dotted).**

Conclusion

We have identified the computational bottleneck of the FMD model as currently implemented in MATLAB; the sequential solve of the corrosion potential and new concentrations. We hypothesize that, by fully coupling these solutions together we can achieve significant speed up. An example matrix solution was provided. A stand-alone Fortran 1D reactive-transport code is currently being developed from scratch to implement this approach. This effort is important for increased efficiency and accuracy in the FMD process model.

References

Buck, E., Jerden, J., Ebert, W., Wittman, R. (2013), Couple the Mixed Potential and Radiolysis Models for Used Fuel Degradation, FCRD-UFD-2013-000290, Argonne National Laboratory.

Jerden, J., Frey, K., Cruse, T., Ebert, W. (2012), Waste Form Degradation Model Status Report: Electrochemical Model for Used Fuel Matrix Degradation Rate, FCRD-UFD-2012-000169, Argonne National Laboratory.

Jerden, J., Copple, J.M., Frey, K.E., Ebert, W. (2015), Mixed Potential Model for Used Fuel Dissolution – Fortran Code, FCRD-UFD-2015-000159, Argonne National Laboratory.

Jerden, J., Gattu, V.K., Ebert, W. (2018), Update on Validation and Incorporation of a New Steel Corrosion Module into Fuel Matrix Degradation Model, M4SF-18AN010301017, Argonne National Laboratory.

Patankar, S.V. (1980). Numerical Heat Transfer and Fluid Flow, Hemisphere Publishing Corporation.

Shoesmith, D.W., Kolar, M., King, F. (2003), A Mixed-Potential Model to Predict Fuel (Uranium Dioxide) Corrosion within a Failed Nuclear Waste Container, Corrosion, 59:802-816.

Wagner, C., Traud, W. (1938), Elektrochem., 44:391-454.

Appendix C. GDSA FRAMEWORK GRAPHICAL WORKFLOW

APPENDIX C. GDSA FRAMEWORK GRAPHICAL WORKFLOW

Introduction

The GDSA computational framework is largely comprised of two primary computational capabilities: PFLOTRAN and Dakota, as described in Section 2.2. An analysis supporting the performance assessment of a geologic repository necessarily requires the development and use of many additional connective computational components beyond these two primary components. These additional computational components are used to develop input files, connect the capabilities of PFLOTRAN and Dakota, submit calculations to computational resources, gather and post-process results, and much more. The collection of these computational components that comprise the complete body of work required to produce results of interest from a computational simulation capability is hereafter referred to as an *analysis workflow*.

Any analysis workflow necessarily requires the development of connective capabilities to support the execution of a computational simulation to produce results of interest, as noted above. These connective capabilities are often developed on an analysis-by-analysis and/or an analyst-by-analyst basis and are not necessarily easy to update and translate to support the development of new analyses or use by new analysts. This can make it difficult to replicate previous analyses, hand-off analyses between analysts, and/or train new analysts to produce analysis workflows. This is a general problem that is faced across the computational simulation community of practice. It therefore is of general interest to develop a more traceable, generalizable, and straightforward approach to the creation of computational simulation analysis workflows.

The Next-Generation Workflow (NGW) capability is an open source engine that was developed at Sandia National Laboratories to provide analysts with a capability to construct, execute, and communicate end-to-end computational simulation analysis workflows [Orient 2020]. This capability is a graphical, node-based interface that includes many pre-programmed support functions which are often utilized within computational simulation analysis workflows. NGW is available within the Dakota Graphical User Interface (GUI) [Ridgway 2020] and is thus available to the GDSA analysis community. A series of NGW analysis workflows for GDSA analysis exemplars were developed in FY 2020 to pilot the use of this capability for the GDSA program. This appendix details the development of these workflows,

provides examples of their use, and proposes a path forward for additional development. The eventual goal of this work is to develop an analysis workflow library that can be made available to the GDSA analysis community.

Next-Generation Workflow (NGW)

The Next-Generation Workflow (NGW) capability was built to graphically define, communicate, and execute the process of building and running analyses with computational simulation capabilities. It is designed to be intuitive and graphical, to allow for hierarchical workflow development through nesting, and to support the development of credibility evidence, communication, and training for computational simulation [Friedman-Hill 2015, Orient 2020]. NGW is available in the Sandia Analysis Workbench (SAW) and as an open source tool that is also available in the Dakota GUI, as described above. The manual for the Dakota GUI provides an example that details setting up and running simulations using the NGW capability [Ridgway 2020]. Nodes within the NGW capability are designed to accomplish common tasks that are undertaken within a computational simulation analysis workflow, including file manipulation, script execution (bash, Python, etc.), results plotting, and more. The NGW capability is currently in active development; releases including updates to this capability are included as new versions of Dakota are released.

Development of GDSA Graphical Workflows

A first step towards developing graphical workflows for GDSA analyses is the development of an understanding of the existing analysis workflow of interest. An example of a basic notional GDSA analysis workflow for a deterministic analysis is shown in Fig. C-1 below. This example shows the development of analysis results using a PFLOTRAN simulation and subsequent visualization software and plotting scripts.

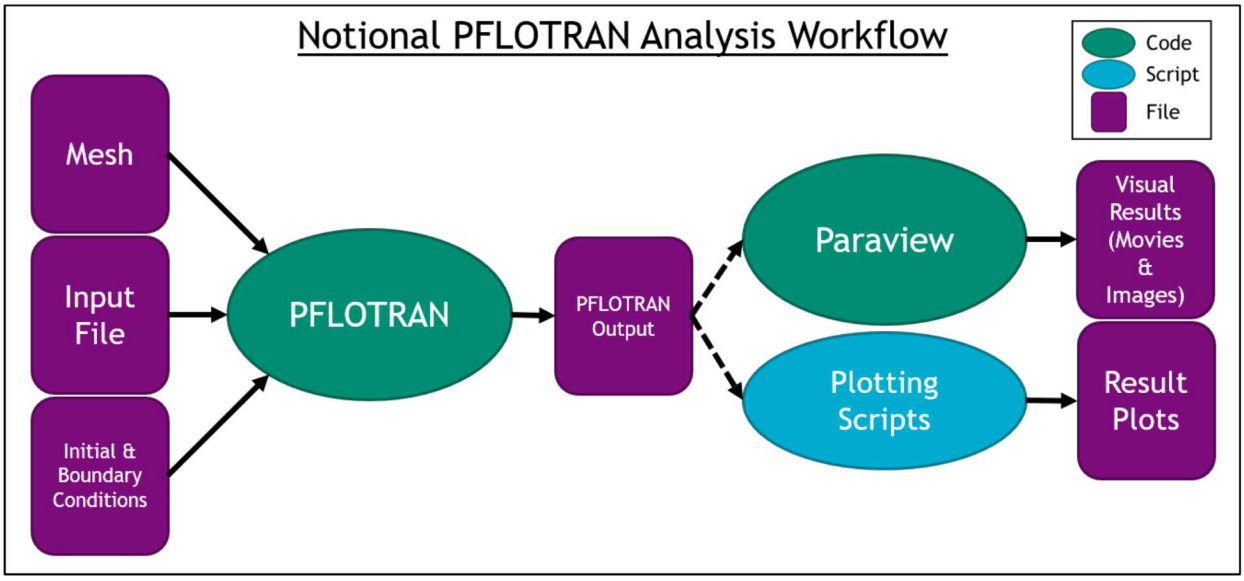

Fig. C-1 Notional Deterministic PFLOTRAN Analysis Workflow

The arrows connecting each component of the workflow shown above may or may not be automated. Solid lines show connections that may be made automatically using bash scripting. Dashed lines show points at which an analyst may take action to move files manually to use as inputs for visualization, as an example. At this level of detail, it is tractable to document and trace each step of this analysis workflow as-is. However, as greater complexity is added to the analysis, this becomes increasingly difficult to thoroughly manage and time consuming to complete.

An example of a probabilistic analysis workflow utilizing both PFLOTRAN and Dakota is shown in Fig. C-2.

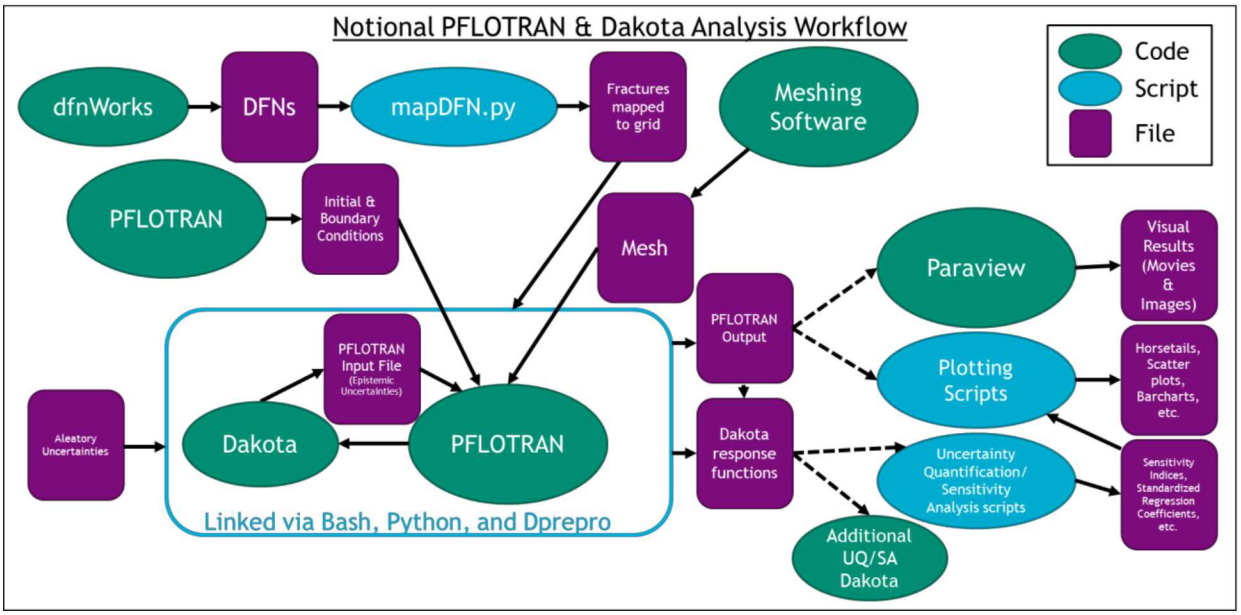

Fig. C-2 Notional Probabilistic PFLOTRAN & Dakota Analysis Workflow.

The additional use of Dakota to develop a probabilistic analysis begins to add a great deal of complexity to this workflow. In addition to Dakota and PFLOTRAN, many software capabilities may be utilized to produce input files, such as the mesh and fracture representation, and to post-process and provide visualization of the results. Handoffs between software capabilities may be complex and dynamic. For instance, Dakota samples parameters of interest, these sampled parameter values are included in the PFLOTRAN input file, PFLOTRAN is run and the results of the simulation are passed back to Dakota to calculate statistics on results and to perform sensitivity analysis. Without the graphical workflow software, this analysis workflow component by itself requires bash scripting and manual intervention from the analyst, which both increases the time it takes to complete the analysis and raises the opportunity for error to be introduced. It quickly becomes intractable for the analysis to be easily re-run or replicated under this paradigm.

A graded approach was taken to develop NGW analysis workflows for GDSA analyses under two examples of interest. First, an analysis workflow was developed for a simple example, similar to the notional example presented in Fig. C-1. This basic workflow was then extended to a complex probabilistic analysis paradigm, similar to the notional example presented in Fig. C-2. The workflows for each of these examples are presented in the sections that follow.

Geologic Disposal Example

A graphical workflow was first developed for the geologic disposal example that is available in the materials for the PFLOTRAN short course [Stein 2020]. This example demonstrates how to use PFLOTRAN's process models developed for performance assessment simulations of deep geologic nuclear waste repositories.

The complete graphical workflow for this example is shown in Fig. C-3 below. This workflow sets parameters of interest, inserts these parameters into the PFLOTRAN input file, collects additional input files, runs PFLOTRAN, and develops and runs a post-processing script.

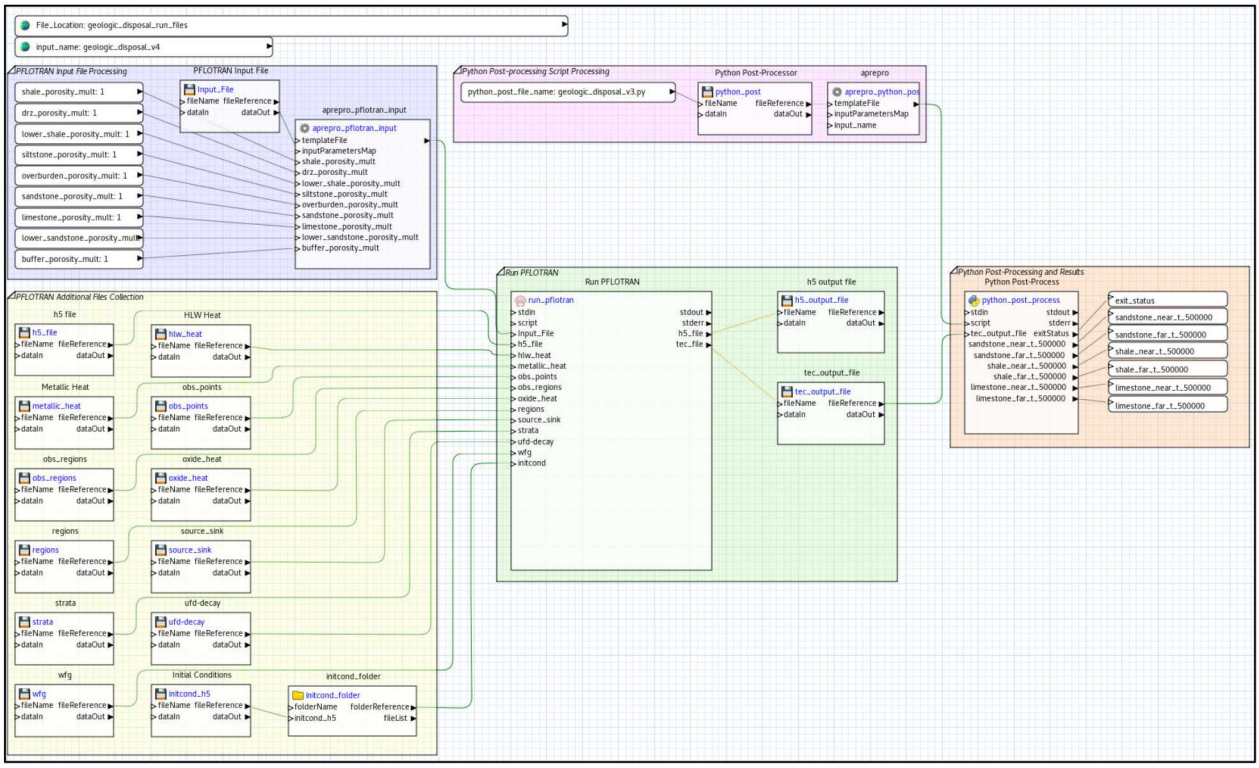

Fig. C-3 Geologic Disposal Example Graphical Workflow

The first step in this simple workflow sets up the PFLOTRAN input file using a text-processing software called ‘aprepro’ to replace strings in a templated input file with calculated parameters of interest, as shown in Fig. C-4. In this example, multipliers on porosity values for each material are passed to the templated input file. Values of the porosity for each material are calculated by multiplying these parameters by a nominal value for porosity. In this way, porosity values could be varied by changing the value of each multiplier. This allows for automatic generation of a PFLOTRAN input file with variations in parameter values, which supports, for example, uncertainty quantification using Dakota. The default values of these multipliers are set to 1, meaning that the PFLOTRAN input file would be populated with the nominal values of each porosity parameter. The output of this processing step is the final PFLOTRAN input file, which will be used in the PFLOTRAN calculation.

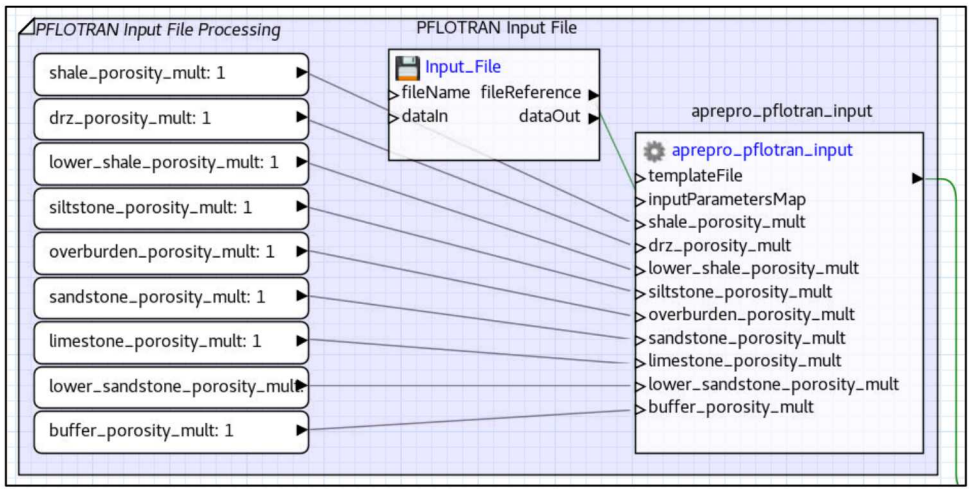

Fig. C-4 PFLOTRAN Input File Processing for Geologic Disposal Example Graphical Workflow

The next section of the graphical workflow for this example collects files that are referenced in the PFLOTRAN input file during the PFLOTRAN calculations, as shown in Fig. C-5. Each file is found at the file location specified by the user and then copied to the directory where the calculation will run. This can be very helpful for traceability purposes; every file that is used in the run is saved along with the input file and results, allowing for the analysis to be reproduced easily. Although this may be trivial for this small example problem, it is significant for more complex analyses.

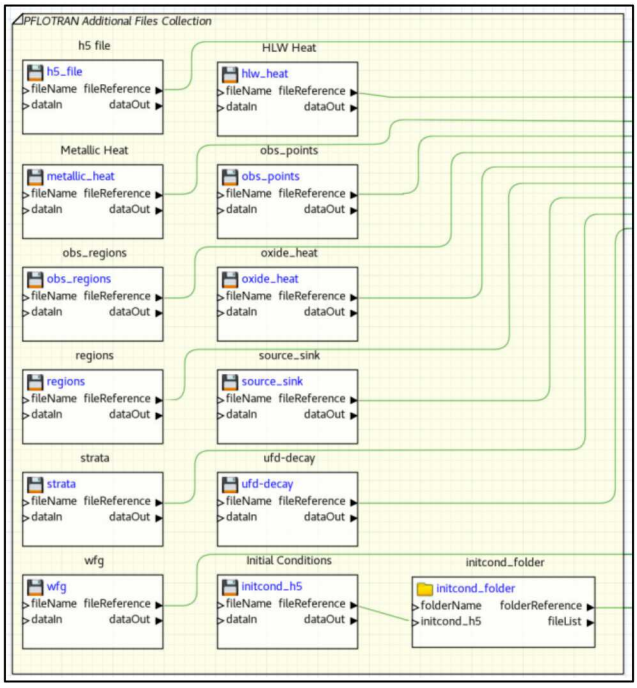

Fig. C-5 Input File Collection for Geologic Disposal Example Graphical Workflow

The PFLOTRAN calculation is executed in the graphical workflow using a bash scripting node that executes a command to run PFLOTRAN, as shown in Fig. C-6, with the input file that was created using

'aprepro' and all of the files that were collected as a preprocessing step. Output files are generated, one of which is sent to a post-processing script to generate plots of results.

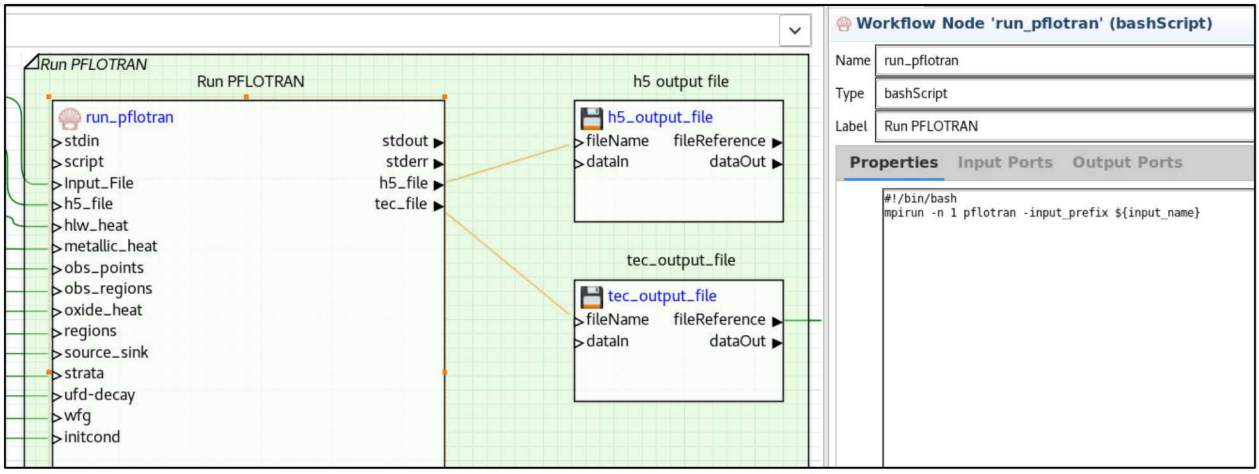

Fig. C-6 PFLOTRAN Calculation for Geologic Disposal Example Graphical Workflow

The final post-processing calculations for this graphical workflow are accomplished in two steps, shown in Fig. C-7 and Fig. C-8. First, the post-processing script itself is processed using 'aprepro' to include the name of the input file as a parameter, allowing for automated flexibility if the input file name were to be changed by the user. Second, the Python post-processing script is run and parameters of interest are output as responses for the workflow.

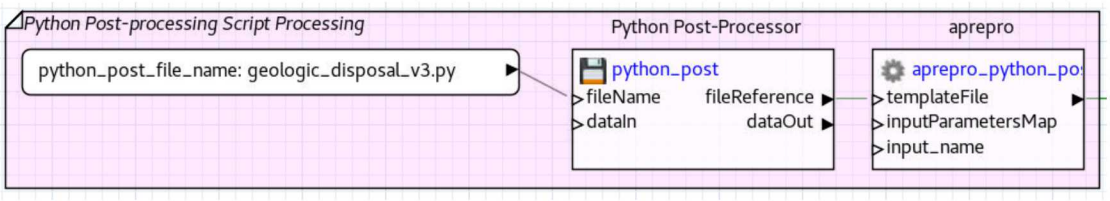

Fig. C-7 Post-processing Script Development for Geologic Disposal Example Graphical Workflow

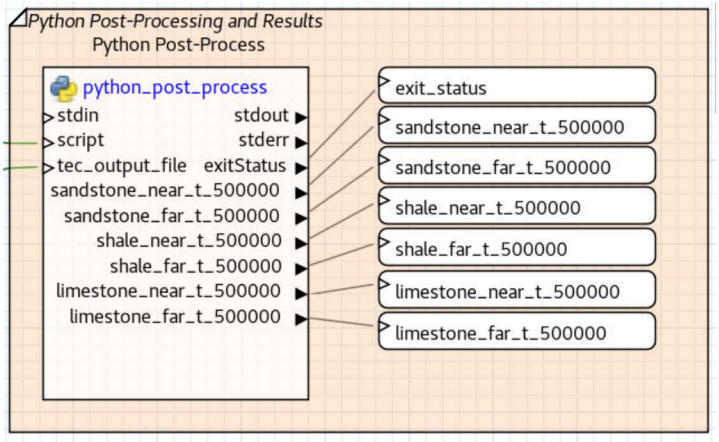

Fig. C-8 Post-processing Script Execution for Geologic Disposal Example Graphical Workflow

The user can select a run directory prior to running the workflow. As the workflow is running, the user can monitor progress using color-coding in which completed nodes are shown in green, nodes that are still running are shown in yellow, and nodes that experience an error are shown in red, as shown in Fig. C-9. This allows the user to both monitor their calculations in real time and to quickly understand where an error might have occurred for debugging purposes.

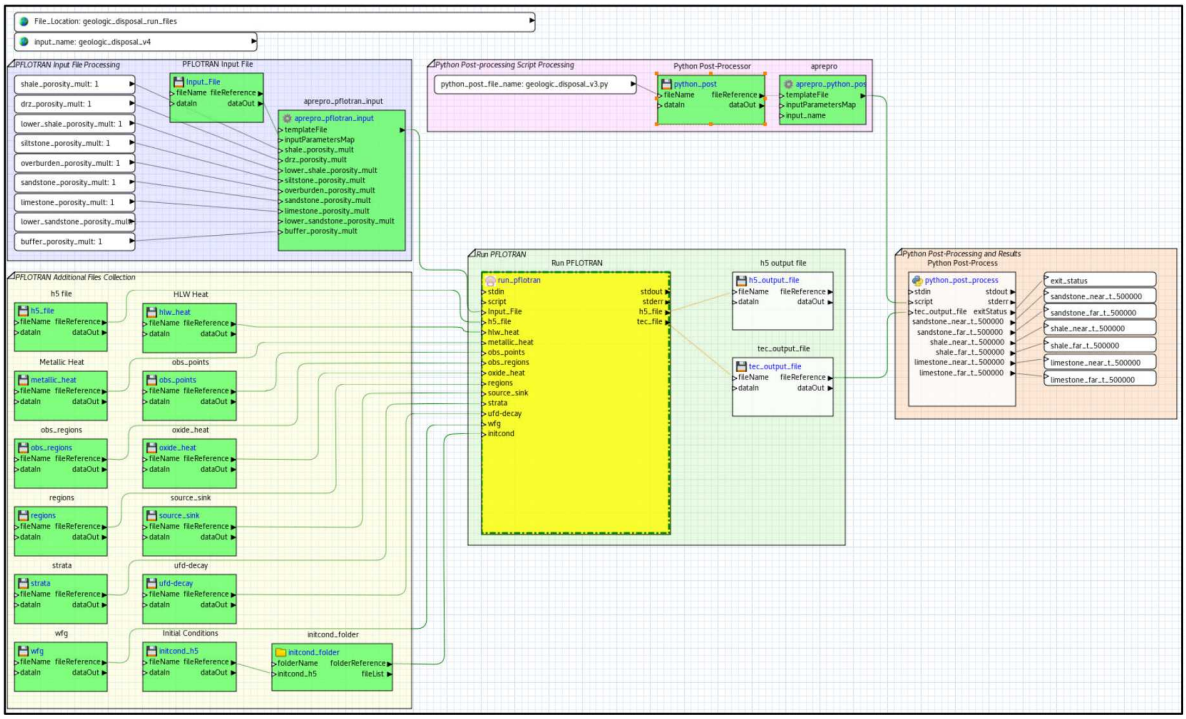

Fig. C-9 Real-time Progress of Geologic Disposal Example Workflow

The final results of the calculations completed in this graphical workflow are shown in Fig. C-10. The plot displayed in this figure is created during the Python post-processing calculations.

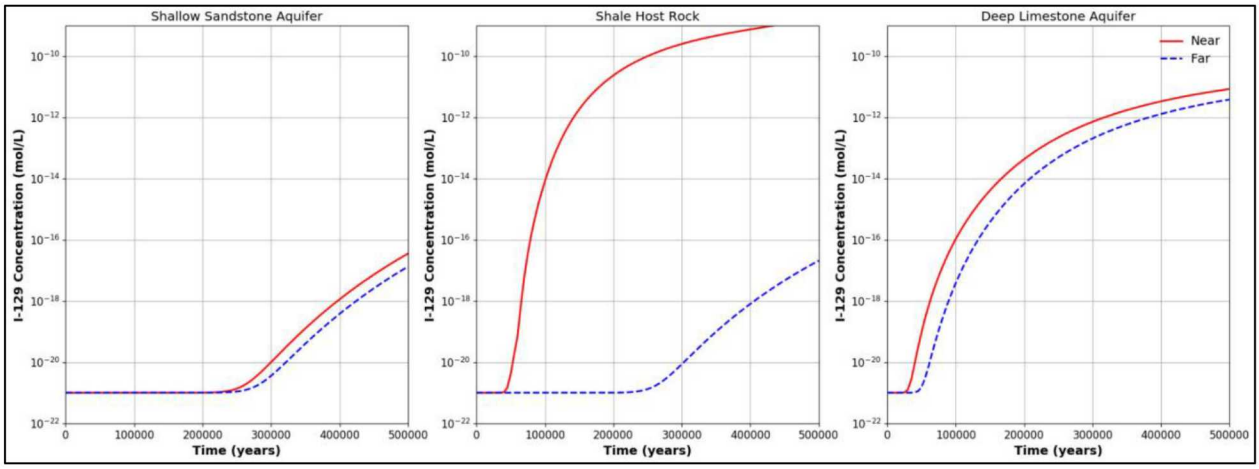

Fig. C-10 Final Results of the Calculations Completed in the Geologic Disposal Example Workflow

Following the development of this graphical workflow, additional capabilities that are available in the NGW software package can be easily utilized. For example, NGW has been developed to work seamlessly with Dakota. Thus, with the parameters and responses specified as described above, the 'Dakota Wizard' can be utilized to develop a Dakota input file for this workflow to study, e.g., how uncertainty in the porosity values for all materials might contribute to uncertainty in the outputs of interest. This Dakota input file can then be developed into another graphical workflow for performing uncertainty quantification, an example of which is shown in Fig. C-11.

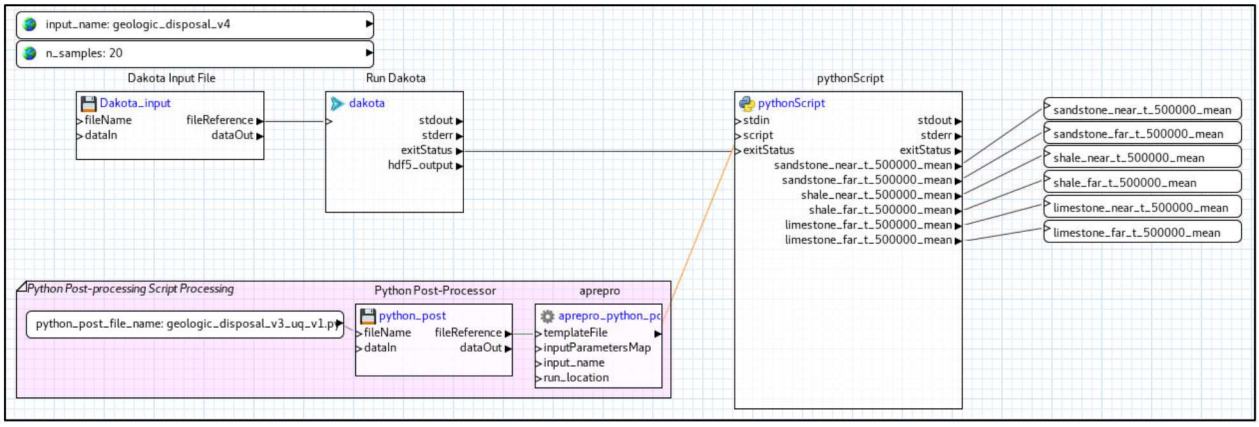

Fig. C-11 Dakota Uncertainty Quantification Workflow for the Geologic Disposal Example

The results of this Dakota uncertainty quantification workflow are shown in Fig. C-12. These results show the affect of uncertainty in the porosity values for all materials defined in the PFLOTRAN input file. These results can be compared to the deterministic results presented in Fig. C-10. The porosity parameters are varied uniformly by ±10% in this uncertainty quantification example, with 80 samples taken using latin hypercube sampling to produce the results presented below.

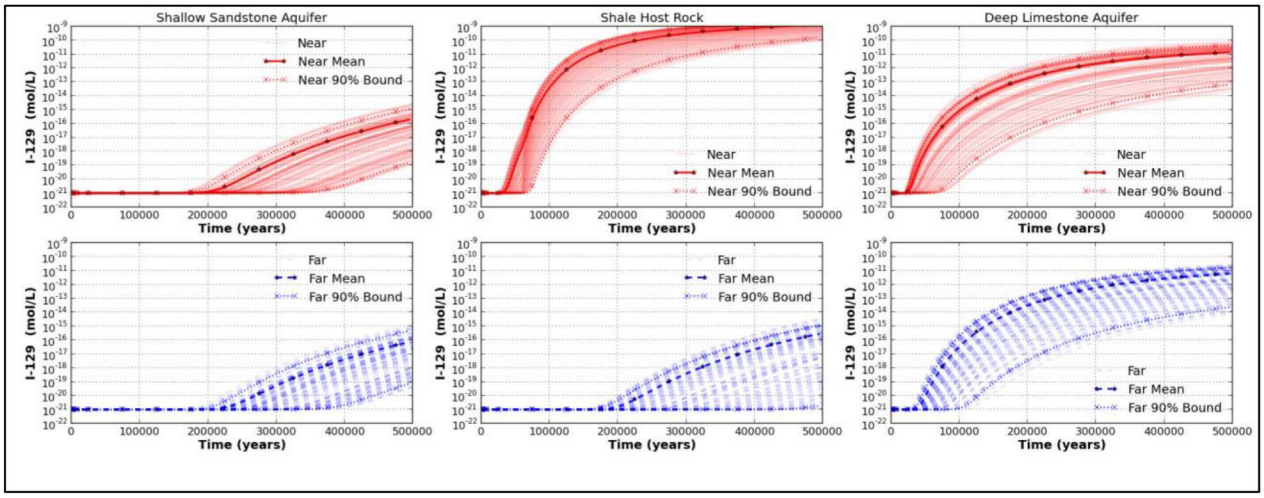

Fig. C-12 Uncertainty Quantification Results for the Geologic Disposal Example

The basic workflow presented above could be modified for a different analysis with a similar structure in several ways. First, all file paths to input files within file nodes would need to be updated to reference the files for the specific analysis of interest. File nodes that are not used by the new analysis would need to be removed. New file nodes for files that were not included in the original workflow would need to be added and connected as appropriate to downstream nodes. If a different PFLOTRAN input file was used and uncertain inputs are of interest, this new file would need to be templated for use with 'aprepro'. If different uncertain parameters were desired, these would need to be updated and connected to subsequent nodes. Finally, depending on the outputs of interest and output files generated by the calculation, the post-processing script would need to be updated or switched out and connected to new response parameters of interest.

HPC Submission and Probabilistic Analysis Example

The simple graphical workflow that was developed for the geologic disposal example was expanded significantly to pilot the use of NGW to support PFLOTRAN simulations that require job submission to Sandia's high-performance computing (HPC) resources. The analysis of interest selected for this demonstration was the Crystalline Reference Case [Swiler et al. 2020]. The analysis workflow for this case includes many computation components and modelers/analysts that are combined to produce analysis results which include those related to uncertainty quantification and sensitivity analysis. The NGW graphical analysis workflow that is under development for this problem is intended to provide an enabling capability to support completing end-to-end uncertainty quantification and sensitivity analysis calculations that are both traceable and can be completed efficiently. The development of the Crystalline Reference Case graphical workflow has been completed in parallel to the development of an updated PFLOTRAN input file, the addition of capabilities for outputting new quantities of interest (QoIs) in PFLOTRAN, and the execution of uncertainty quantification and sensitivity analyses. The graphical workflow that is presented below represents a portion of the overall analysis workflow for the Crystalline Reference Case. Future work will include the remaining components of the analysis workflow for this case to develop a finalized end-to-end analysis product. The notional analysis workflow for this complete analysis is presented in Fig. C-2.

The first step towards developing a graphical analysis workflow for the Crystalline Reference Case was to develop the deterministic analysis workflow that includes running PFLOTRAN and post-processing results using Python. This is, at a high level, nearly the same as the steps presented for the geologic

disposal analysis example. However, due to the complexity of the Crystalline Reference Case simulation and input file, additional development was required.

The execution of the Crystalline Reference Case deterministic simulation was split into two workflows. The first is a local workflow that collects supporting files that are used during the run, sets global parameters including those required for submission to the HPC queue, processes the run script, PFLOTRAN input file, and Python post-processing script based on user inputs and parameter selections, and sends all information and files required for running the PFLOTRAN simulation on the HPC resource to a remote nested workflow. This remote nested workflow is the second workflow, which intakes information and files from the first workflow and uses a run script to submit the PFLOTRAN simulation to the HPC queue.

The local workflow for the Crystalline Reference Case deterministic simulation is shown in Fig. C-13 below. The user input parameters are set in the top left and include options required for HPC submission and directory information that is used to manipulate and manage files under the set of nested workflows that comprise the double-looped uncertainty quantification analysis workflow, which will be described later. Run files are collected in five groups based on input type and source files location, as shown in the bottom left. The Crystalline Reference Case PFLOTRAN input file references additional files in five separate file locations. This workflow copies these files into a local directory and then replaces the file references in the input file, allowing for greater transparency and traceability in this analysis.

The local workflow processes the run script for the analysis and input file using the same text-replacement software ‘aprepro’ that was applied for the geologic disposal example. This step is shown along with the connection to the remote HPC submission workflow in the top right of Fig. C-13.

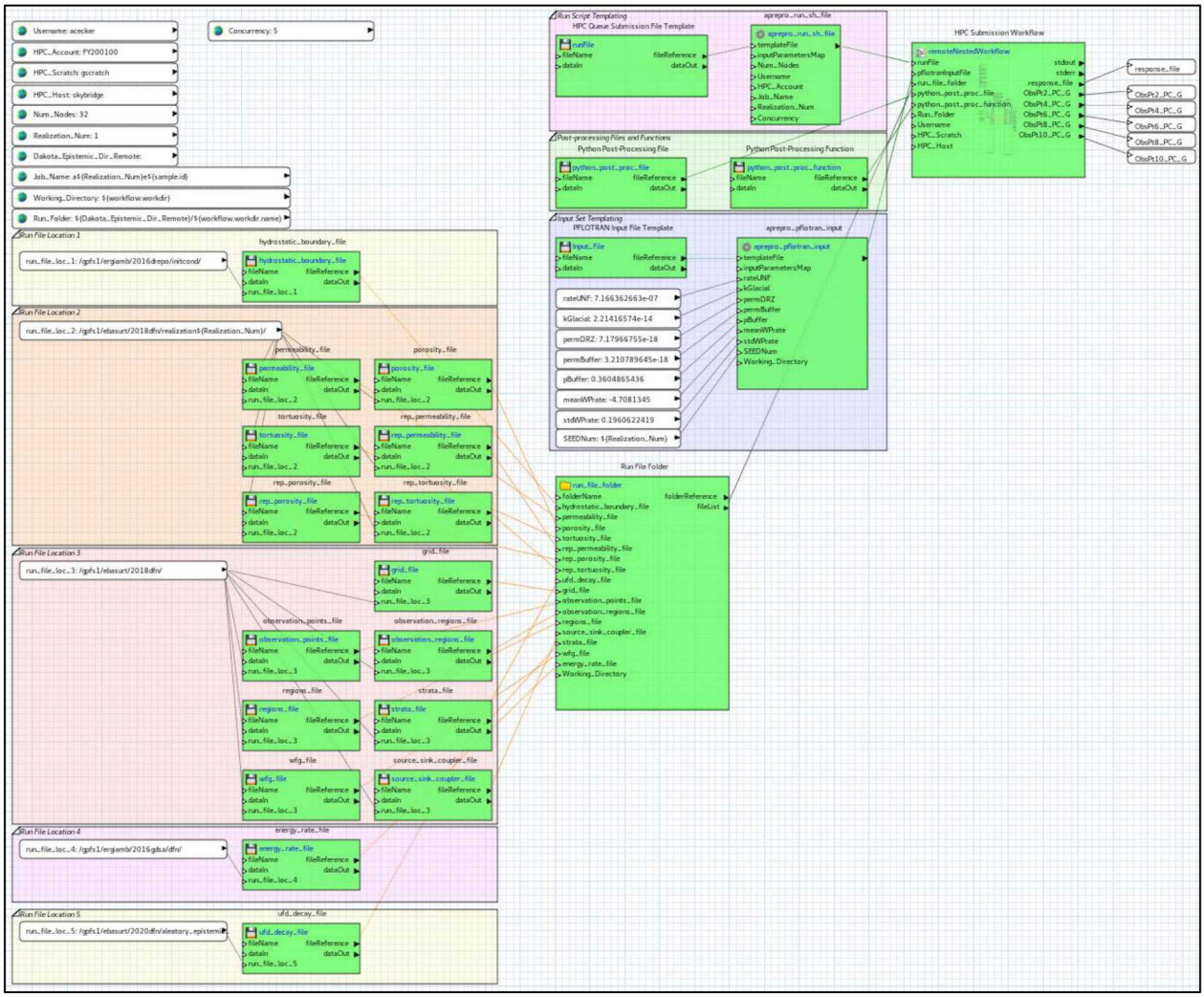

Fig. C-13 Local Workflow for Crystalline Reference Case Deterministic Simulation

The local workflow for the Crystalline Reference Case deterministic simulation sends all of the information and files required for the PFLOTRAN run to be submitted to the HPC queue to a remote nested workflow, which connects to a second graphical workflow for HPC submission. This second workflow is shown in Fig. C-14. The second workflow uses the run script and PFLOTRAN input file developed in the local workflow to submit the PFLOTRAN simulation to the queue using a bash scripting node. This bash node runs the run script, which includes the sbatch options that set up the queue submission, and monitors the run status by continuously checking the queue status as the run is in the queue, running, and completed. This monitoring allows the workflow to wait for the calculation to complete prior to the next step. When the calculation completes, results files are sent to a Python post-processing node, which produces responses of interest that are sent back to the local workflow.

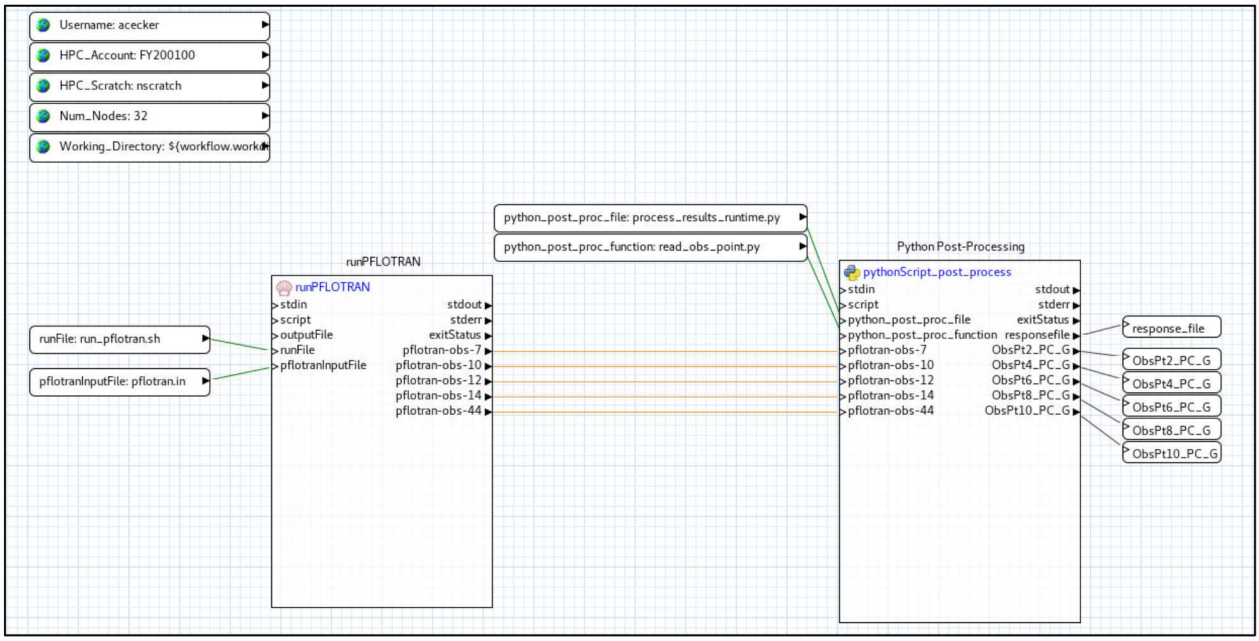

Fig. C-14 Remote HPC Submission Workflow for the Crystalline Reference Case Deterministic Simulation

The execution of the local workflow that calls the HPC submission workflow for the Crystalline Reference Case deterministic simulation encompasses a single PFLOTRAN run. The purpose of the Crystalline Reference case analysis is to perform uncertainty quantification in a nested aleatory and epistemic loop structure. Thus, this deterministic calculation must first be connected to Dakota to allow for the propagation of parametric uncertainty, which is the epistemic loop of the Crystalline Reference Case uncertainty analysis. This workflow is shown in Fig. C-15. The Dakota input file for this portion of the analysis samples the eight parameters of interest and runs the deterministic simulation by changing these parameter values to run the simulation many times.

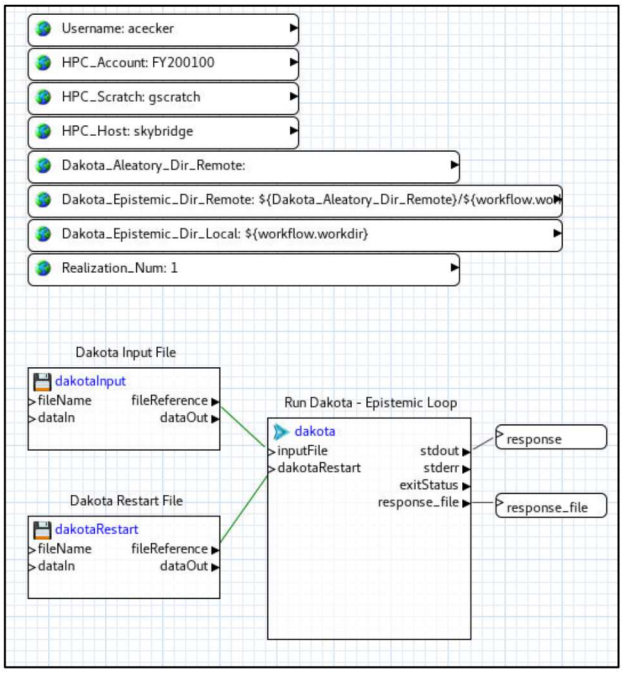

Fig. C-15 Epistemic Loop Workflow for the Crystalline Reference Case

A second Dakota workflow was developed to sample twenty discrete fracture networks (DFNs), which represent the aleatory uncertainty included in the overall uncertainty quantification structure of the Crystalline Reference Case. The DFN inputs are saved in folders labeled with their DFN realization number. Thus, the Dakota input file used for this portion of the analysis uses a list parameter study to change the value of the realization number that is sent to the epistemic loop. Each aleatory sample of a DFN initializes a full epistemic sampling loop of 40 samples. Each of these 40 epistemic samples uses the DFN inputs for the single aleatory realization, effectively completing the nested sampling approach that has been developed for the Crystalline Reference Case. This workflow is shown in Fig. C-16.

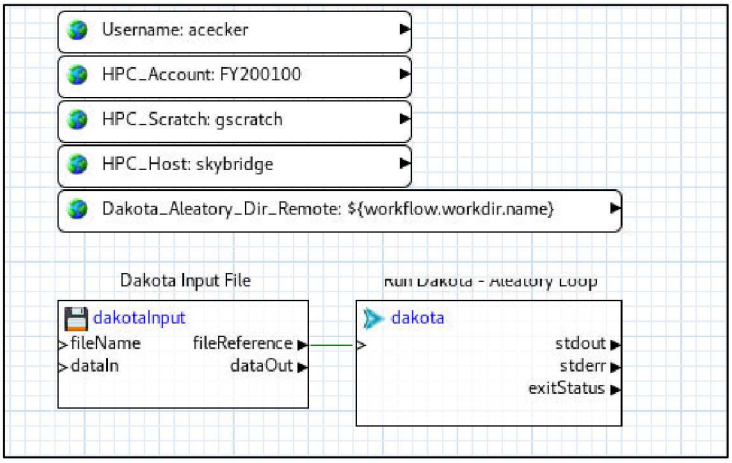

Fig. C-16 Aleatory Loop Workflow for the Crystalline Reference Case

As shown in Fig. C-15 and Fig. C-16, the two workflows that comprise the nested-loop sampling structure for the crystalline reference case are fairly simplistic. Despite this simple implementation, these

workflows represent a significant step forward in automating the process of uncertainty quantification for the Crystalline Reference Case, which will be a powerful tool that will enable faster turnaround of these analyses in the future. In addition, future work will supplement these workflows with post-processing, plotting, and sensitivity analysis at each sampling level, allowing for results generation as the calculations are running.

Development Path Forward

The development of graphical analysis workflows using NGW in support of the GDSA Framework effort in FY 2020 has been primarily a pilot effort centered on the study of specific examples and use-cases. This effort has demonstrated that NGW can be utilized with PFLOTRAN and supporting capabilities to develop graphical analysis workflows of varying complexity for problems in the GDSA program area. Future work and a path forward for the graphical workflow component of the GDSA project are presented as follows.

The current workflow for the Crystalline Reference case [Swiler et al. 2020] as described above includes a nested workflow for input setup and HPC submission that has been wrapped in Dakota workflows for nested double-looped aleatory and epistemic sampling in support of uncertainty quantification analyses. Although this workflow represents a step forward towards the automation of this analysis in a graphical analysis workflow, additional steps must be taken to include further analysis components. These include scripts to post-process data at intermediate levels under each sampling loop, plotting scripts to generate results of interest, and sensitivity analysis capabilities including both further Dakota studies and related post-processing and plotting scripts. Further, faster execution of PFLOTRAN uncertainty quantification runs under the graphical workflow framework could be enabled by the use of PFLOTRAN restart capabilities, which may be implemented as a part of continued input file development. The additional development of these capabilities and the completion of an end-to-end Crystalline Reference case graphical workflow that includes post-processing and sensitivity analysis capabilities is planned for the beginning of FY21.

The generalization and extension of the piloted graphical workflow examples from FY 2020 to a wider variety of problems is an important next step in this development. The current pilot graphical analysis workflows cover a small problem set (geologic disposal). It is important to identify additional analyses and problems for which graphical analysis workflows could be piloted in a strategic way such that examples might be available across the GDSA framework problem space of interest.

Finally, the ultimate path forward for the graphical analysis workflow effort is to develop and deploy a library of both examples and workflow templates for the GDSA framework user community. The realization of this goal requires the development of supporting documentation and a methodology for both delivering these graphical workflows and ensuring that they will continue to run successfully as PFLOTRAN is continuously updated. The development of strategies and capabilities for deploying workflow examples to the GDSA framework user community is planned for FY21.

References

Friedman-Hill, E., Hoffman, E., Gibson, M., Clay, R., & Olson, K., 2015. Incorporating Workflow for V&V/UQ in the Sandia Analysis Workbench. Proceedings of the NAFEMS World Congress, June 2015.

Orient, G., Clay, R., Friedman-Hill, E., & Hoffman, E., 2020. Next Generation Workflow – an Open Source Software System for Computational Modeling to Support Agile VVUQ. Presented at the ASME V&V Symposium, May 20-22, 2020.

Ridgway, E., 2020. Dakota. GUI Version 6.12 User Manual – Next-Gen Workflow. https://dakota.sandia.gov/content/next-gen-workflow. Accessed August 5, 2020.

Swiler, L.P, Basurto, E., Brooks, D.M., Eckert, A.C., Mariner, P.E., Portone, T., & Stein, E.R., 2020. Status Report on Uncertainty Quantification and Sensitivity Analysis Tools in the Geologic Disposal Safety Assessment (GDSA) Framework. Sandia Report – SAND2020-XXXX. In preparation.

Stein, E., 2020. PFLOTRAN Short Course Geologic Disposal Example. https://bitbucket.org/pflotran/pflotran/src/master/shortcourse/exercises/geologic_disposal/. Accessed April 2, 2020.

(This page is intentionally blank.)

Appendix D. NEAR-TERM GDSA THRUSTS IN THE DISPOSAL RESEARCH R&D 5-YEAR PLAN

APPENDIX D. NEAR-TERM GDSA THRUSTS IN THE DISPOSAL RESEARCH R&D 5-YEAR PLAN

Disposal Research 5-Year Plan Thrusts - Near Term

Thrust	Description	Tech. Area	Term
	Geologic Disposal Safety Assessment		
G01	*Advanced simulation capability*	*GDSA*	*Near*

GDSA Framework integrates coupled physical and chemical process models and material-specific constitutive models in PFLOTRAN (Lichtner et al. 2019), a multiphase flow and reactive transport simulator. Near term advancements in capability will focus on high priority topical areas identified in the 2019 Disposal Research R&D Roadmap Update, including high temperature processes, coupled thermo-hydro-mechanical processes affecting buffer evolution, waste package degradation models, criticality, and coupled thermo-hydro-chemical processes affecting radionuclide transport. Multi-fidelity model implementation including mechanistic models derived from detailed process understanding, reduced order models, and machine learning emulators enhances computational efficiency and dovetails with integration of advanced uncertainty and sensitivity analysis methods.

Other software development tasks will include implementation and testing of advanced solvers and physics-based convergence criteria to improve computational efficiency when solving the nonlinear systems of equations that arise in simulation of complex systems; development of open-source biosphere simulation software; and release of an open source version of Vorocrust (Abdelkader et al. 2020), an automated meshing tool for generating conforming meshes of complex engineered and geologic features.

G02	*Uncertainty and sensitivity analysis*	*GDSA*	*Near*

Uncertainty and sensitivity analysis (UQ/SA) methods in GDSA Framework are primarily available through Dakota (Adams et al. 2020), an open source HPC interface for coupling physics simulations to both tried-and-true and cutting-edge methods of UQ/SA, optimization, and parameter estimation. In the next 1 to 2 years, GDSA will identify and demonstrate methods consistent with the current standard of practice that add value to deep geologic repository performance assessment (e.g., metamodeling, variance decomposition); prototype multi-fidelity UQ/SA methods in coordination with development of multi-fidelity simulation capability; and contribute to development of an international consensus on best practices for sensitivity analysis in the context of repository performance assessment.

Thrust	Description	Tech. Area	Term
	Geologic Disposal Safety Assessment		
G03	*Workflow*	*GDSA*	*Near*

Transparent, traceable workflows increase stakeholder confidence and user-friendliness. In the next 1 to 2 years, three important workflows will be established: an open source framework (scripted in Python) that automates software (PFLOTRAN) verification testing; a workflow that streamlines data transfer from the geologic model to the meshing software and ultimately to the simulator; and an automated, traceable workflow for performing probabilistic uncertainty and sensitivity analyses.

G04 *Repository systems analysis* — *GDSA* *Near*

Reference cases describing generic repositories in argillite, salt, crystalline, and unsaturated host rocks provide a platform for integrating concepts, demonstrating capability, and driving development of simulation software and analysis methods. In the next 1 to 2 years, conceptual models and simulations that account for high temperature impacts (associated with direct disposal of DPCs) in generic argillite and unsaturated repositories will be advanced. Integration with the DPC technical area will also address the consequences of criticality for repository performance.

International collaborations will focus on crystalline and salt concepts. The GDSA team is leading a 4-year task for DECOVALEX2023 in which performance assessment (PA) simulation and analysis methods applied to generic crystalline and salt reference cases will be compared. Ten teams from 7 countries are participating. A US/German joint project will finalize a report to be published by the international Nuclear Energy Agency that documents FEP in salt repositories; and a broader coalition of countries will initiate a collaborative effort to establish best practices for development of scenarios for evolution of salt repositories from FEP.

G05 *Geologic modeling* — *GDSA* *Near*

Geologic modeling involves two primary efforts: generation of representative 3-dimensional (3D) regional geology models that inform reference case concepts and simulations, and development of an interactive web-based application (https://gis1.inl.gov/regionalgeology/) for visualizing argillite, salt, and crystalline formations in the US. In the next 1 to 2 years, geologic models of a generic unsaturated alluvial basin and of regional argillite stratigraphy will be linked into the meshing workflow described above; and 3D subsurface visualization tools will be developed within the web application.

(This page is intentionally blank.)

Appendix E. NEAR-TERM GDSA THRUSTS AND THEIR MAPPED ROADMAP ACTIVITIES

APPENDIX E. NEAR-TERM GDSA THRUSTS AND THEIR MAPPED ROADMAP ACTIVITIES

5-Year Plan Thrusts and their Related Roadmap Activities

Thrust	Act. ID	Activity	Tech. Area	Term
Geologic Disposal Safety Assessment				
G01		*Advanced simulation capability*	*GDSA*	*Near*
	P-06	(Pseudo) colloid-facilitated transport model		
	P-07	Intrinsic colloid model		
	P-08	Other missing FEPs (processes) in PA-GDSA		
	P-09	Surface processes and features		
	P-11	Pitzer model		
	P-12	WP degradation model framework		
	P-13	Full representation of chemical processes in PA		
	P-14	Generic capability development for PFLOTRAN		
	P-15	Species and element properties		
	P-16	Solid solution model		
	P-17	Multi-component gas transport		
G02		*Uncertainty and sensitivity analysis*	*GDSA*	*Near*
	P-05	Disruptive events		
	P-10	Uncertainty and sensitivity analysis		
G03		*Workflow*	*GDSA*	*Near*
	P-10	Uncertainty and sensitivity analysis		
G04		*Repository systems analysis*	*GDSA*	*Near*
	P-01	CSNF repository argillite reference case		
	P-02	CSNF repository crystalline reference case		
	P-03	CSNF repository bedded salt reference case		
	P-04	CSNF repository unsaturated zone (alluvium) reference case		
	P-05	Disruptive events		
	P-06	(Pseudo) colloid-facilitated transport model		
	P-07	Intrinsic colloid model		
	P-09	Surface processes and features		
	P-10	Uncertainty and sensitivity analysis		
	P-11	Pitzer model		
	P-12	WP degradation model framework		
	P-13	Full representation of chemical processes in PA		
	P-17	Multi-component gas transport		
G05		*Geologic modeling*	*GDSA*	*Near*

Thrust	Act. ID	Activity	Tech. Area	Term
		Geologic Disposal Safety Assessment		
G05	*Geologic modeling*		*GDSA*	*Near*
	P-01	CSNF repository argillite reference case		
	P-02	CSNF repository crystalline reference case		
	P-03	CSNF repository bedded salt reference case		
	P-04	CSNF repository unsaturated zone (alluvium) reference case		
	P-09	Surface processes and features		
	P-13	Full representation of chemical processes in PA		